STATIC AND ROTORDYNAMIC ANALYSIS OF A PLAIN ANNULAR (LIQUID) SEAL IN THE LAMINAR REGIME WITH A SWIRL BRAKE FOR THREE CLEARANCES

A Thesis

by

OVAIS AHMED BIN NAJEEB

Submitted to the Office of Graduate and Professional Studies of
Texas A&M University
in partial fulfillment of the requirements for the degree of

MASTER OF SCIENCE

Chair of Committee,	Dara W. Childs
Committee Members,	Luis San Andrés
	Wayne Hung
Head of Department,	Andreas A. Polycarpou

December 2017

Major Subject: Mechanical Engineering

ABSTRACT

The author conducts tests using a smooth annular seal with a radius of 101.6 mm (4.00 in) with three radial clearances (0.127, 0.254 and 0.381 mm) referred as 1X, 2X and 3X respectively, producing the radial clearance to radius ratios (C_r/R) of 0.0025,0.005 and 0.0075. The seals have axial length of 45.72 mm (1.80 in), producing the length to diameter ratio (L/D) of 0.45. ISO VG 46 oil is used as the testing fluid at a temperature range of 46.0-49.0 ℃ to keep fluid flow laminar. A high pre-swirl insert is used to induce high fluid swirl to the swirl brakes (SBs). Each SB comprises of 36 square cuts with an axial depth of 5.08 mm (0.2 in), radial height of 6.35 mm (0.25 in) and circumferential width of 6.35 mm (0.25 in). The author conducts static and dynamic measurements at ω = 2, 4, 6, 8 krpm, ΔP = 2.07, 4.14, 6.21, 8.27 bar (30, 60, 90, 120 psi), and eccentricity ratios, ε_0 = 0.00, 0.27, 0.53, and 0.80. Static measurements include leakage rate, pre-swirl ratio and outlet swirl ratio, and the static load required to produce the eccentricity ratios.

Dynamic measurements comprise rotor-stator relative displacements, stator acceleration, and applied dynamic load. The measurements are used to calculate stiffness, damping, virtual mass and effective damping coefficients for the seals.

Most importantly, SBs are shown to be effective in minimizing inlet fluid rotation at the 3X clearance but ineffective at the 1X and 2X clearance. When SBs are used with the 3X clearance seal, the cross-coupled stiffness variables have the same sign meaning that the seal would have a WFR of zero and would not produce destabilizing forces on a pump rotor. However, at the 3X clearance, the smooth annular seal has a negative direct

stiffness *K* that could eventually "suck" the rotor into contact with the stator wall, along with dropping the natural frequency of the pump rotor, further reducing its dynamic stability.

Dynamic measurements are compared to predictions based on a model developed by Zirkelback and San Andrés [16]. Most of the predictions agree well with the test data. Notable exceptions are the direct and cross-coupled stiffness coefficients for the 3X clearance. Predictions showed positive direct stiffness and opposite signs for the cross-coupled stiffness coefficients; whereas, the data showed negative direct stiffness and the same positive sign for the cross-coupled stiffness coefficients. Also, for the 1X clearance seal, measured direct damping was higher than predicted at $\omega > 2$krpm by about 25%. For the 1X clearance seal, measured cross-coupled damping was lower than predicted by approximately 2-5 times.

At most of the test conditions, measured direct virtual mass coefficients are about 6 times greater than predicted but follow the same general trend. For the 1X and 3X clearance seals, predictions are lower than measured data while predictions match test data well for the 2X clearance seals.

The model predicts the whirl frequency ratio WFR very well for the 1X and 2X clearance seals at all test conditions but fails to predict zero WFR for the 3X clearance seal.

DEDICATION

I dedicate this work to the lovely mothers I have in my life; the mother that gave birth to me and the adorable grandmothers I cannot live without.

ACKNOWLEGEMENTS

First and foremost I would like to be thankful to my Creator. The countless blessings that I have in my life are only because of the Almighty. I pray for more successes in this life and the hereafter.

Dr. Childs is the reason why this thesis was possible. I could not have had a better supervisor. Thank you for bringing a stranger into this wonderful research family of yours. My masters would not have been possible without your generous support. You are an inspiration and May God Bless you.

My colleagues here at the turbolab deserve the praise too. Alex Moreland, thank you for being a great mentor. I do not exaggerate, when I say I could not have done this without you. I hope that you may be successful in whatever you do. Josh Bullock, thank you for giving me the initial support that I needed, starting off at the lab. Nathan Eitrheim, thank you for your help whenever I needed it the most. Nathan Balke, thank you for all your support. Patricio and Connor, thank you for doing anything and everything I asked you guys to do. All of you were an integral part of this journey.

Last but not the least, I would like to thank my Mama, Baba and Vicky. My family is the only reason I have achieved anything in life. Without your love, guidance, sacrifices and belief in me, I wouldn't be here today. I wish you all the happiness and success in this life and the hereafter.

CONTRIBUTORS AND FUNDING SOURCES

Contributors

This work was supervised by a thesis committee consisting of Professor Dara Childs (Chair of Committee) and Professor Luis San Andrés of the Department of Mechanical Engineering and Professor Wayne Hung of the Department of Engineering Technology and Industrial Distribution.

All work for the thesis was completed independently by the student.

Funding Sources

Graduate study was supported by a Research Assistantship from Texas A&M University and Turbomachinery Research Consortium funding.

NOMENCLATURE

$\boldsymbol{A_{ij}}$	Frequency domain stator acceleration [L/T^2]
C_{eff}	Seal effective damping defined in Eq. (26) [FT/L]
C_{ij}	Seal damping coefficients [FT/L]
C_r	Seal radial clearance [L]
D	Seal diameter [L]
$\boldsymbol{D_{ij}}$	Frequency domain stator displacement [L]
e_0	Static eccentricity [L]
f_{sX}, f_{sY}	Seal reaction force components in X and Y directions [F]
F_s	Applied static load magnitude [F]
f_X, f_Y	Applied dynamic loads in X and Y directions [F]
$\boldsymbol{F_X}, \boldsymbol{F_Y}$	Frequency domain excitation forces in X and Y directions [F]
$\boldsymbol{H_{ij}}$	Frequency domain dynamic stiffness coefficient [F/L]
$\boldsymbol{j}$	Complex operator [-]
K_{ij}	Seal stiffness coefficients [F/L]
L	Seal axial length [L]
M_{ij}	Seal virtual mass coefficients [M]
M_s	Stator mass [M]
$\dot{Q}$	Seal volumetric leakage [L^3/T]
R	Shaft radius [L]

Re_a	Axial Reynolds number [-]
Re_c	Circumferential Reynolds number [-]
Re_t	Vector Reynolds number [-]
v_i, v_o	Inlet and outlet circumferential fluid velocity [L/T]
w	Axial fluid velocity [L/T]
X, Y	Cartesian coordinate system [-]
1X,2X,3X	New radial clearance, two times the new radial clearance and three times the new radial clearance [-]

Greek symbols

ΔP	Seal differential pressure [F/L^2]
$\Delta X, \Delta Y$	Rotor-stator relative displacement components [L]
$\Delta \dot{X}, \Delta \dot{Y}$	Rotor-stator relative velocity components [L/T]
$\Delta \ddot{X}, \Delta \ddot{Y}$	Rotor-stator relative acceleration components [L/T^2]
$\boldsymbol{\varepsilon_0}$	Static eccentricity ratio vector [-]
$\varepsilon_{0X}, \varepsilon_{0Y}$	Static eccentricity ratio components in X and Y directions [-]
μ	Fluid dynamic viscosity [FT/L^2]
ρ	Fluid density [M/L^3]
ω	Ω [1/T]
Ω	Excitation frequency [1/T]
ϕ	Attitude angle [-]
θ	Angle between eccentricity ratio vector and the Y-axis [-]

Subscripts

i, j	Interchangeable X and Y directions
X, Y	X and Y directions
r, t	Radial coordinate system [-]

Abbreviations

DE	Drive end
NDE	Non drive end
OSI	Onset speed of instability
OSR	Outlet swirl ratio
PSR	Pre-swirl ratio
SBs	Swirl brakes
SSSBs	Smooth seals with swirl brakes
WFR	Whirl frequency ratio

TABLE OF CONTENTS

Page

ABSTRACT ii

DEDICATION iv

ACKNOWLEGEMENTS v

CONTRIBUTORS AND FUNDING SOURCES vi

NOMENCLATURE vii

LIST OF FIGURES xii

LIST OF TABLES xvi

1. INTRODUCTION 1

2. TEST RIG DESCRIPTION 10

    2.1 Main Test Section 11
    2.2 Oil Supply System 18
    2.3 Instrumentation 19

3. TEST HARDWARE 21

4. STATIC TEST PROCEDURE 22

    4.1 Cold Clearance Measurements 22
    4.2 Dry Dynamic Baseline Measurements 22
    4.3 Hot Clearance Measurements 23
    4.4 Static Measurements 24

5. TEST MATRIX 26

6. STATIC RESULTS 27

    6.1 Leakage 27
    6.2 Reynolds Number 29
    6.3 Pre-Swirl and Outlet Swirl Ratio 31
    6.4 Required Applied Static Load and Attitude Angle 41

7. DYNAMIC RESULTS 45

7.1 Dynamic Measurement Approach 45
7.2 Dynamic Data Analysis and Curve Fit 45
7.3 Dynamic Stiffness Coefficients 47
7.4 Load and Position Control Systems 52
7.5 Rotordynamic Coefficients 55
7.6 Whirl Frequency Ratio 81

8. SUMMARY & CONCLUSIONS 83

8.1 Summary 83
8.2 Static Results 83
8.3 Dynamic Results Summary 85
8.4 Dynamic Results Conclusions and Recommendations 87

REFERENCES 89

APPENDIX A TABULATED RESULTS 92

APPENDIX B UNCERTAINTY ANALYSIS 128

APPENDIX C NON-DIMENSIONAL ROTORDYNAMIC COEFFICIENTS 130

LIST OF FIGURES

Page

Figure 1. Impeller-diffuser-seal arrangements at the exit of a straight-through multi-stage centrifugal pump reprinted from [1]. 1

Figure 2. Pressure distribution for a displaced rotor in a fluid film annulus reprinted from [1]. 3

Figure 3. Lomakin effect. 4

Figure 4. Effect of changing inlet swirl on WFR for a smooth seal reprinted from [1]. 7

Figure 5. Balance-piston seal swirl brake reprinted from [15]. 8

Figure 6. Axonometric view of the main test rig. 10

Figure 7. Cross-sectional view of the main test section. 11

Figure 8. Drive Side (DS) view of the shaker assembly reprinted from [17]. 13

Figure 9. 1X clearance seal with SBs. 14

Figure 10. Cross-sectional view of high pre-swirl insert. 15

Figure 11. Stator assembly schematic. 16

Figure 12. Stator and lubricant flow path. 17

Figure 13. Non-Drive end (NDE) side of test rig displaying the static loader system reprinted from [17]. 18

Figure 14. Assembled stator and instrumentation. 20

Figure 15. Detailed drawing of new clearance seal with swirl brakes. All dimensions are in mm 21

Figure 16. (a) Definition of coordinate system in the rig coordinate system. (b) Presented coordinate system. 25

Figure 17. Measured and predicted $\dot{Q}$ versus ε_0 for ω = 6 krpm at (a) ΔP = 2.07 bar, (b) ΔP = 4.14 bar, (c) ΔP = 6.21 bar and (d) ΔP = 8.27 bar. 27

Figure 18. Measured and predicted $\dot{Q}$ versus ω for centered position at a ΔP of 4.14 bar. 28

Figure 19. Measured and Predicted $\dot{Q}$ versus ω for centered position for the 1X clearance seal at ΔP = 8.27 bar. 29

Figure 20. (a) Re_a versus ω at a range of ΔP for the 3X clearance, (b) Re_c versus ω at a range of ΔP for the 3X clearance. 30

Figure 21. Re_t versus ω at ε_0 = 0.00 and at (a) ΔP = 2.07 bar, (b) ΔP = 4.14 bar, (c) ΔP = 6.21 bar and (d) ΔP = 8.27 bar. 31

Figure 22. (a) Axial positions of the pitot tubes. (b) Radial location of the inlet pitot tube. All dimensions in mm reprinted from [20]. 32

Figure 23. Radial position of the inlet pre-swirl pitot tube. Note that the Figure is not drawn to scale. 33

Figure 24. Radial position of outlet swirl pitot tube. Note that the Figure is not drawn to scale. 33

Figure 25. v_i versus ω at ε_0 = 0.00 and (a) ΔP = 2.07 bar, (b) ΔP = 4.14 bar, (c) ΔP = 6.21 bar and (d) ΔP = 8.27 bar. 35

Figure 26. PSR versus ω at ΔP = 8.27 bar. 36

Figure 27. PSR versus ΔP at ε_0 = 0.00 and $\omega = 4$ krpm. 37

Figure 28. v_o versus ω at ε_0 = 0.00 and (a) ΔP = 2.07 bar, (b) ΔP = 4.14 bar, (c) ΔP = 6.21 bar and (d) ΔP = 8.27 bar. 38

Figure 29. OSR versus ω at ΔP = 8.27 bar. 39

Figure 30. OSR versus ΔP at ε_0 = 0.00 and $\omega = 4$ krpm . 40

Figure 31. Measured ϕ versus ε_0 at ω = 8krpm and (a) ΔP = 2.07 bar, (b) ΔP = 4.14 bar, (c) ΔP = 6.21 bar and (d) ΔP = 8.27 bar. 42

Figure 32. Measured and predicted F_s versus ε_0 at ω = 8krpm and (a) ΔP = 2.07 bar, (b) ΔP = 4.14 bar, (c) ΔP = 6.21 bar and (d) ΔP = 8.27 bar. 44

Figure 33. (a) Imaginary component of direct dynamic stiffness, (b) Imaginary component of cross-coupled stiffness, (c) Real component of direct dynamic stiffness, (d) Real component of cross-coupled stiffness

versus Ω at ε_0= 0.00, ΔP = 4.14 bar, ω = 4krpm for the 1X clearance seal. 49

Figure 34. (a) Imaginary component of direct dynamic stiffness, (b) Imaginary component of cross-coupled stiffness, (c) Real component of direct dynamic stiffness, (d) Real component of cross-coupled stiffness versus Ω at ε_0= 0.00, ΔP = 8.27 bar, ω = 8krpm for the 3X clearance seal. 51

Figure 35. (a) Ideal load control, (b) Ideal position control. 53

Figure 36. Coordinate transformation from cartesian coordinate system to r and t coordinate system. 54

Figure 37. Measured K_{tt} and K_{rr} versus ε_0 at ΔP = 2.07 bar and ω = 4krpm. 56

Figure 38. ΔP = 2.07 bar and ω = 4krpm (a) Measured and predicted K_{rr} versus ε_0. (b) Measured and predicted K_{tt} versus ε_0. 57

Figure 39. Measured K_{tt} and K_{rr} versus ΔP at ε_0 = 0.80 and ω = 4 krpm. 58

Figure 40. ε_0 = 0.80 and ω = 4 krpm (a) Measured and predicted K_{rr} versus ΔP. (b) Measured and predicted K_{tt}versus ΔP. 59

Figure 41. Measured K_{tt} and K_{rr} versus ω at ε_0 = 0.00 and ΔP = 4.14 bar. 60

Figure 42. ε_0 = 0.00 and ΔP = 4.14 bar (a) Measured and predicted K_{rr} versus ω. (b) Measured and predicted K_{tt} versus versus ω..... 61

Figure 43. ΔP = 2.07 bar and ω = 4krpm (a) Measured K_{tr} and K_{rt} versus ε_0. (b) Predicted K_{tr} and K_{rt} versus ε_0. 62

Figure 44. ε_0 = 0.27 and ω = 6 krpm (a) Measured K_{tr} and K_{rt} versus ΔP. (b) Predicted K_{tr} and K_{rt} versus ΔP. 63

Figure 45. ε_0 = 0.27 and ΔP = 4.14 bar (a) Measured K_{tr} and K_{rt} versus ω. (b) Predicted K_{tr} and K_{rt} versus ω..... 65

Figure 46. Measured C_{tt} and C_{rr} versus ε_0 at ΔP = 2.07 bar and ω = 2 krpm..... 66

Figure 47. ΔP = 2.07 bar and ω = 2 krpm (a) Measured and Predicted C_{rr} versus ε_0. (b) Measured and Predicted C_{tt} versus ε_0..... 67

Figure 48. Measured and Predicted C_{rr} versus ΔP at ε_0 = 0.00 and ω = 6 krpm. 68

Figure 49. Measured and Predicted C_{rr} versus versus ω at ε_0 = 0.00 and ΔP = 8.28 bar. 69

Figure 50. ΔP = 6.21 bar and ω = 4 krpm (a) Measured and predicted C_{tr} versus ε_0. (b) Measured and predicted C_{rt} versus ε_0. 71

Figure 51. $Im(H_{XY})$ and $Im(H_{YX})$ versus Ω at ε_0= 0.8, ΔP = 6.21 bar and ω = 4 krpm for the 1X clearance seal 71

Figure 52. ε_0 = 0.80 and ω = 4 krpm (a) C_{tr} versus ΔP. (b) C_{rt} versus ΔP..... 73

Figure 53. ε_0 = 0.00 and ΔP = 6.21 bar (a) Measured and predicted C_{tr} versus ω. (b) Measured and predicted C_{rt} versus versus ω. 74

Figure 54. Measured M_{tt} and M_{rr} versus ε_0 at ΔP = 2.07 bar and ω = 4 krpm. 75

Figure 55. $Re(H_{XX})$ and $Re(H_{YY})$ versus Ω at ε_0 =0.8, ΔP = 2.07 bar, ω = 4 krpm for the 1X clearance seal. 76

Figure 56. ΔP = 2.07 bar and ω = 4 krpm (a) Measured and predicted M_{rr} versus ε_0. (b) Measured and predicted M_{tt} versus ε_0..... 77

Figure 57. Measured M_{rr} and M_{tt} versus ΔP at ε_0 = 0.00 and ω = 2 krpm. 78

Figure 58. Measured and predicted M_{tt} versus ΔP at ε_0 = 0.00 and ω = 2 krpm. 79

Figure 59. Measured M_{tr} and M_{rt} versus ε_0 at ΔP = 6.21 bar and ω = 6 krpm. 80

Figure 60. Measured and Predicted WFR versus ε_0 at ΔP = 4.14 bar and ω = 6 krpm. 82

LIST OF TABLES

Page

Table 1. Hot clearance measurements of each assembly. 23

Table 2. Test matrix 26

Table 3. Stability impact of M_{tr}, M_{rt} at ΔP = 6.21 bar and ω = 6krpm..... 81

1. INTRODUCTION

Pumps and compressors use annular seals to reduce leakage between multiple stages of differing pressures. Annular seals are non-contacting; there is a clearance between the rotor and the seal stator. Figure 1, shows the types of annular seals and their locations typical to a centrifugal pump.

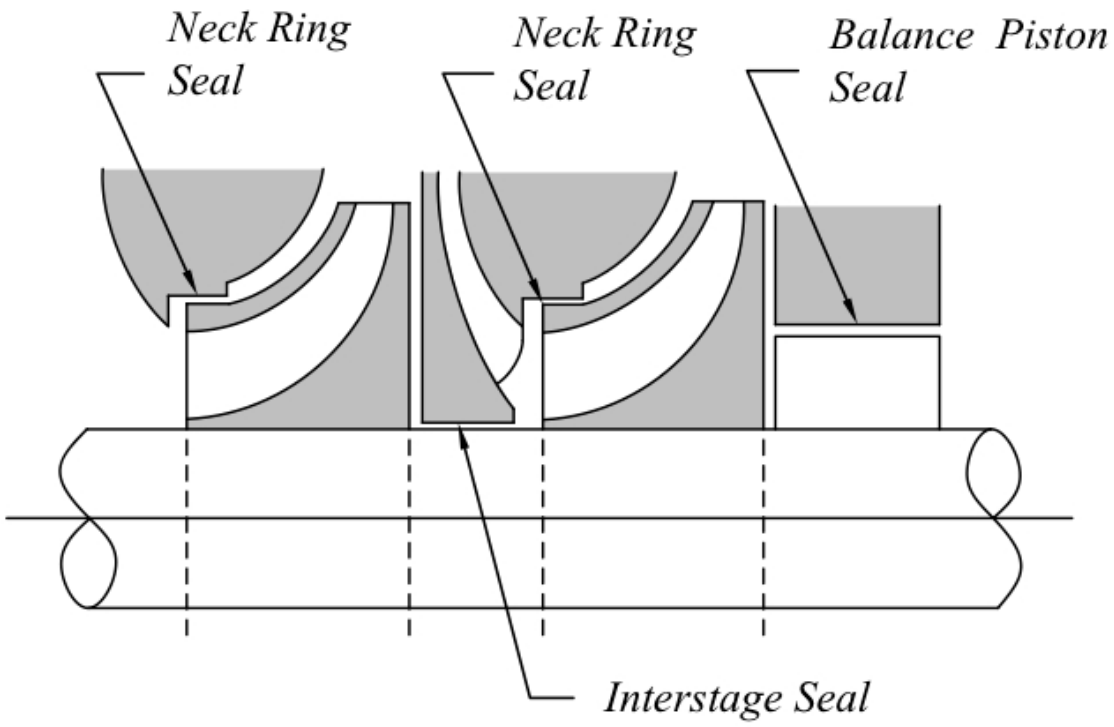

Figure 1. Impeller-diffuser-seal arrangements at the exit of a straight-through multi-stage centrifugal pump reprinted from [1].

Seal annular clearances tend to have a major impact on the rotordynamic characteristics of pumps. Low clearance to radius ratios ($C_r/R \sim 0.001$) [2] that are usual

for journal bearings encourage shear-driven circumferential flow. Since annular seals have higher clearance to radius ratios ($C_r/R \sim 0.003 - 0.005$), for low viscosity fluids, shear forces were thought to be of reduced importance. It was also thought that the seals provided so much damping that rotordynamic analysis was not needed [2]. However, Henry Black [3, 4] showed that fluid inertia effects and higher Reynolds numbers cause the annular seals to have a significant impact on the rotordynamic characteristics of pumps.

Shaft centering forces are developed in annular seals by mainly two means, (1) the hydrodynamic effect (fluid rotation), and, (2) the Lomakin effect [5]. Starting from the hydrodynamic effect, Fig. 2 shows a rotor displaced eccentrically in an annular seal. The eccentric position of the shaft in the annulus produces a converging region where pressure is higher and a diverging region where pressure is lower. The difference in circumferential pressure distribution thus produces a shaft reaction force arising from the hydrodynamic effect. The hydrodynamic effect is pronounced in hydrodynamic bearings where shear flow due to shaft rotation is dominant due to lower C_r/R. The hydrodynamic effect is discussed in detail by Pinkus and Sternlicht [6].

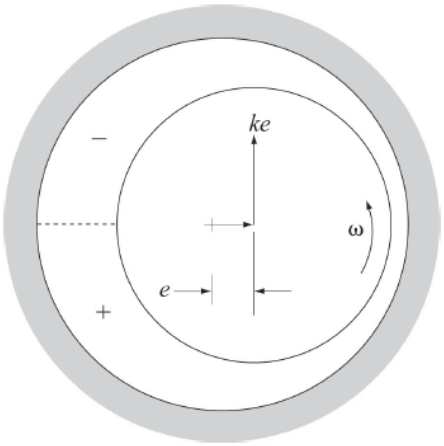

Figure 2. Pressure distribution for a displaced rotor in a fluid film annulus reprinted from [1].

Figure 3 helps in explaining the Lomakin effect [5]. Initially, the rotor is centered in the seal. The high $\Delta P = P_{supplied} - P_{exit}$ causes the inlet fluid to accelerate. This leads to pressure drop at the seal entrance followed by a pressure drop through the seal due to wall friction. As the rotor is displaced from the center of the seal, clearance at the top decreases, leading to lower axial velocity, lower Reynolds number, and higher friction factor. Whereas, the clearance at the bottom increases, which leads to higher axial velocity, higher Reynolds number, and lower friction factor. A combination of these factors results in an axial pressure distribution (shown as gray areas in Figure 3) that leads to a resultant centering force, *F*.

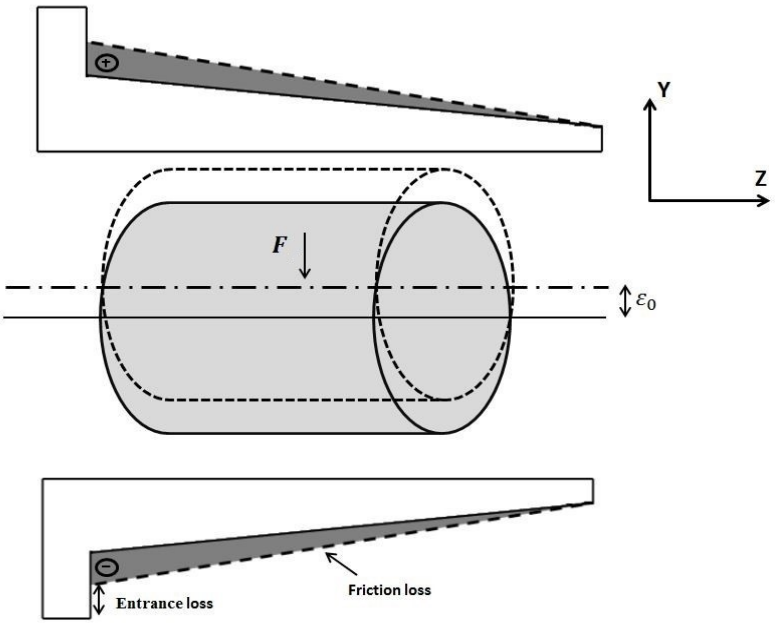

Figure 3. Lomakin effect.

Note that the conditions where the Lomakin effect is appreciable in seals varies. It greatly depends on the type of fluid flow. The flow inside the seal can be stated in terms of a average circumferential component and an average axial component characterized by the circumferential Reynolds number (Re_c) and axial Reynolds number (Re_a), respectively. Total Reynolds number, Re_t refers to the resultant of Re_c and Re_a. For an annular seal the hydraulic diameter is $2C_r$. Hence, the definitions are as follows

$$Re_c = \frac{\rho R \omega C_r}{\mu} \tag{1}$$

$$Re_a = \frac{\rho 2(C_r) w}{\mu} \tag{2}$$

$$Re_t = \sqrt{Re_a^2 + Re_c^2}, \tag{3}$$

where μ is lubricant viscosity and $w = \dot{Q}/2\pi RC_r$ is the average axial velocity. At tighter clearances and laminar flow conditions ($Re_t < 1800$), seals generally act more like bearings as fluid rotation effects are more important.

For Electric Submersible Pumps (ESPs), as the clearances increase, viscous forces due to fluid rotation decrease, and the Lomakin effect becomes more pronounced even when the fluid flow is laminar [7].

The following KCM rotordynamic-coefficient model is used to represent the reaction forces developed by the fluid film of a centered seal.

$$-\begin{Bmatrix} f_{sX} \\ f_{sY} \end{Bmatrix} = \begin{bmatrix} K & k \\ -k & K \end{bmatrix} \begin{Bmatrix} \Delta X \\ \Delta Y \end{Bmatrix} + \begin{bmatrix} C & c \\ -c & C \end{bmatrix} \begin{Bmatrix} \Delta \dot{X} \\ \Delta \dot{Y} \end{Bmatrix} + \begin{bmatrix} M & m \\ -m & M \end{bmatrix} \begin{Bmatrix} \Delta \ddot{X} \\ \Delta \ddot{Y} \end{Bmatrix} \tag{4}$$

f_{sX} and f_{sY} represent the seal reaction forces in the orthogonal directions, *K* and *C* are the direct stiffness and damping coefficients, respectively; *k* and *c* are the cross-coupled stiffness and damping coefficients, respectively. The model also accounts for virtual mass terms as direct virtual mass terms *M* and cross-coupled mass terms *m.* Relative rotor-stator displacement components are ΔX and ΔY. Childs [2] and Black [3] developed models that are similar to Eq. (4) but without the *m* virtual mass terms.

Improving on the work of Childs [2], Nelson and Nguyen [8], [9] developed a method to calculate rotordynamic coefficients of seals where the rotor was operating at eccentric positions within the seal. The fluid-film reaction force components are

$$-\begin{Bmatrix} f_{sX} \\ f_{sY} \end{Bmatrix} = \begin{bmatrix} K_{XX}(e_0) & K_{XY}(e_0) \\ K_{YX}(e_0) & K_{YY}(e_0) \end{bmatrix} \begin{Bmatrix} \Delta X \\ \Delta Y \end{Bmatrix} + \begin{bmatrix} C_{XX}(e_0) & C_{XY}(e_0) \\ C_{YX}(e_0) & C_{YY}(e_0) \end{bmatrix} \begin{Bmatrix} \Delta \dot{X} \\ \Delta \dot{Y} \end{Bmatrix}$$

$$+\begin{bmatrix} M_{XX}(e_0) & M_{XY}(e_0) \\ M_{YX}(e_0) & M_{YY}(e_0) \end{bmatrix} \begin{Bmatrix} \Delta\ddot{X} \\ \Delta\ddot{Y} \end{Bmatrix} \tag{5}$$

where e_0 represents the static offset/eccentricity.

An important measure of the annular seal's effectiveness in stabilizing a turbomachine is its whirl-frequency ratio (WFR). For a flexible rotor rotating on hydrodynamic bearings, it is defined as the ratio of the rotor's first flexural, natural frequency ω_{n1} to its onset speed of instability (OSI), or

$$WFR = \frac{\omega_{n1}}{OSI} \rightarrow OSI = \frac{\omega_{n1}}{WFR} \tag{6}$$

Lund [10] was the first to come up with an equation for the WFR of a journal bearing in terms of rotordynamic coefficients. The equation is shown as

$$(WFR)^2 = \frac{(K_{eq} - K_{XX})(K_{eq} - K_{YY}) - K_{XY}K_{YX}}{\omega^2(C_{XX}C_{YY} - C_{XY}C_{YX})}, \tag{7}$$

where ω is the running speed and K_{eq} is

$$K_{eq} = \frac{K_{XX}C_{YY} + K_{YY}C_{XX} - K_{XY}C_{YX} - K_{YX}C_{XY}}{C_{XX} + C_{YY}} \tag{8}$$

San Andrés [11] provided a model that included the direct and cross-coupled virtual mass terms of Eq. (5) and showed that Eqs. (7-8) remain valid provided that M_{XY} and M_{YX} are negligible.

Annular seals that operate with high viscosity fluids such as the fluid in this study tend to have a WFR of 0.5. This means that the rotor bearing system can run up to twice

its first natural speed before the seal becomes destabilizing. For stability, WFR should be as close to zero as possible.

Instability in a rotor-bearing system is primarily caused by fluid rotation in the bearing/seal annulus [1]. Black et al. [12] were the first to analyze the effect of inlet pre-swirl of the fluid flow on the seals' rotordynamic characteristics. Figure 4 from Childs [1] shows the predicted WFR versus length to diameter ratio, L/D, of a seal ($C_r/R = 0.005$) with changing inlet pre-swirl. WFR decreases as inlet/pre-swirl is decreased. k is also a function of the inlet pre-swirl, and it decreases as inlet swirl goes down [1]. A lower WFR and k thus would reduce the seal's ability to destabilize a pump.

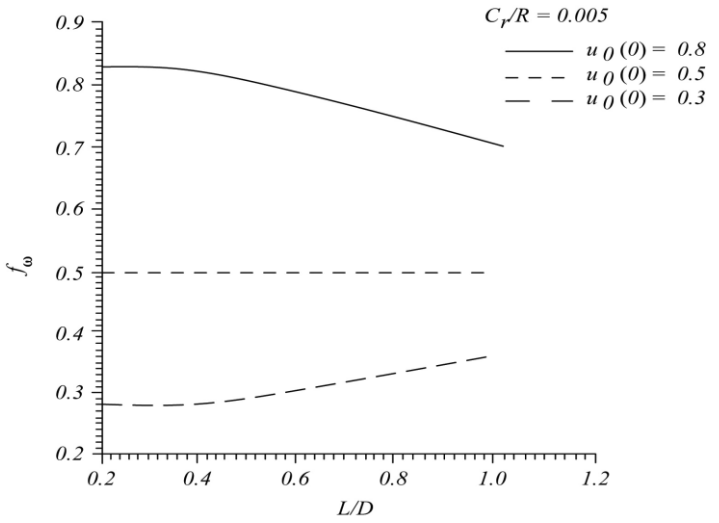

Figure 4. Effect of changing inlet swirl on WFR for a smooth seal reprinted from [1].

Decreasing fluid rotation at the inlet of a seal brings us to the idea of using swirl brakes (SBs). SBs use a series of circumferential slots at the seal inlet to lower the inlet pre-swirl of the fluid entering a seal. Figure 5 shows an SB design used by Massey [13] to

stabilize a pump. Benchert and Wachter [14] were the first to use SBs for gas labyrinth seals, referring to them as “swirl webs” to effectively reduce WFR and k.

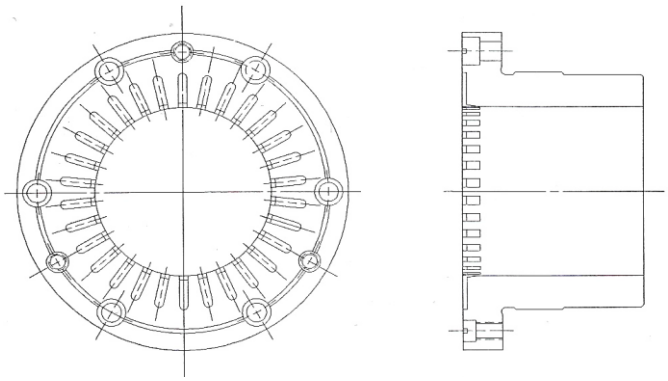

Figure 5. Balance-piston seal swirl brake reprinted from [15].

Massey’s [13] pump operated with a light hydrocarbon with low viscosity at elevated temperatures. It was unstable, and an SB at the balance-piston seal was required to stabilize it. SBs have been shown to be effective in machines handling low viscosity fluids such as Massey’s pump. On the other hand, the effectiveness of installing SBs on seals operating with higher viscosity fluids is still uncertain.

Childs et al. [15] measured the rotordynamic coefficients and leakage characteristics of a short ($L/D = 0.21$) smooth annular seal as formerly used for buffer seals in injection compressors in laminar flow conditions. The clearance to radius ratios of these seals are comparable to journal bearings, and the results are not directly applicable to this study.

With a viscous fluid at low seal clearances, shear forces due to shaft rotation are large and dominate the inlet pre-swirl condition, and the bulk-flow circumferential velocity

is $R\omega/2$. SBs are predicted to be ineffective in these conditions. As clearance and leakage increase due to wear in a pump, the hydrodynamic effect becomes less effective, and the Lomakin effect becomes more important. Using predictions from the model of [16] for seal rotordynamic coefficients, Childs and Norrbin [7] predicted that SBs would be effective in lowering the WFR of seals in these enlarged-clearance circumstances. This study aims to experimentally investigate the predictions of seal rotordynamic coefficients of smooth seals with SBs, operating with a higher viscosity fluid at enlarged clearances.

2. TEST RIG DESCRIPTION

The test rig shown in Fig. 6 was used to conduct static and dynamic measurements of the smooth seals with swirl brakes (SSSBs). It was initially designed by Kaul [17] to test annular oil bushing seals for compressors. Since Kaul, the test rig has gone through several modifications to be discussed henceforth. As discussed below, the test rig can be classified into three main sections consisting of a main test section, oil supply system and instrumentation.

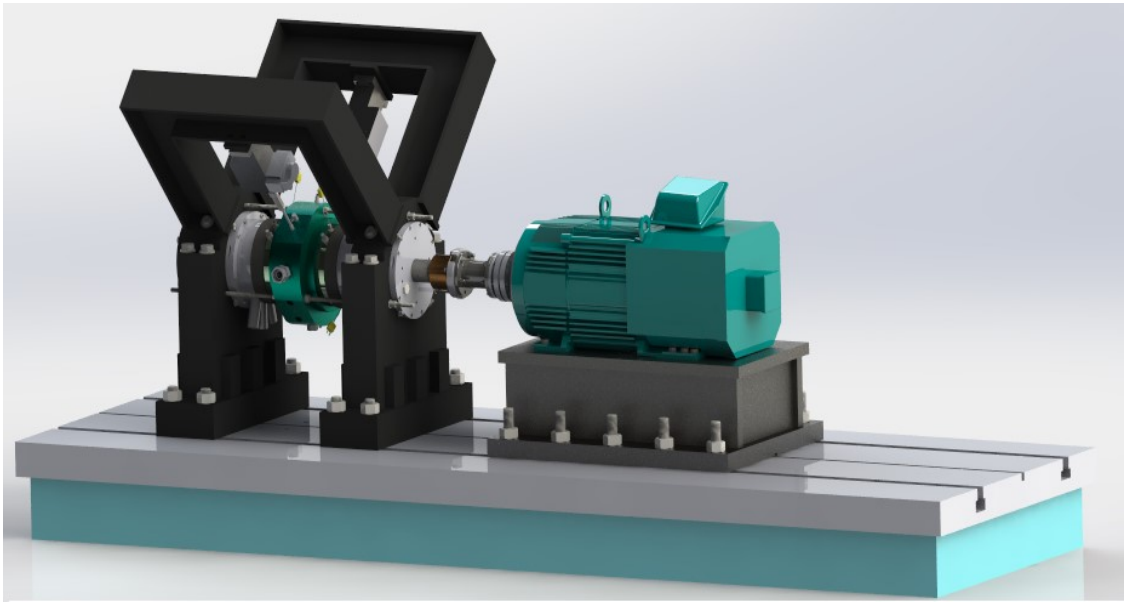

Figure 6. Axonometric view of the main test rig.

2.1 Main Test Section

"Ground" for the main test section is formed by mild steel plates that support the electric motor, the motor mount and the two pedestals. Figure 7 shows the cross section view of the main test section.

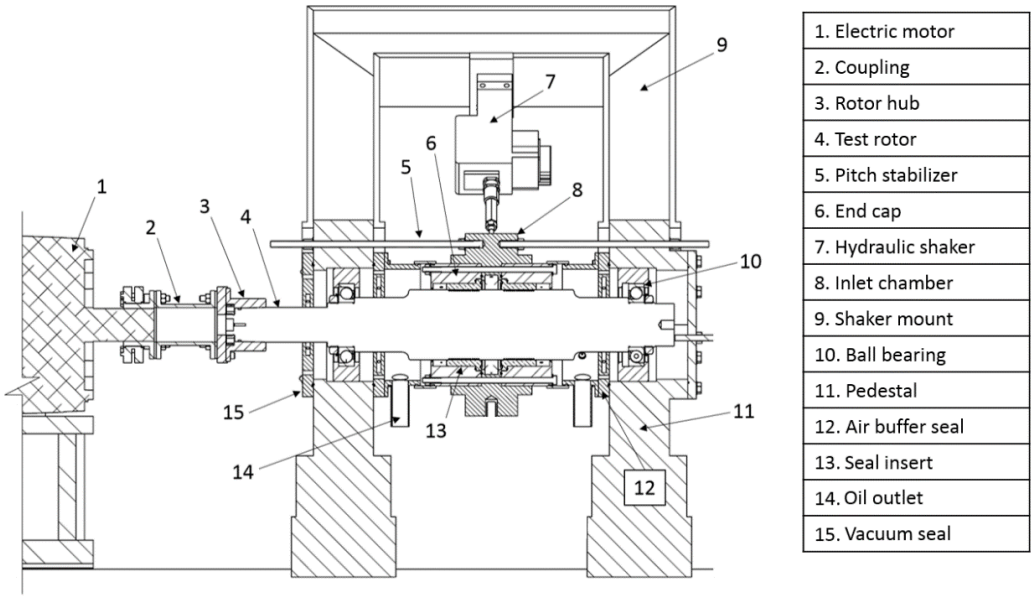

Figure 7. Cross-sectional view of the main test section.

The pedestal assemblies are made of AISI 1040 steel and are spaced 38 mm (15 in) apart. The assemblies have an upper half and a lower half. The lower half supports angular contact ball bearings that in turn support the smooth rotor with a span of 640.1 mm (25.2 in) and maximum diameter of 101.6 mm (4 in). The rotor is connected to the variable frequency drive 29.8 kW (40 hp) electric motor by the coupling. The rotor maximum speed is 8 krpm. As shown in Fig. 7 and described in detail in [17], other peripherals that form the main test section include pitch stabilizers, collection chambers,

end cap, air buffer seals and vacuum seal. Pitch stabilizers are 6 long threaded bolts that are screwed between the pedestals and the stator to keep the stator parallel to the rotor [17]. The collection chambers collect the oil as it leaves the stator during testing. End caps seal the non-drive end (NDE) of the main test section stopping oil flow. The air buffer seals form an air flow that prevents oil from entering the ball bearings, and the vacuum seal functions similarly to prevent oil flow from the drive end (DE) of the test section.

The upper half of the pedestal assembly contains the two hydraulic shaker assemblies. Shaker heads are connected to the stator via stingers as shown in Fig. 8. The stinger helps isolate the stator from dynamic interference of hydraulic shaker itself. The hydraulic shaker assembly includes a load cell mounted on each of the orthogonal X and Y axes to measure the force applied in each direction. Two 3000 psi pumps that are controlled by a dual-loop master controller power the orthogonal shakers. As mentioned earlier, the shaker assembly tends to "float" the stator such that the SSSBs are never in contact with the rotor surface. The shakers can excite the stator up to 1kHz and provide a maximum tension and compression of 4450 N.

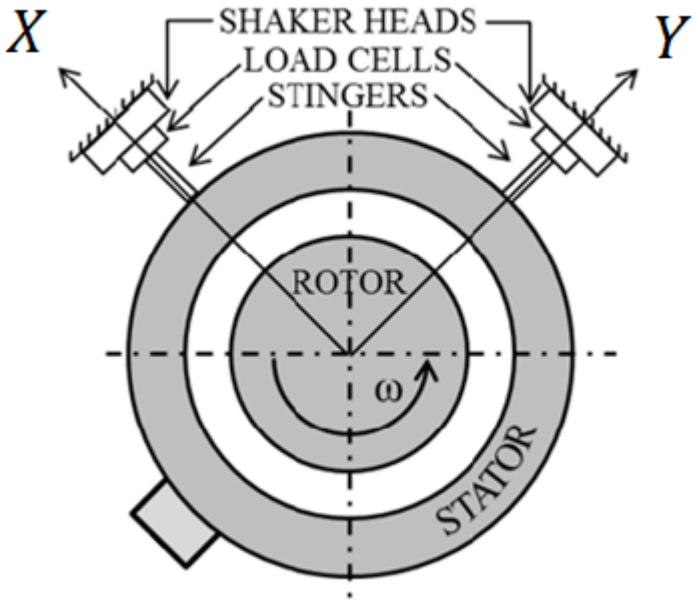

Figure 8. Drive Side (DS) view of the shaker assembly reprinted from [17].

Figure 9 is a photo of the 1X clearance seal used for testing. The SB design is inspired from Massey's SB design [13] as shown previously in Fig. 5. The SB consists of 36 cuts. Its rugged construction would resist wear and tear due to particulates in the flow. A better design for inlet circumferential flow control could probably be developed using CFD. With the data provided in this study, the design could be further improved using CFD analysis.

Figure 9. 1X clearance seal with SBs.

Figure 10 shows the insert used to induce the pre-swirl. The insert has 12 nozzles. Each nozzle has a diameter of 4.039 mm (0.1590 in). It was designed to produce inlet pre-swirl ratio (defined in Eq. (13)) ranging from 0-0.8 depending on rotor speed and ΔP. Note that the injection angle is such that the fluid stream leaving the pre-swirl insert nozzles is tangential to the rotor surface as shown in Fig. 10.

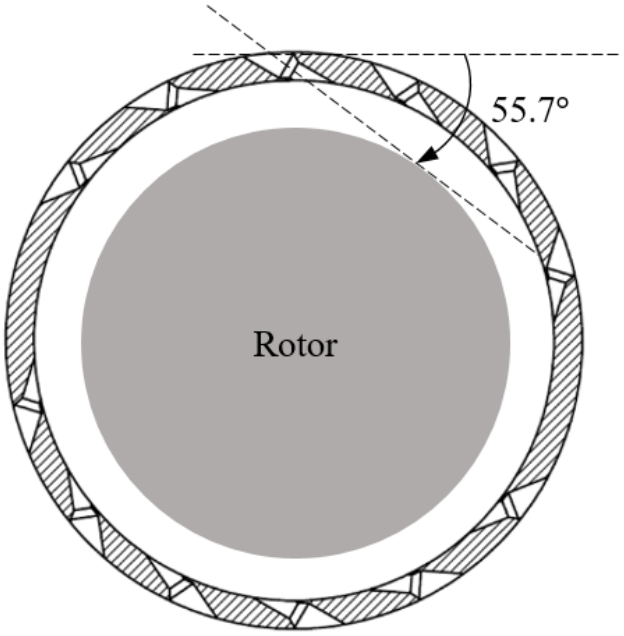

Figure 10. Cross-sectional view of high pre-swirl insert.

As shown in Fig. 11, the stator assembly consists of the following three main parts: inlet chamber, seal holders, SSSBs. The pre-swirl insert described above is part of the inlet chamber. Both SSSBs are made of 660 bronze. They are press fitted into a set of seal holders that are in turn assembled into the inlet chamber. ISO VG 46 oil enters through the Oil Inlet and passes through the pre-swirl insert designed to swirl oil flow before the fluid enters the SSSBs

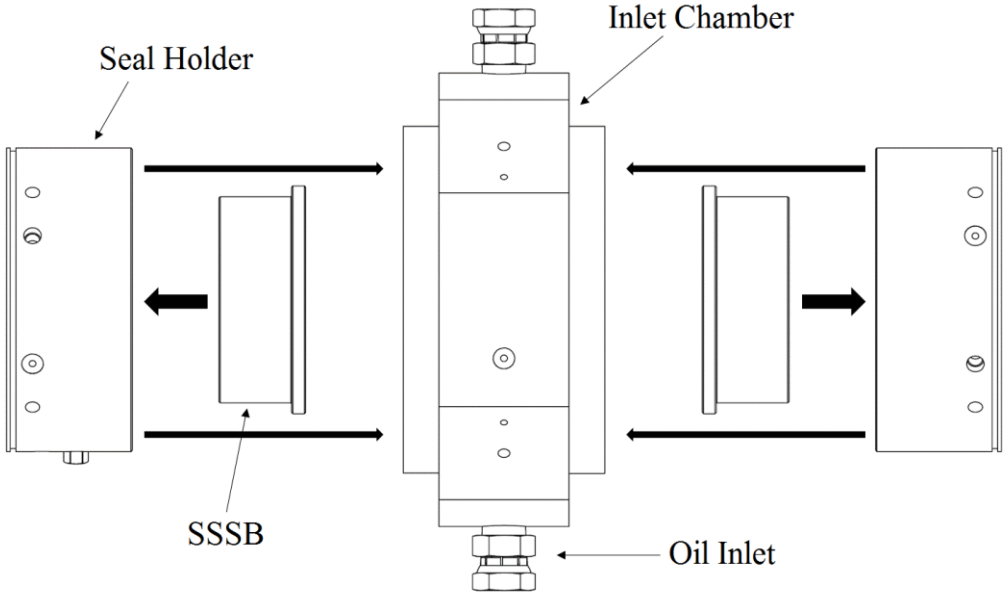

Figure 11. Stator assembly schematic.

Figure 12 shows the test-fluid flow path. After passing through the pre-swirl insert, the swirling fluid is then met by the SBs that reduce the fluid's circumferential flow. Oil then enters the seals and eventually leaves the stator into the collection chambers. Note that a labyrinth tooth at the end of the seal holder is present to avoid cavitation at the seal's exit.

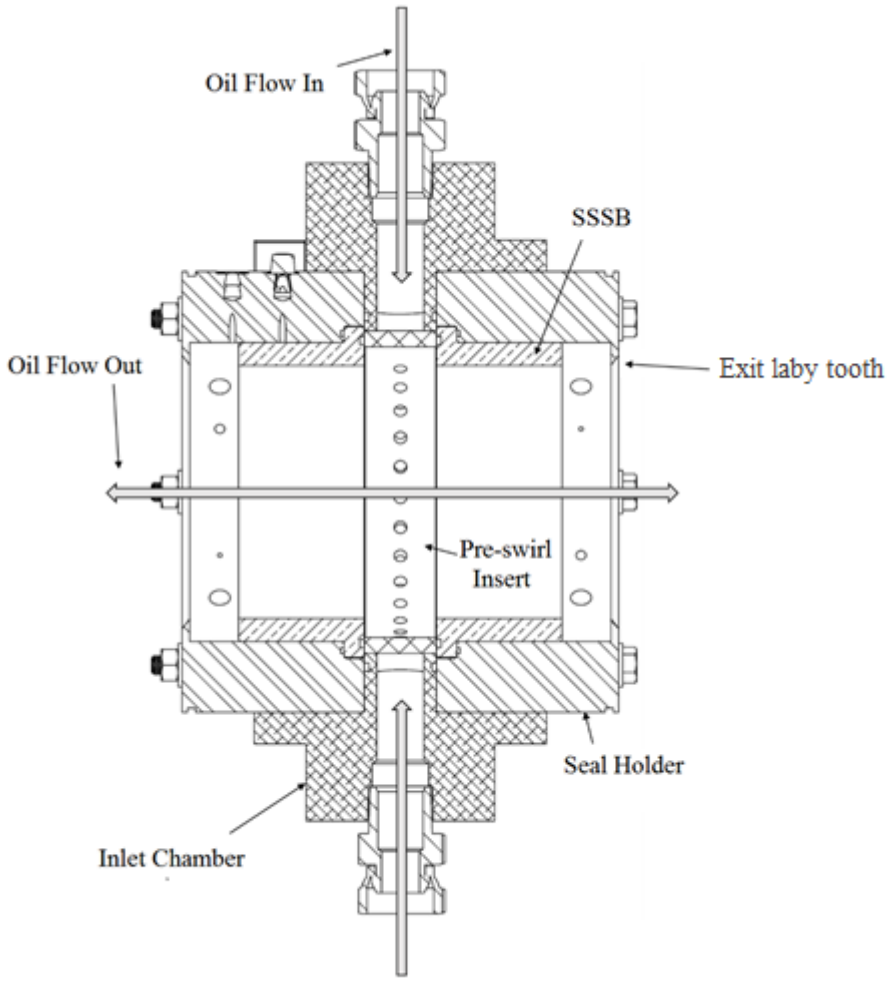

Figure 12. Stator and lubricant flow path.

The Static loader, shown in Fig. 13 completes the main test section. The yoke connects the static loader to the stator. The static loader provides static loads up to 22.2 KN. A static loader is used when a required static load exceeds the loading capacity of the hydraulic shakers.

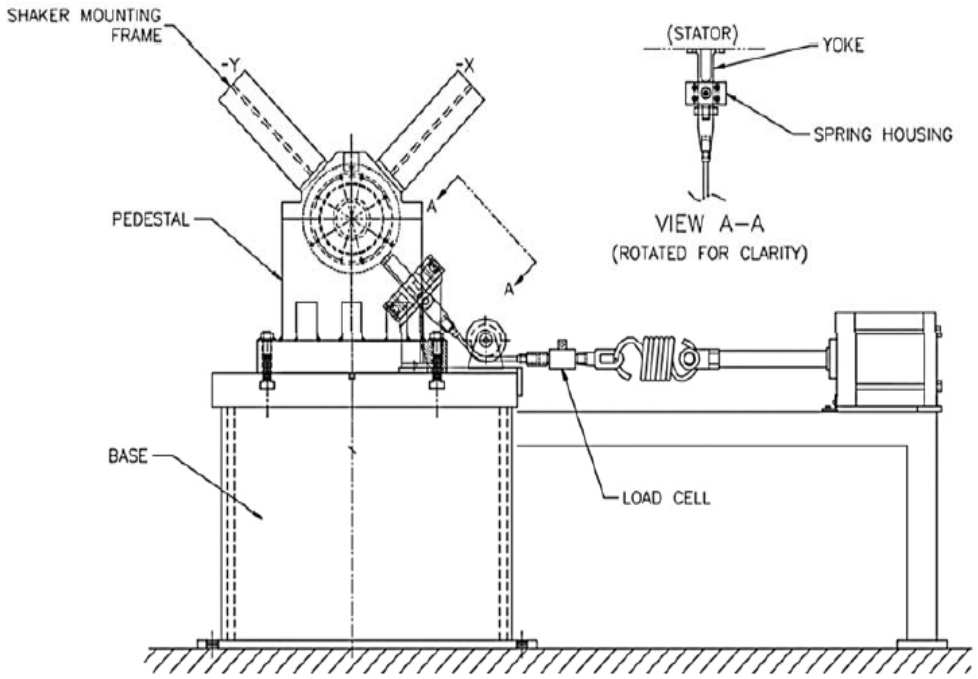

Figure 13. Non-Drive end (NDE) side of test rig displaying the static loader system reprinted from [17].

2.2 Oil Supply System

The oil supply system consists of: (1) 950 liter (250 gallon) main tank, (2) a 380 liter (100 gallon) sump tank, (3) two Viking spur gear pumps, (4) electro-pneumatic control valves, (5) heat exchanger and fan, (6) 15.8 kW circulation heater, and (7) a piping network to and from the main test section. The circulation heater heats the oil from the main-tank to a steady state temperature of 46.1°C (115°F), reaching a predicted oil viscosity of 23.4 cP. The main-tank Viking pump pushes the fluid through the piping network towards the main test section. After passing through the test seals, the oil leaves the main test section

through the collection chambers and back to the sump tank where it is cooled by a heat exchanger and a fan. Oil temperature rises as it flows through the test rig mainly due to pressure drop across the seals. Oil is then either returned to the main tank or directly fed into the main Viking pump to be pumped back to the main test section.

2.3 Instrumentation

The investigator uses the instrumentation shown in Fig. 14 to measure the dynamic and static characteristics of the test rig. Zonic Corporation load cells (4) measure the applied static and dynamic force to the stator, PCB accelerometers (6) measure the acceleration in the orthogonal axis, four Lion precision eddy current proximity probes (8), two each in the X and Y directions, measure the relative displacement between the SSSBs and the rotor, Kulite XTM-190 pressure transducers (7) and Type J Omega thermocouples (2) measure the inlet and outlet fluid pressures and lubricant temperatures of SSSBs respectively. $\dot{Q}$, the volumetric flow rate across the test rig, is measured by a Flow Technology turbine flow-meter, located upstream of the main test section. The rotor's running speed ω is determined by a once-per-revolution output from the PHILTEC fiber-optic displacement sensor. Kleutinberg [18] describes the instrumentation in detail.

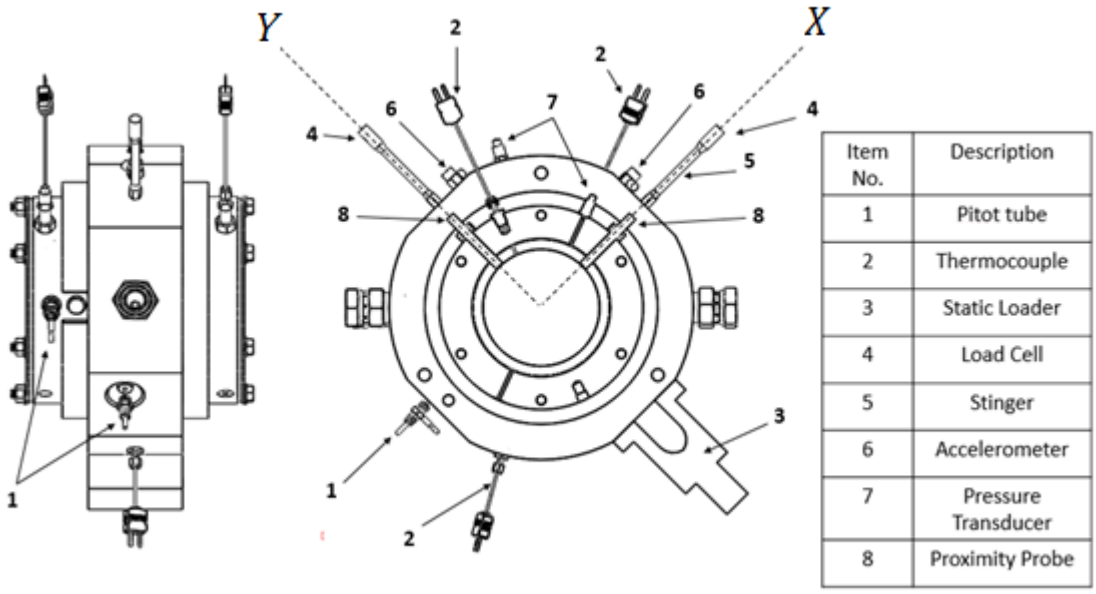

Item No.	Description
1	Pitot tube
2	Thermocouple
3	Static Loader
4	Load Cell
5	Stinger
6	Accelerometer
7	Pressure Transducer
8	Proximity Probe

Figure 14. Assembled stator and instrumentation.

Two United Sensor custom made pitot tubes (1) measure the inlet and DE outlet swirl velocity at specified location. The outer diameter of the pitot tube is 1.65 mm while the inner diameter is 0.71 mm. The investigator uses precision blocks to align the pitot tubes tangentially to the rotor.

3. TEST HARDWARE

The test seals are smooth with axial length L= 45.720 mm (1.800 in) and clearances $C_r = 127\mu m, 254\mu m, 381\mu m$ (1X, 2X and 3X respectively) and use SBs as shown in Fig. 9. The corresponding radial clearance to radius ratios (C_r/R) were 0.0025, 0.005, 0.0075. The length to diameter ratio (L/D) was 0.45. Figure 15 presents a detailed drawing of the seal with SBs. Each SB has a total of 36 square cuts with axial length D_{sb} = 5.08 mm (0.2 in), radial height H_{sb} = 6.35 mm (0.25 in) and circumferential width W_{sb} = 6.35 mm (0.25 in).

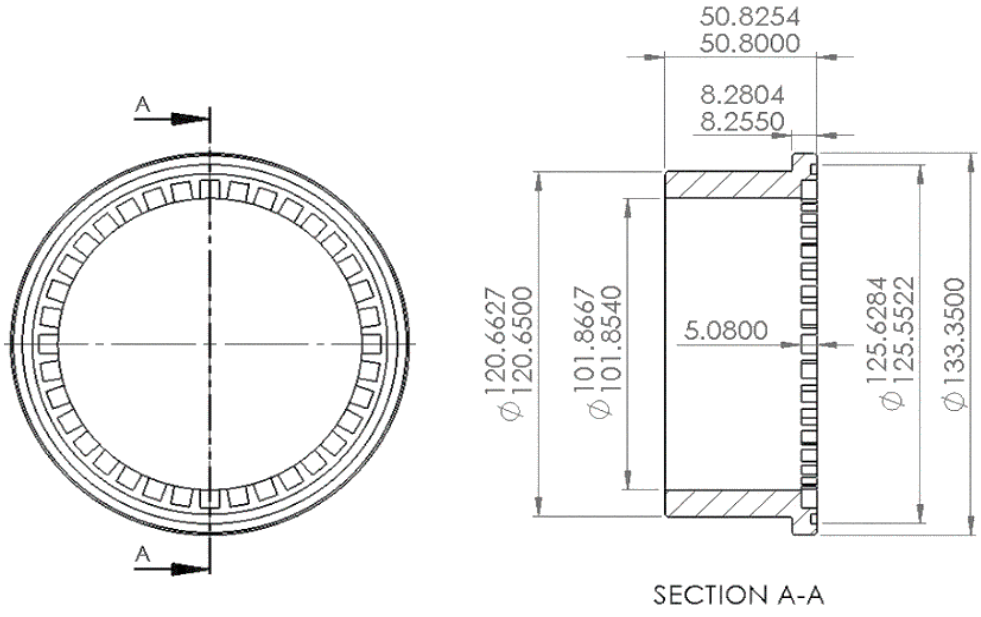

Figure 15. Detailed drawing of new clearance seal with swirl brakes. All dimensions are in mm

4. STATIC TEST PROCEDURE

4.1 Cold Clearance Measurements

The operator measures the "Cold" clearance of the seal without any oil in the system and at zero ω. Cold refers to the measurement that is taken at room temperature. As shown in Fig. 14, Four-eddy current sensors, located orthogonally in two different axial planes, measure the gaps between the seal and journal (radial clearance). Measurement in two different planes are used to minimize the pitch between the seal and the rotor. To measure the clearance circle, the seal housing is forced to touch the rotor with an applied force from the Zonic hydraulic shakers. The housing is then rotated 360° around the rotor by adjusting the force from X and Y shaker units while maintaining a contact force. Continuous acquisition of the clearance data throughout this process captures the clearance circle of the test seal. The cold clearance circle also provides the geometric center of the seal, which aids the next step in the process.

4.2 Dry Dynamic Baseline Measurements

The next step involves separately measuring the "dry" baseline characteristics of the test-rig including seal housing and additional supporting structures of the test-rig. The measurements utilize the "floating stator" method developed by Gilienicke [19]. Actual dynamic measurements include both the annular fluid reaction forces and the reactions from the test rig itself. To isolate the dynamic stiffness of the seals and the test rig, the operator applies dynamic excitations to the stator with no oil running through the test rig.

These dry baseline results are then subtracted from the measured dynamic stiffness while testing with lubricant resulting solely in the fluid-film dynamic stiffness.

4.3 Hot Clearance Measurements

After the baseline test, the operator supplies oil to the test-rig oil until the lubricant temperature reaches a steady test condition of 115±5°F (46.1°C). At this point, oil flow is stopped, and the clearance circle is immediately measured. This clearance circle is the "hot" clearance circle. It is smaller than the cold clearance circle measured earlier due to thermal expansion. The hot clearance is used for predicting the static and dynamic characteristics of the seal. Table 1 shows the measured hot clearances at the test condition of 46.1℃. They are used to calculate the rotor offset and the eccentricity ratios.

Table 1. Hot clearance measurements of each assembly.

Assembly Configuration	Assembly 1 New Clearance (1X)	Assembly 2 2X	Assembly 3 3X
C_r [μm]	111	239	350

4.4 Static Measurements

At each steady-state condition, sensors are used to measure the following parameters:

- ω
- ΔP (Subtracting supplied and exit pressures)
- Eccentricity, e_0 (relative rotor position in the X and Y coordinate system)
- Inlet and Outlet temperatures
- Leakage, $\dot{Q}$
- Applied Static load, F_s

Note that the measured values of $\dot{Q}$ and F_s are for both of the back-to-back test seals. They need to halved to get values for each seal.

Figure 16 shows the coordinate system used for determining the rotor's center within the seal. Figure 16a shows the test rig coordinate system. Position of the rotor is described in a stator-fixed reference frame.

For the results presented here, the coordinate system is modified to represent a traditional view with F_s acting in the $-Y$ direction and ω in the counter-clockwise direction as shown in 16b.

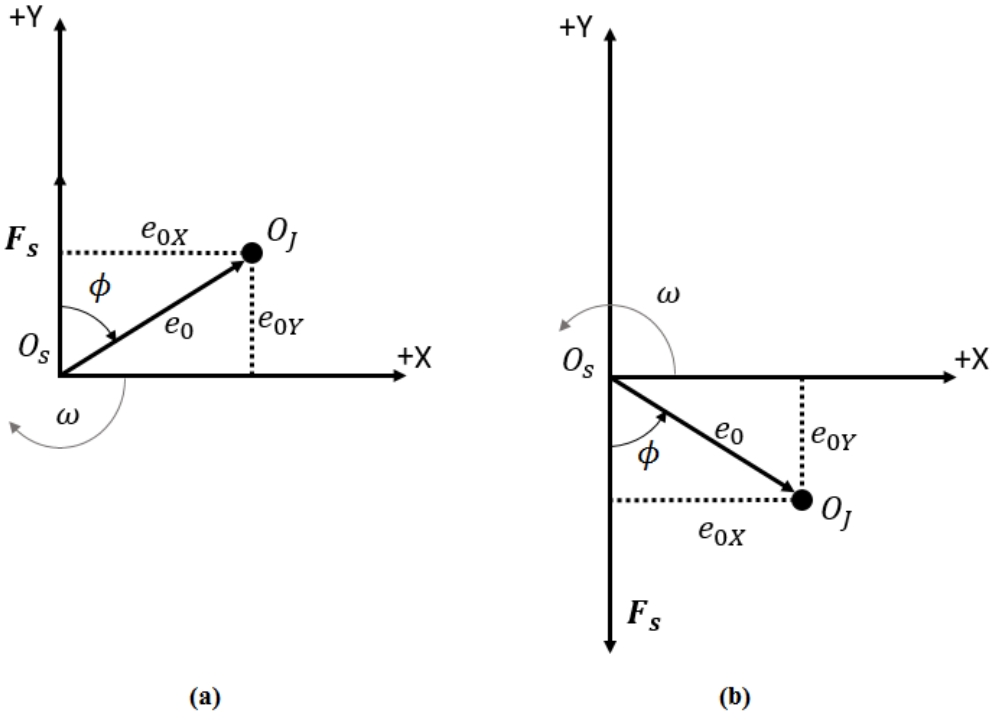

Figure 16. (a) Definition of coordinate system in the rig coordinate system. (b) Presented coordinate system.

O_S represents the geometric center of the seal, O_J represents the center of the rotor located at the eccentric position e_{0X}, e_{0Y}. The journal/rotor's position can be described relative to the stationary seal position as follows.

$$\varepsilon_0 = \sqrt{\varepsilon_{0X}^2 + \varepsilon_{0Y}^2} \tag{9}$$

where

$$\varepsilon_{0X} = \frac{e_{0X}}{C_r}, \varepsilon_{0X} = \frac{e_{0X}}{C_r} \tag{10}$$

The attitude angle, ϕ of $\boldsymbol{\varepsilon_0}$ with respect to $\boldsymbol{F_s}$ is calculated as

$$\phi = \tan^{-1}\frac{\varepsilon_{0X}}{\varepsilon_0 Y} \tag{11}$$

5. TEST MATRIX

The study reports on tests to measure the effect of swirl brakes on the static and rotordynamic characteristics of smooth seals using ISO VG 46 oil. Table 2 summarizes the conditions at which the measurements were taken. Note that tests were taken out to an ε_0 = 0.8. Testing was not done for ε_0 higher than 0.8 because the amplitude of each shake is around 10% of the clearance. The rotor could rub the stator for higher eccentricity ratios.

Table 2. Test matrix

ω (krpm)	ΔP (bar)	ε_0	ω (krpm)	ΔP (bar)	ε_0
2	2.07	0.00	6	2.07	0.00
		0.27			0.27
		0.53			0.53
		0.80			0.80
	4.14	0.00		4.14	0.00
		0.27			0.27
		0.53			0.53
		0.80			0.80
	6.21	0.00		6.21	0.00
		0.27			0.27
		0.53			0.53
		0.80			0.80
	8.27	0.00		8.27	0.00
		0.27			0.27
		0.53			0.53
		0.80			0.80
4	2.07	0.00	8	2.07	0.00
		0.27			0.27
		0.53			0.53
		0.80			0.80
	4.14	0.00		4.14	0.00
		0.27			0.27
		0.53			0.53
		0.80			0.80
	6.21	0.00		6.21	0.00
		0.27			0.27
		0.53			0.53
		0.80			0.80
	8.27	0.00		8.27	0.00
		0.27			0.27
		0.53			0.53
		0.80			0.80

6. STATIC RESULTS

6.1 Leakage

Figure 17 shows predicted and measured $\dot{Q}$ versus ε_0 for all clearances and ΔPs. A Turbolab in-house code, XLanSeal® based on a model discussed in [16] is used for predictions. Note that Exp X and XLan X in the graph refer to measured and predicted $\dot{Q}$ for the 1X clearance seal, respectively, and the naming convention is repeated for the 2X and 3X clearance seal, accordingly. Uncertainty values are very small compared to measured data and are difficult to see in the figure. As expected, $\dot{Q}$ increases as C_r and ΔP increase. $\dot{Q}$ is predicted well for the 1X and the 2X clearance seal. However, measured $\dot{Q}$ is 1.25 times higher than predicted $\dot{Q}$ for the 3X clearance seal.

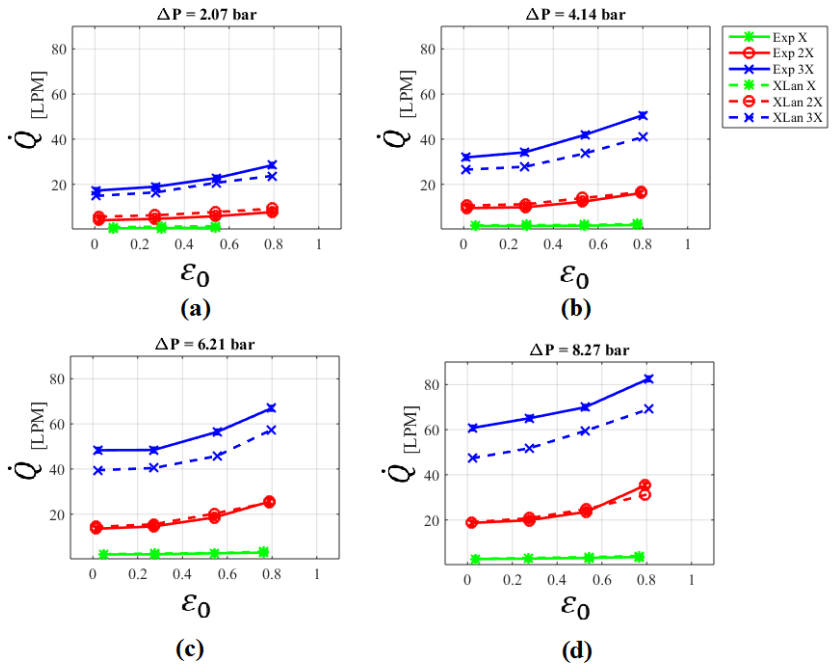

Figure 17. Measured and predicted $\dot{Q}$ versus ε_0 for ω = 6 krpm at (a) ΔP = 2.07 bar, (b) ΔP = 4.14 bar, (c) ΔP = 6.21 bar and (d) ΔP = 8.27 bar.

Note that ΔP was measured upstream of the SBs and not immediately upstream of the seal inlet. The same ΔP was used to predict $\dot{Q}$ across the seal. The $\dot{Q}$ discrepancy between measurements and predictions was speculated to be due to the SBs converting the velocity head due to circumferential flow into a pressure head, thereby increasing the ΔP across the seal. The increase in ΔP across the seal could therefore increase the leakage in the actual measurements compared to predictions that do not account for the head rise. However, assuming that the inlet circumferential velocity head $\rho v_i^2/2$ is converted to pressure, the model does not significantly improve in predicting $\dot{Q}$ for the 3X clearance seal.

Figure 18 shows $\dot{Q}$ versus ω for all clearances at ΔP = 4.14 bar. For the 1X and 2X clearance seals, $\dot{Q}$ is not dependent on ω. $\dot{Q}$ increases as clearance increases. The agreement between measurements and predictions is about the same as in Fig. 17. Note that the uncertainties are small and difficult to see in the figure.

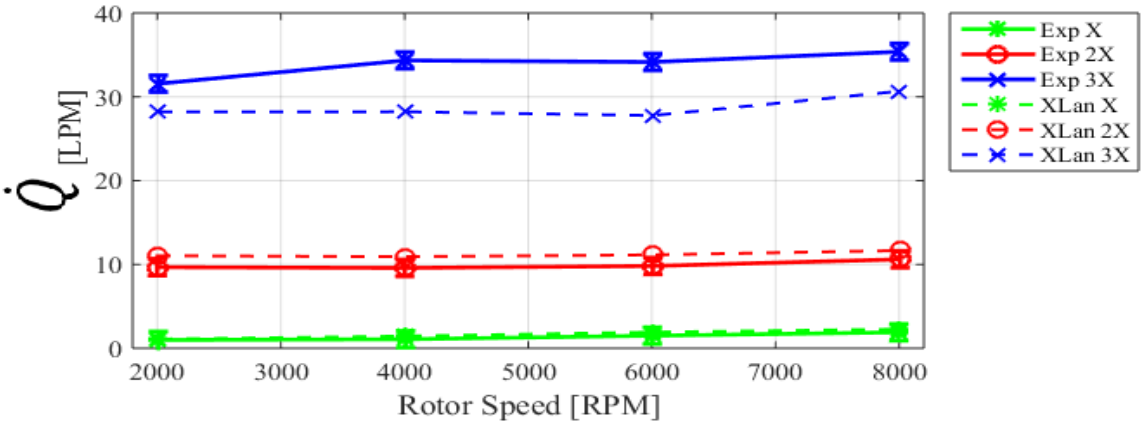

Figure 18. Measured and predicted $\dot{Q}$ versus ω for centered position at a ΔP of 4.14 bar.

Because of the scaling, for the 1X clearance seal, Fig. 18 does not clearly show the dependency of $\dot{Q}$ on ω. For the 1X clearance seal, Fig 19 shows that $\dot{Q}$ increases as ω increases. A possible explanation for this outcome is that in laminar flow conditions, the wall friction factor decreases with an increase in ω [1]. Predictions match the data very well.

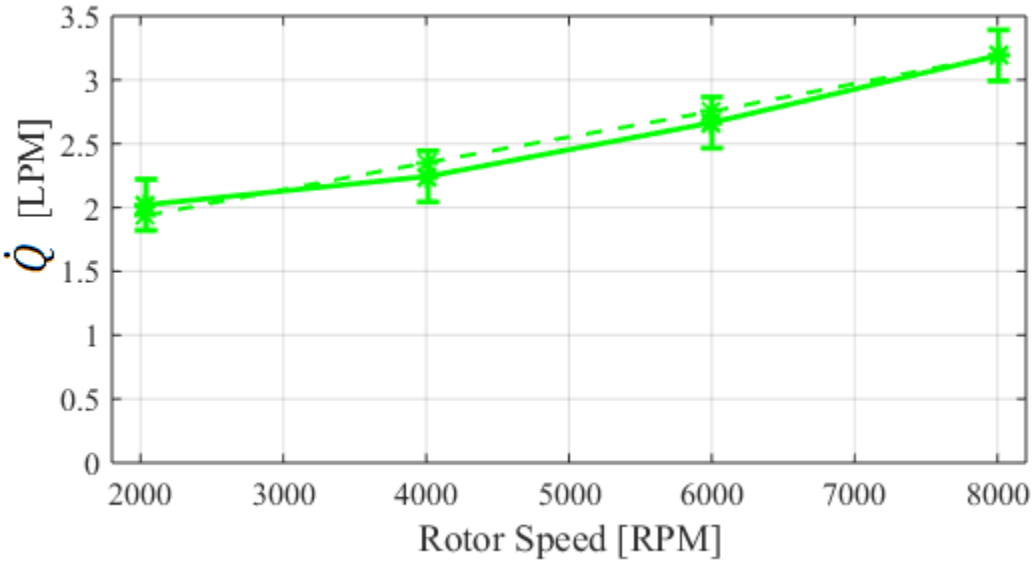

Figure 19. Measured and Predicted $\dot{Q}$ versus ω for centered position for the 1X clearance seal at ΔP = 8.27 bar.

6.2 Reynolds Number

Figure 20 shows Re_c and Re_a versus ω for the 3X clearance seal at a range of ΔPs. Re_a is independent of ω but increases as ΔP increases. Re_c increases as ω increases but is independent of ΔP. Re_c is more than twice as large as Re_a except at ΔP = 8.27 bars and ω

= 2000 rpm. Reynolds numbers for the 1X and 2X clearances are smaller compared to the 3X clearance seal and are not shown.

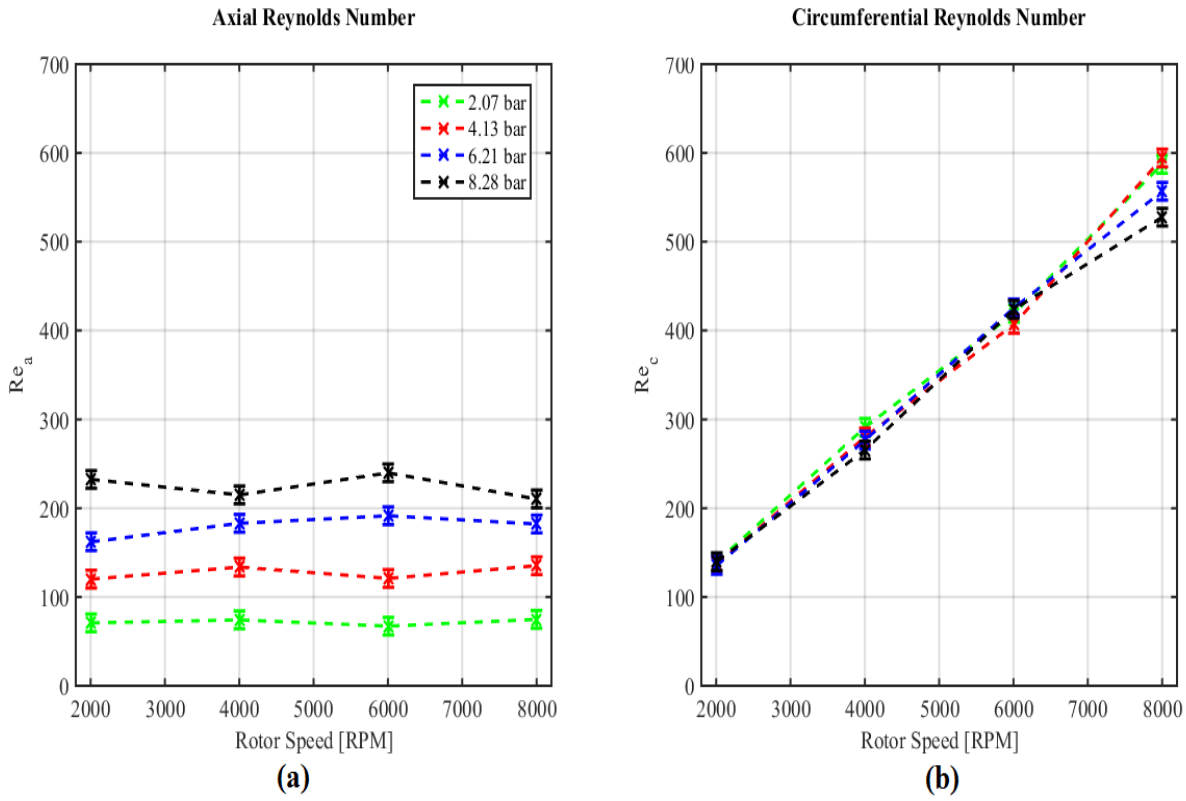

Figure 20. (a) Re_a versus ω at a range of ΔP for the 3X clearance, (b) Re_c versus ω at a range of ΔP for the 3X clearance.

Figure 21 shows Re_t versus ω for all C_r and ΔP values at the centered location. Note that the maximum Re_t does not exceed 650. Thus the flow is comfortably laminar. Re_t increases as C_r and ω increase. Re_t does not seem to be a function of ΔP.

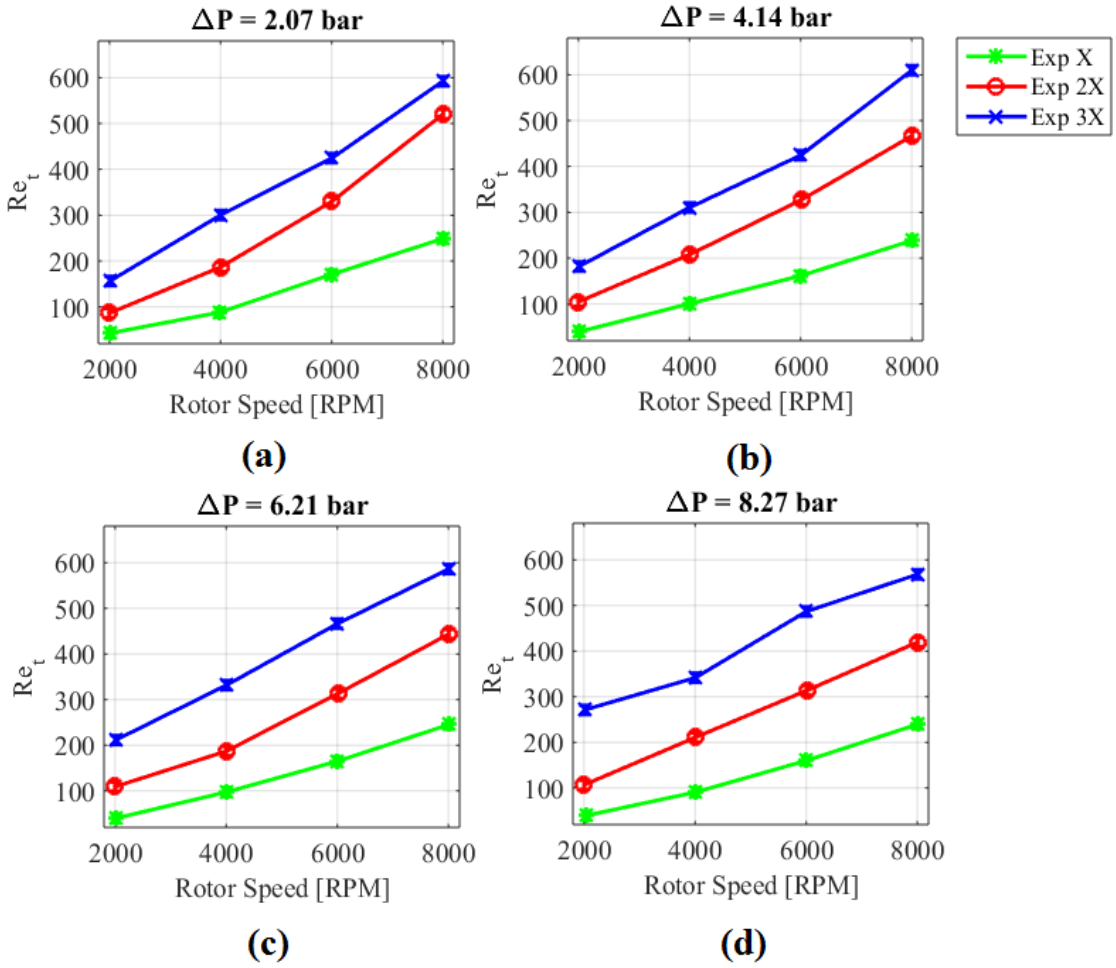

Figure 21. Re_t versus ω at ε_0 = 0.00 and at (a) ΔP = 2.07 bar, (b) ΔP = 4.14 bar, (c) ΔP = 6.21 bar and (d) ΔP = 8.27 bar.

6.3 Pre-Swirl and Outlet Swirl Ratio

As mentioned earlier, two pitot tubes measure the dynamic and static pressure at the inlet and outlet of the liquid annular seal. They are used to calculate the inlet and outlet circumferential velocities (v_i and v_o) respectively. The defining equation is

$$v = \sqrt{\frac{2\Delta P_{pitot}}{\rho}} \tag{12}$$

where ΔP_{pitot} is the pressure difference between the static and dynamic pressure measurements, and ρ is the density of the fluid. The swirl ratio is the ratio of the fluid inlet circumferential velocity to the rotor's surface speed. The pre-swirl ratio (PSR) is

$$PSR = \frac{v_i}{\omega R} \tag{13}$$

The outlet swirl ratio (OSR) is

$$OSR = \frac{v_o}{\omega R} \tag{14}$$

Figure 22a shows the axial positions of the inlet and outlet pitot tubes. Figure 22b shows an enlarged axial view of the inlet pitot tube.

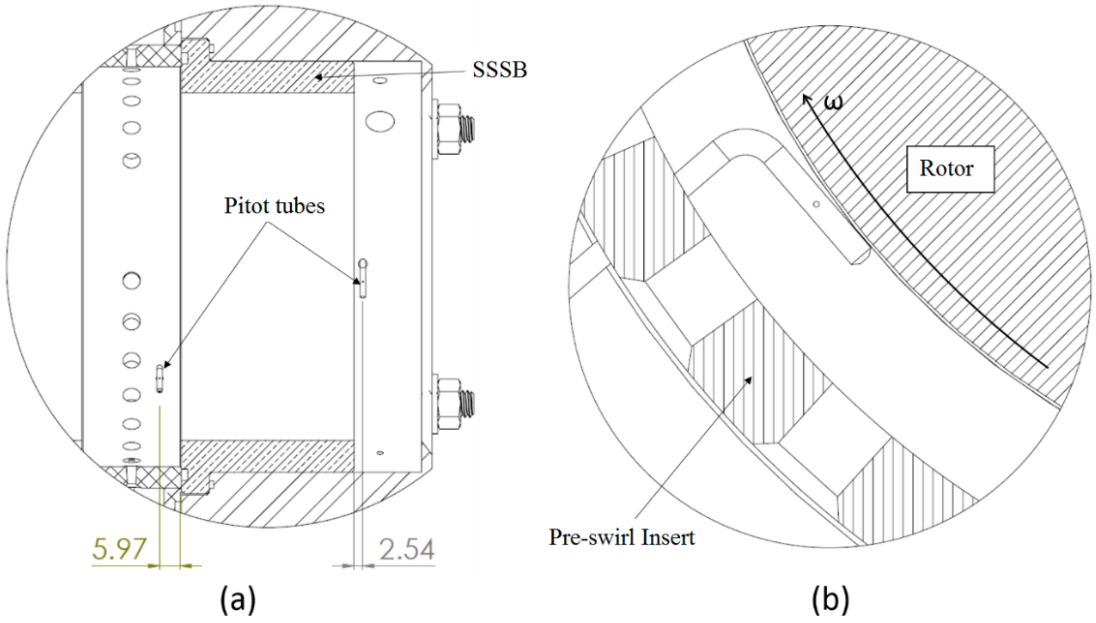

Figure 22. (a) Axial positions of the pitot tubes. (b) Radial location of the inlet pitot tube. All dimensions in mm reprinted from [20].

Figure 23 shows the radial location of the pre-swirl pitot tube. Note that the radial location of the pre-swirl pitot tube differs for each of the SSSBs. The pre-swirl pitot tube radial clearance is always equal to the radial clearance C_r of the seal; specifically 0.127, 0.254 and 0.381 mm for 1X, 2X and 3X C_r, respectively.

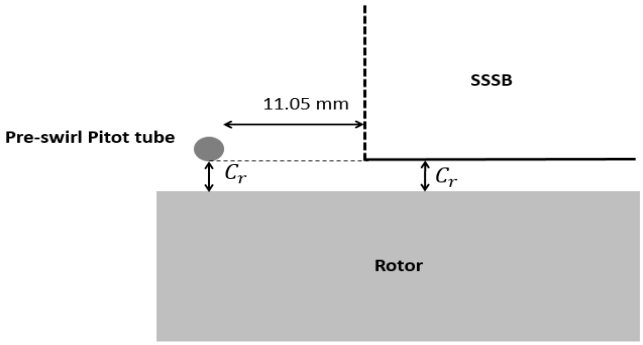

Figure 23. Radial position of the inlet pre-swirl pitot tube. Note that the Figure is not drawn to scale.

The radial location of the outlet swirl pitot tube varies in the same manner. Figure 24 shows that the outlet swirl pitot tube radial location is always the displaced distance C_r from the rotor.

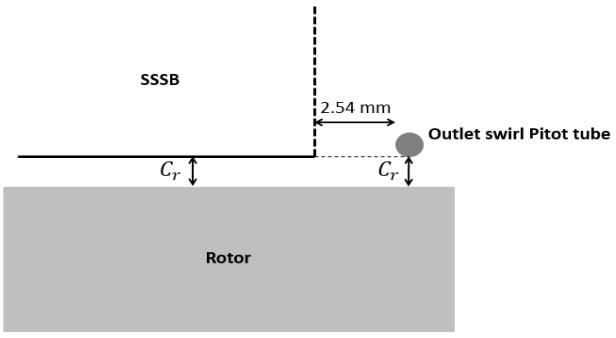

Figure 24. Radial position of outlet swirl pitot tube. Note that the Figure is not drawn to scale.

We will first look at the measured trends of PSR. Figure 25 shows the measured inlet circumferential velocity, v_i versus ω for a range of ΔP. The solid lines represent measured v_i. The dashed lines represent the fluid velocity leaving the pre-swirl insert, v_{insert} calculated as follows

$$v_{insert} = \frac{\dot{Q}}{12\pi r_{nozzle}^2} \tag{15}$$

where r_{nozzle} is the radius of each hole in the pre-swirl insert.

The black line represents $R\omega$, the fluid circumferential velocity at the rotor surface assuming no slip conditions. Figure 25 shows that v_i increases as ω and ΔP increase for all the clearances. The v_i magnitudes are higher than v_{insert}, especially for the 2X and the 3X clearance seals. For the 3X clearance seal, v_{insert} is higher than v_i at ω = 2krpm and all ΔPs. The data of Fig. 25 shows a slight relationship between v_{insert} and v_i to the extent that generally v_i (3X) > v_i (2X) > v_i (1X) but changes in ω have a clear impact on v_i. One explanation for this impact is the induced circumferential flow due to shaft rotation, particularly with the high fluid viscosity used here. Another possible explanation could be the location of the pitot tube. As C_r increases, the distance between the pitot tube and the rotor also increases (refer to Fig. 23). Thus the fluid velocity measurement location changes from seal to seal. v_i does increase with increasing ω indicating an induced pre-swirl due to shearing force from the shaft rotation. As ΔP increases, v_i tends to trend more with v_{insert} and less with $R\omega$. v_i is closer to the average fluid circumferential velocity $(R\omega/2)$ for the 3X clearance seal.

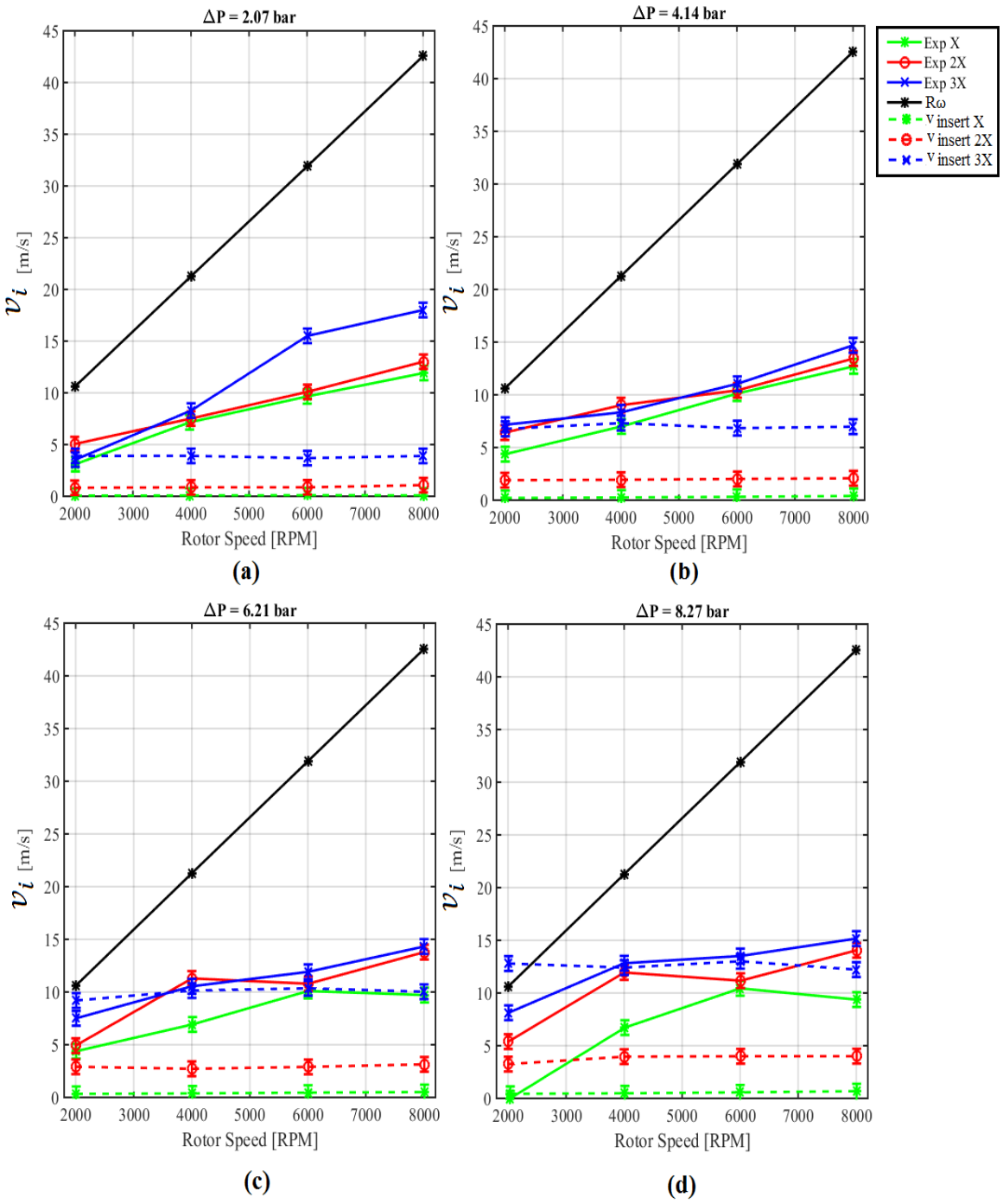

Figure 25. v_i versus ω at ε_0 = 0.00 and (a) ΔP = 2.07 bar, (b) ΔP = 4.14 bar, (c) ΔP = 6.21 bar and (d) ΔP = 8.27 bar.

Figure 26 shows PSR versus ω at the centered position. As expected from Eq. (13), PSR generally decreases with increasing ω for all the seal clearances even though Fig. 25 shows that v_i increases as ω increases.

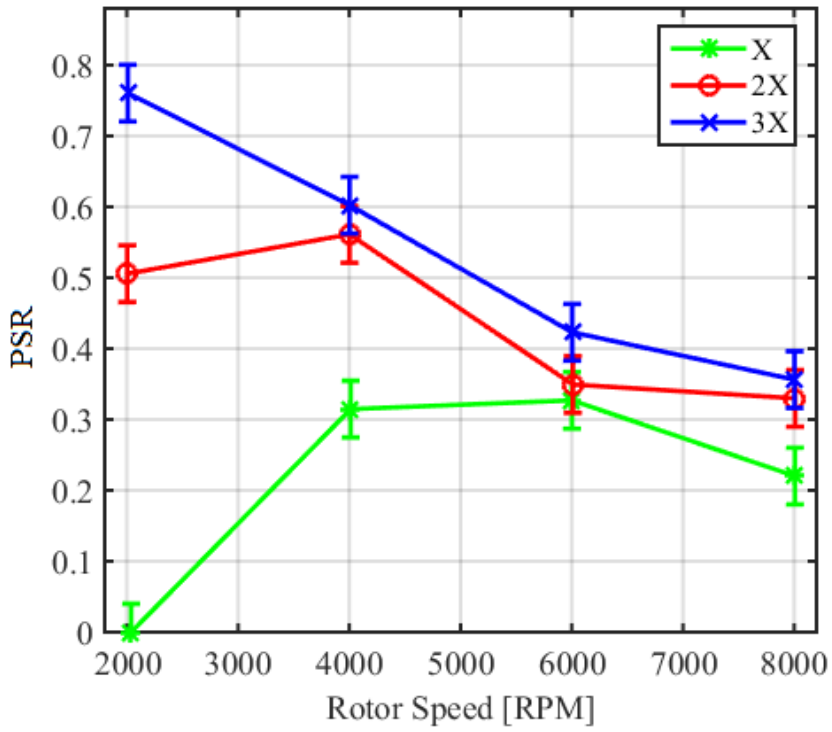

Figure 26. PSR versus ω at ΔP = 8.27 bar.

Figure 27 shows PSR versus ΔP at the centered location with $\omega = 4$ krpm. For 2X and 3X clearance seals, increasing ΔP increases PSR. However, for the 1X clearance seal, PSR decreases slightly as ΔP increases. PSR also tends to increase in moving from 1X to 2X and 3X clearance seals. However there is little difference of PSR between 2X and 3X clearance seal.

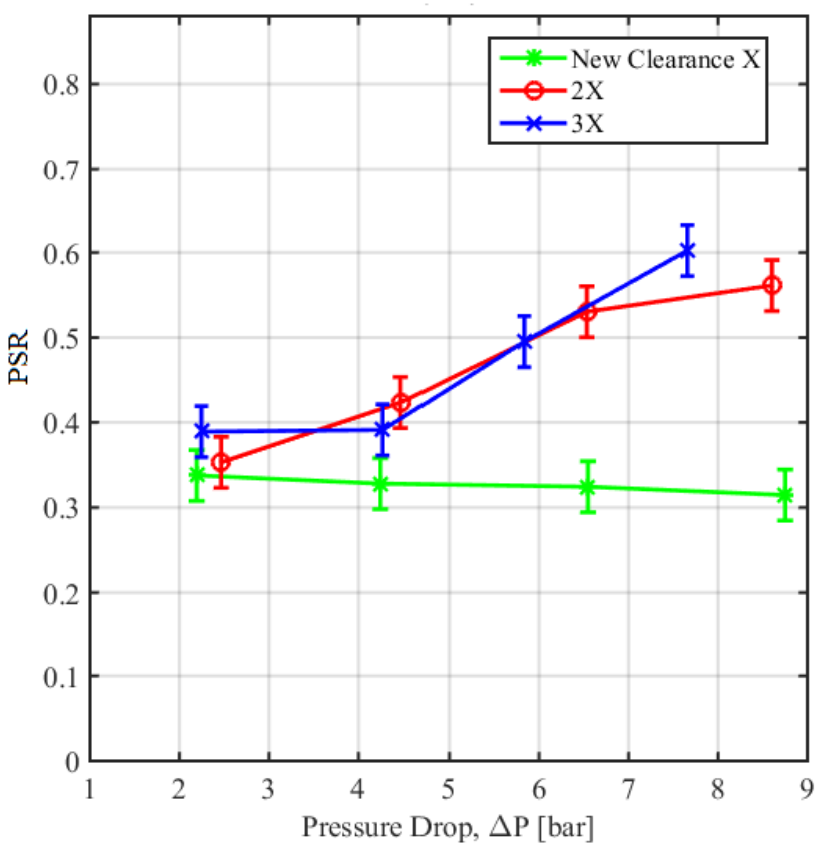

Figure 27. PSR versus ΔP at ε_0 = 0.00 and ω = 4 krpm.

Figure 28 shows the measured exit circumferential velocity, v_o versus ω for a range of ΔP. For the 1X clearance seal, v_o seems to be independent of ω. At ΔP ≤ 6.21 bar, For the 2X and 3X clearance seals, there is no clear relation between v_o and ω. However, at ΔP = 8.27 bar, for the 2X and 3X clearance seals, v_o increases as ω increases. There is no clear relation between v_o and ΔP for any of the clearances. Measured v_o is also less than the average bulk fluid velocity ($R\omega/2$) for all clearances.

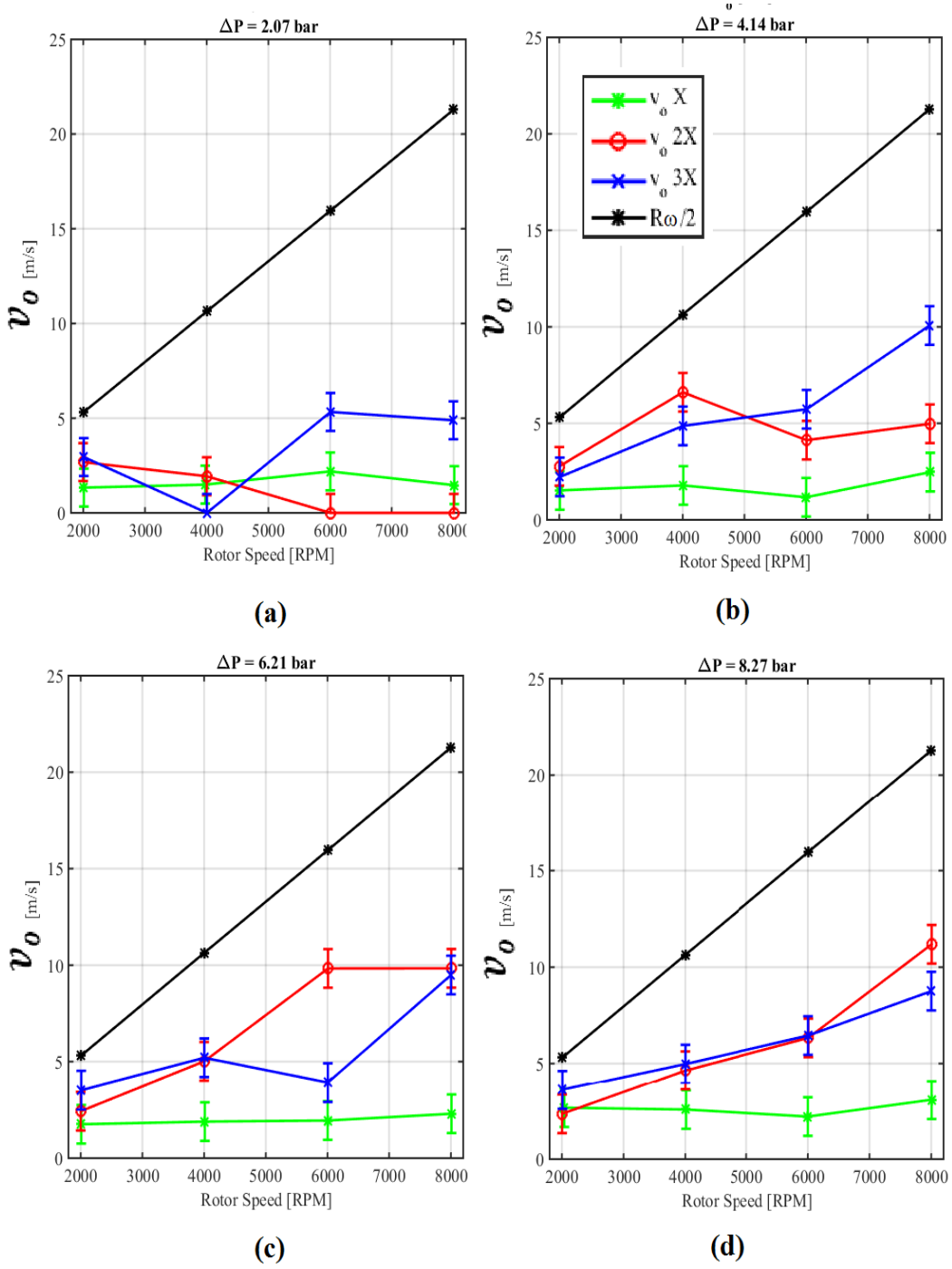

Figure 28. v_o versus ω at ε_0 = 0.00 and (a) ΔP = 2.07 bar, (b) ΔP = 4.14 bar, (c) ΔP = 6.21 bar and (d) ΔP = 8.27 bar.

Figure 29 shows OSR versus ω at the centered position at ΔP = 8.27 bar. For the 1X and 3X clearance seals OSR behaves similarly and tends to decrease with increasing speed. However, there is no clear relation between OSR and ω for the 2X clearance seal. The average circumferential velocity of the fluid *exiting the seal* is expected to be $R\omega/2$ for all seals. However, measured OSR values are found to be lower than 0.5. This discrepancy may be explained by the position of the outlet pitot tube position (refer to Fig 24). OSR values closer to 0.5 might be obtained, if the outlet pitot tube were closer to the trailing edge of the seal, which is not physically possible.

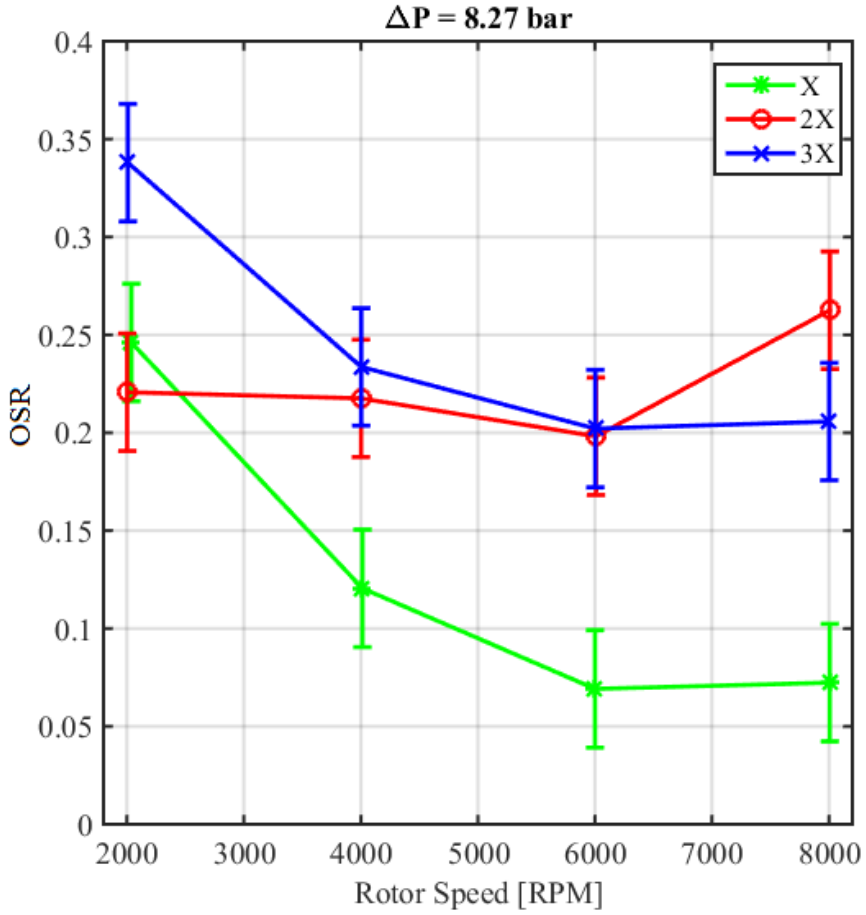

Figure 29. OSR versus ω at ΔP = 8.27 bar.

Figure 30 shows OSR versus ΔP at the centered location at $\omega = 4$ krpm. For the 1X clearance seal, OSR increases with an increase in ΔP. However for the 2X and 3X seals, OSR shows no clear correlation with ΔP.

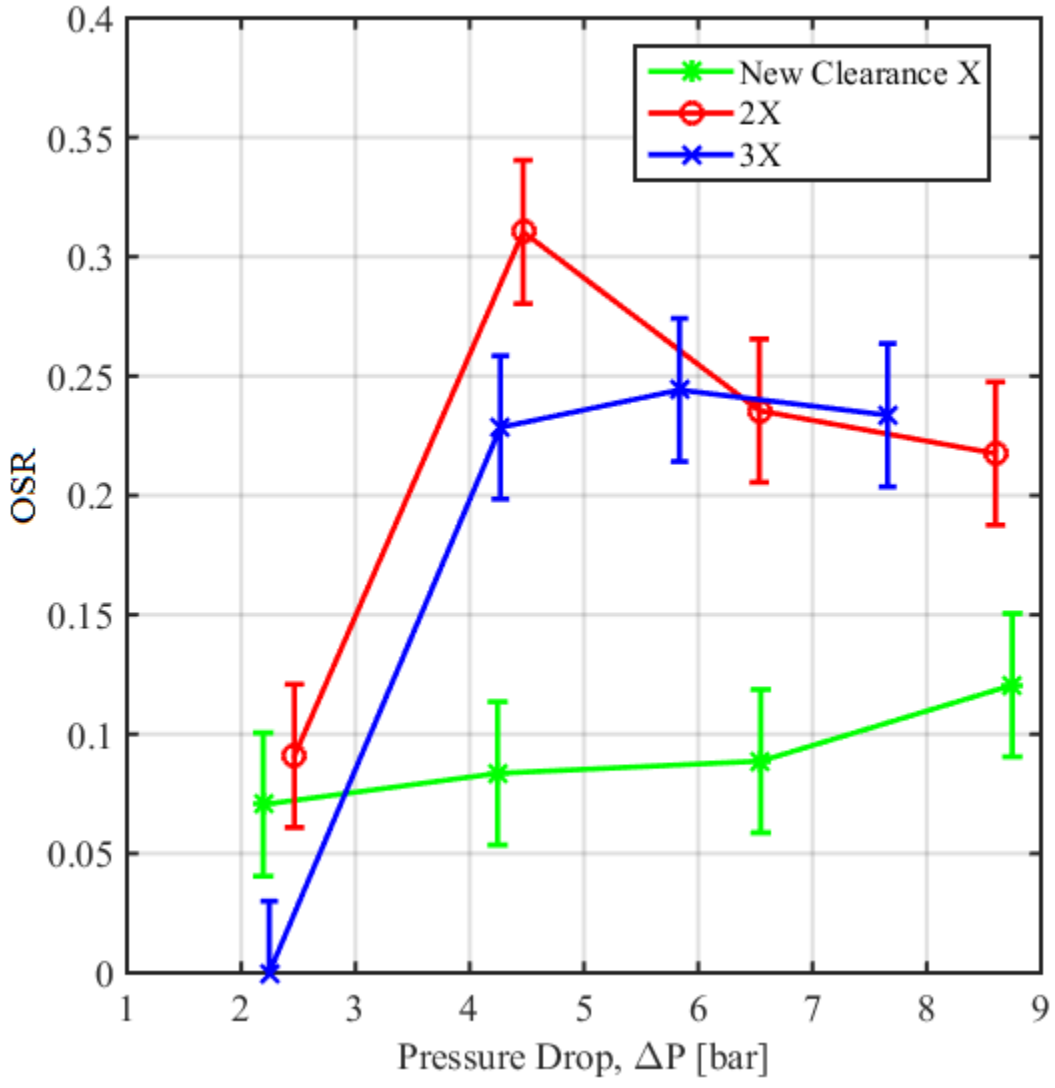

Figure 30. OSR versus ΔP at ε_0 = 0.00 and ω = 4 krpm .

6.4 Required Applied Static Load and Attitude Angle

Figure 31 shows measured attitude angle ϕ versus ε_0 at ω = 8krpm and all ΔPs. Recall Fig. 16 for the definition of ϕ. At ε_0 = 0.00, ϕs could not be determined because both the force and eccentricity vectors were zero. For the 1X clearance seal at ε_0 = 0.27, $\phi \geq 90°$ is an indication that fluid inertia effects are important [21]. Destabilizing forces exist, and there is presence of decentering forces. For the 1X seal, as expected, ϕ generally decreases as ε_0 increases. At $\varepsilon_0 > 0.27$, $\phi < 90°$, suggesting the presence of a centering force and a forward direction force in the ω direction. For 1X clearance seal, ϕ largely remains unaffected by a change in ΔP.

For the 2X clearance seal at ε_0 = 0.27, $\phi \cong 90°$. In such a situation, no centering force component exists; only a destabilizing force component exists. ϕ decreases as ε_0 increases and remains unaffected by a change in ΔP.

For the 3X clearance seal, $\phi \cong 180°$ at ε_0 = 0.27, 0.53 and ΔP = 2.07 bar. This implies that there is no forward destabilizing force and that the centering force is negative. $\phi < 90°$ for all other test conditions. Note that the uncertainties are small and difficult to see in the figure.

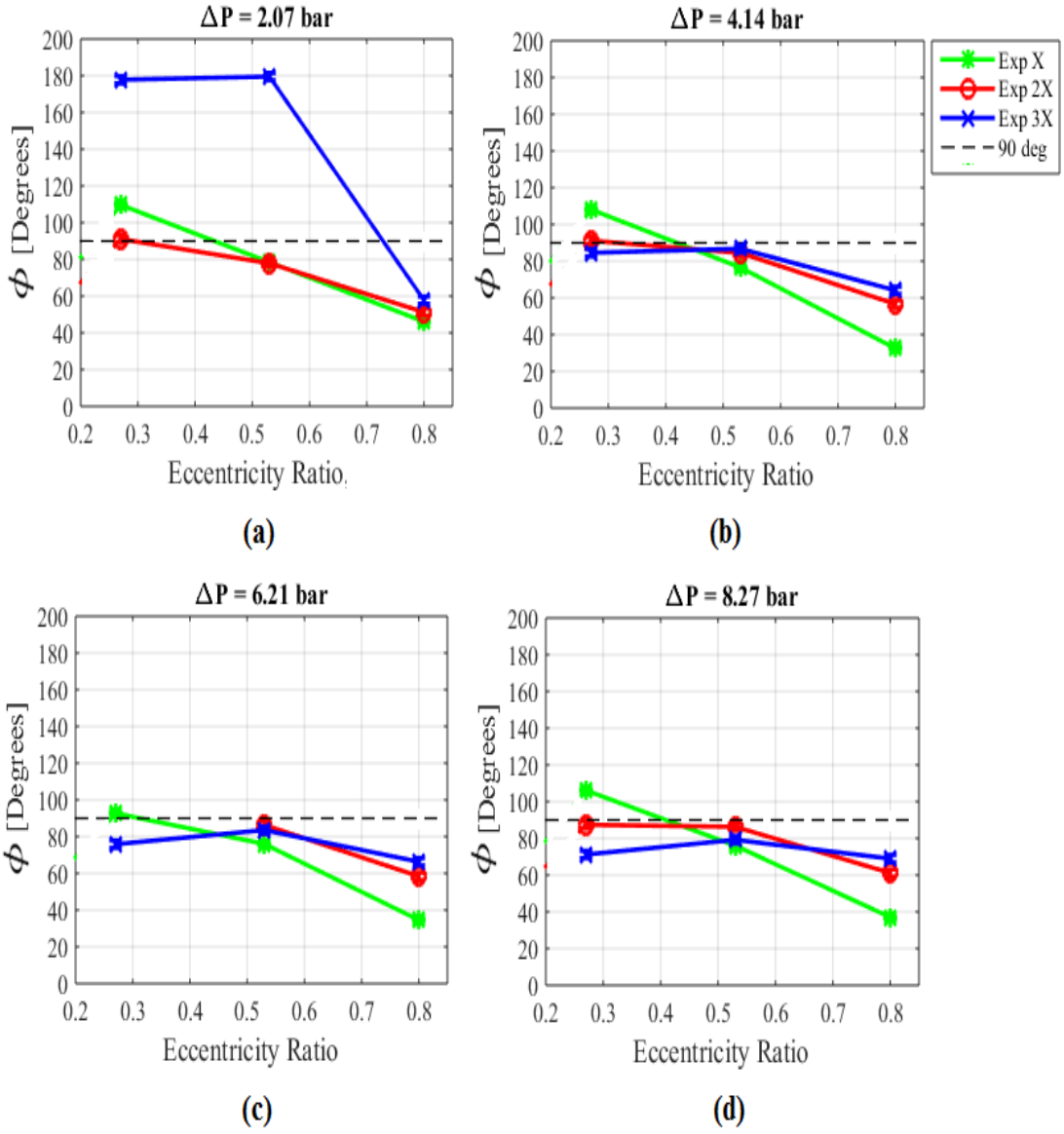

Figure 31. Measured ϕ versus ε_0 at ω = 8krpm and (a) ΔP = 2.07 bar, (b) ΔP = 4.14 bar, (c) ΔP = 6.21 bar and (d) ΔP = 8.27 bar.

Figure 32 shows the measured and predicted static load F_s required to produce each specified ε_0 for all clearances and ΔPs. While testing in load control (refer to section 7.4),

the load F_s is increased to achieve a specified ε_0; hence, for the 1X and 2X clearance seals, required F_s is a function of ε_0 not vice versa.

F_s increases as ε_0 increases and C_r decreases. There is generally good agreement between predictions and measurements. However for the 1X clearance seal at ε_0 = 0.80, measured F_s is consistently larger than predicted.

For the 3X clearance at ε_0 = 0.23, 0.57 at ΔP = 2.07 bar and ω = 8krpm, measured F_s is negative. This outcome is in perfect correlation to the ϕ = 180° results shown in Fig. 31a. Direct stiffness would be expected to be negative in these cases. The model fails to predict negative F_s at ε_0 = 0.23, 0.57 at ΔP = 2.07 bar and ω = 8krpm. The rest of the predicted data agrees well with measurements. Note that the uncertainties are small and difficult to see in the figure.

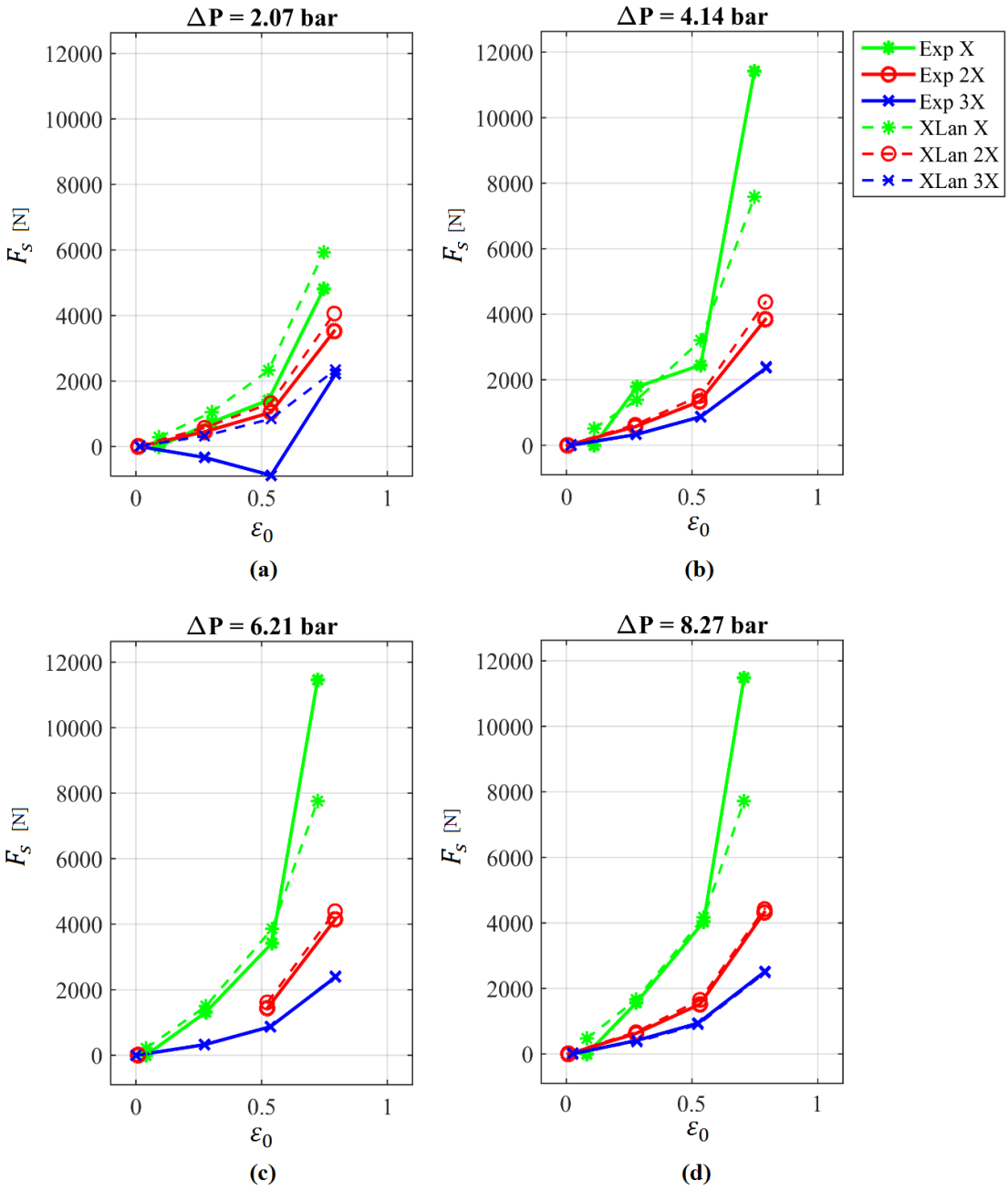

Figure 32. Measured and predicted F_s versus ε_0 at ω = 8krpm and (a) ΔP = 2.07 bar, (b) ΔP = 4.14 bar, (c) ΔP = 6.21 bar and (d) ΔP = 8.27 bar.

7. DYNAMIC RESULTS

7.1 Dynamic Measurement Approach

The multiple frequency excitation method employed by Rouvas and Childs [22], and Childs and Hale [23] was used here to measure the seal dynamic-stiffness coefficients. The input shake frequency is a pseudo random waveform optimized to provide maximum excitation at a range of frequencies between ~10-200 Hz. The stator acceleration components, relative rotor stator displacement components, and applied dynamic load components are measured as the hydraulic shakers shake the stator in each of the orthogonal (X & Y) directions. The stator is shaken for a total of 32.77 seconds consisting of 320 cycles in one direction at a time. Each cycle lasts about 0.1024 seconds and occurs at intervals of 9.765 Hz in order to reduce electrical noise. The data acquisition system samples measurements at 10 kHz.

7.2 Dynamic Data Analysis and Curve Fit

A model for Extracting meaningful stiffness, damping and mass coefficients begins by stating the equation of motion for the seal-rotor system

$$M_s \begin{Bmatrix} \ddot{X} \\ \ddot{Y} \end{Bmatrix} = \begin{Bmatrix} f_X \\ f_Y \end{Bmatrix} + \begin{Bmatrix} f_{sX} \\ f_{sY} \end{Bmatrix} \tag{16}$$

where M_s is the mass of the stator, f_{sX} and f_{sY} are the fluid-film reaction-force components in the X and Y directions, respectively, and f_X and f_Y represent the applied force components in the X and Y directions. Inserting Eq. (16) into Eq. (5) gives

$$\begin{Bmatrix} f_X \\ f_Y \end{Bmatrix} - M_s \begin{Bmatrix} \ddot{X} \\ \ddot{Y} \end{Bmatrix} = \begin{bmatrix} K_{XX}(e_0) & K_{XY}(e_0) \\ K_{YX}(e_0) & K_{YY}(e_0) \end{bmatrix} \begin{Bmatrix} \Delta X \\ \Delta Y \end{Bmatrix} + \begin{bmatrix} C_{XX}(e_0) & C_{XY}(e_0) \\ C_{YX}(e_0) & C_{YY}(e_0) \end{bmatrix} \begin{Bmatrix} \Delta \dot{X} \\ \Delta \dot{Y} \end{Bmatrix} + \begin{bmatrix} M_{XX}(e_0) & M_{XY}(e_0) \\ M_{YX}(e_0) & M_{YY}(e_0) \end{bmatrix} \begin{Bmatrix} \Delta \ddot{X} \\ \Delta \ddot{Y} \end{Bmatrix} \tag{17}$$

The force, acceleration and relative-displacement data component obtained in the time domain is transformed into the frequency domain using the fast Fourier transform (FFT) method. Equation (17) is thus rewritten in the frequency domain as

$$\begin{Bmatrix} \boldsymbol{F_X} - M_s \boldsymbol{A_X} \\ \boldsymbol{F_Y} - M_s \boldsymbol{A_Y} \end{Bmatrix} = \begin{bmatrix} \boldsymbol{H_{XX}} & \boldsymbol{H_{XY}} \\ \boldsymbol{H_{YX}} & \boldsymbol{H_{YY}} \end{bmatrix} \begin{Bmatrix} \boldsymbol{D_X} \\ \boldsymbol{D_Y} \end{Bmatrix} \tag{18}$$

where the applied force components ($\boldsymbol{F_X}$, $\boldsymbol{F_Y}$), acceleration components ($\boldsymbol{A_X}$, $\boldsymbol{A_Y}$), and relative displacement components ($\boldsymbol{D_X}$, $\boldsymbol{D_Y}$) are all in the frequency domain. The real and imaginary parts of the complex frequency response function, $\boldsymbol{H_{ij}}$ can be related to the stiffness, damping and virtual-mass coefficients by

$$\boldsymbol{H_{ij}} = \left(K_{ij} - \Omega^2 M_{ij}\right) + \boldsymbol{j}\left(\Omega C_{ij}\right) \tag{19}$$

where Ω is the excitation frequency and $\boldsymbol{j}$ is $\sqrt{-1}$. Equation (18) can be extended to include shakes in the two orthogonal directions as follows

$$\begin{bmatrix} \boldsymbol{F_{XX}} - M_s\boldsymbol{A_{XX}} & \boldsymbol{F_{XY}} - M_s\boldsymbol{A_{XY}} \\ \boldsymbol{F_{YX}} - M_s\boldsymbol{A_{YX}} & \boldsymbol{F_{YY}} - M_s\boldsymbol{A_{YY}} \end{bmatrix}$$

$$= \begin{bmatrix} \boldsymbol{H_{XX}} & \boldsymbol{H_{XY}} \\ \boldsymbol{H_{YX}} & \boldsymbol{H_{YY}} \end{bmatrix} \begin{bmatrix} \boldsymbol{D_{XX}} & \boldsymbol{D_{XY}} \\ \boldsymbol{D_{YX}} & \boldsymbol{D_{YY}} \end{bmatrix} \tag{20}$$

Using Eq. (19), the extraction of the rotordynamic coefficient is done by the regression analysis applied separately to the real and imaginary parts of the dynamic stiffness as explained by Beckwith et al. [24]. Their curve fit assumes a linear relationship between the input, Inp and the output, Out so that

$$Out = a \cdot Inp + b \tag{21}$$

In Eq. (19), this relationship is used directly to solve for C_{ij}. In solving for K_{ij} and M_{ij}, the independent variable is Ω^2, not Ω. the intercept, b in Eq. (21) is calculated from a set of inputs and outputs as

$$b = \frac{\sum Out \sum Inp^2 - \sum Inp \sum Inp \cdot Out}{n \sum Inp^2 - (\sum Inp)^2} \tag{22}$$

and the slope, a is

$$a = \frac{n \sum Inp \cdot Out - \sum Inp \sum Out}{n \sum Inp^2 - (\sum Inp)^2} \tag{23}$$

7.3 Dynamic Stiffness Coefficients

Characteristic of the entire data set, Fig. 33 shows the fluid-film's imaginary and real dynamic stiffness components respectively, versus Ω, for the 1X clearance seal at ε_0=

0.00, ΔP = 4.14 bar and ω = 4krpm. Clearly with an exception of a few erratic points that were discarded, the overall data agrees well with the KCM model cited in Eq. (19).

Figure 33a shows $Im(\boldsymbol{H}_{XX})$ and $Im(\boldsymbol{H}_{YY})$ increasing linearly with increasing Ω, which means that $C_{XX} > 0$, and $C_{YY} > 0$.

Figure 33b shows $Im(\boldsymbol{H}_{XY})$ increasing with increasing Ω, whereas $Im(\boldsymbol{H}_{YX})$ decreases. They also have opposite signs, an indication that $C_{XY} > 0$, and $C_{YX} < 0$.

Figure 33c shows $Re(\boldsymbol{H}_{XX})$ and $Re(\boldsymbol{H}_{YY})$ decreasing quadratically with Ω with a positive Y intercept showing that $K_{XX} > 0$, $K_{YY} > 0$, $M_{XX} > 0$, $M_{YY} > 0$.

Figure 33d shows $Re(\boldsymbol{H}_{XY})$ and $Re(\boldsymbol{H}_{YX})$ having equal and opposite signs and being very weak functions of Ω. An absence of curvature indicates that $M_{XY} \cong M_{YX} \cong 0$. The data was fit to 200 Hz, which is about 1.5 times the maximum running speed of 8krpm. The data for the 2X clearance seal was also fit to 200 Hz which is about 1.5 times the maximum running speed of 8krpm.

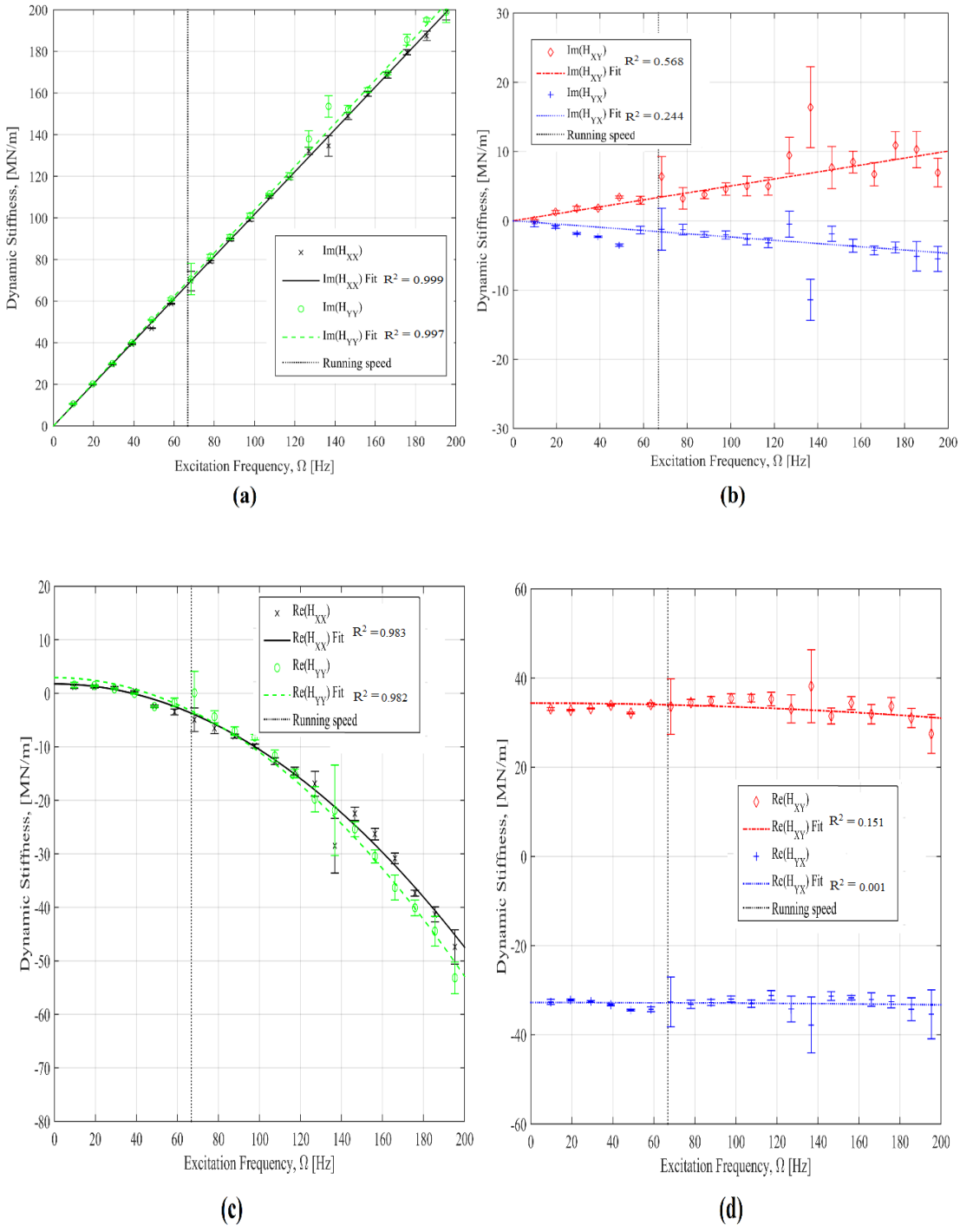

Figure 33. (a) Imaginary component of direct dynamic stiffness, (b) Imaginary component of cross-coupled stiffness, (c) Real component of direct dynamic stiffness, (d) Real component of cross-coupled stiffness versus Ω at ε_0= 0.00, ΔP = 4.14 bar, ω = 4krpm for the 1X clearance seal.

For the 3X clearance seal, at ε_0= 0.00, ΔP = 8.27 bar and ω = 8 krpm, Fig. 34 shows the fluid-film's imaginary and real dynamic stiffness components, versus Ω. Figure 34a shows $Im(\boldsymbol{H}_{XX})$ and $Im(\boldsymbol{H}_{YY})$ increasing linearly with Ω which means that the $C_{XX} > 0$, and $C_{YY} > 0$.

Figure 34b shows $Im(\boldsymbol{H}_{XY})$ increasing with increasing Ω, whereas $Im(\boldsymbol{H}_{YX})$ decreases. $Im(\boldsymbol{H}_{XY}) > 0$ implies that $C_{XY} > 0$; $Im(\boldsymbol{H}_{YX}) < 0$ implies that $C_{YX} < 0$.

Figure 34c shows $Re(\boldsymbol{H}_{XX})$ and $Re(\boldsymbol{H}_{YY})$ decreasing quadratically with Ω with a negative Y intercept showing that K_{XX}, K_{YY} would be negative and M_{XX}, M_{YY} would be positive. Note that K_{XX}, K_{YY} will have different magnitudes.

Figure 34d shows $Re(\boldsymbol{H}_{XY})$ and $Re(\boldsymbol{H}_{YX})$ have the same sign but different magnitudes. Hence K_{XY} and K_{YX} have the same sign and are not destabilizing. $Re(\boldsymbol{H}_{XY})$ and $Re(\boldsymbol{H}_{YX})$ have a negligible curvature. Hence, M_{XY} and M_{YX} would be zero. Overall, the data obtained fits very well up to 100 Hz and then seems to diverge from the KCM model. Keeping this in mind, the data for the 3X clearance seal was fit to about a 100 Hz.

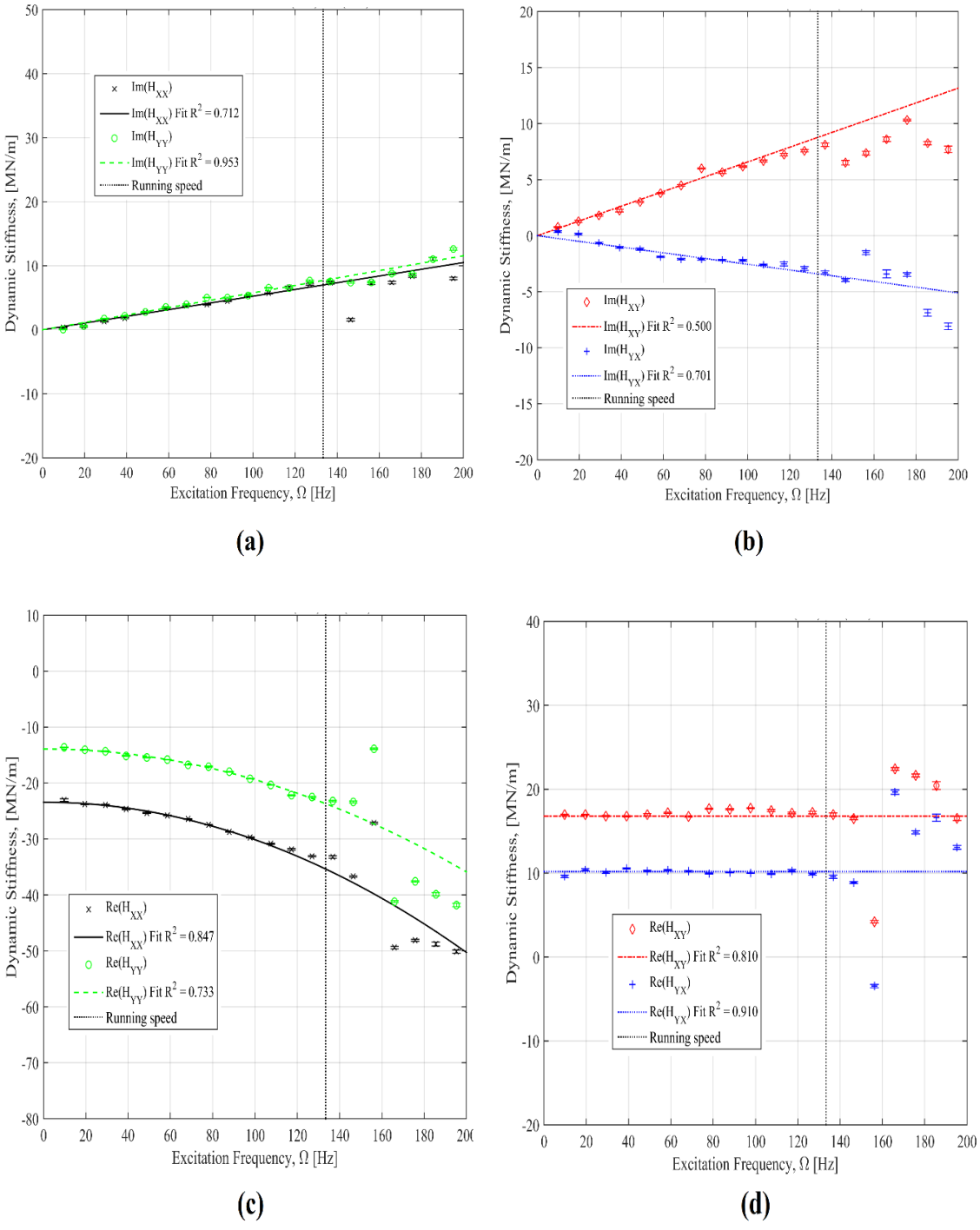

Figure 34. (a) Imaginary component of direct dynamic stiffness, (b) Imaginary component of cross-coupled stiffness, (c) Real component of direct dynamic stiffness, (d) Real component of cross-coupled stiffness versus Ω at ε_0= 0.00, ΔP = 8.27 bar, ω = 8krpm for the 3X clearance seal.

7.4 Load and Position Control Systems

Dynamic measurements at various eccentricity ratios can be set from the test rig in the following two modes (a) Load Control, (b) Position control. As shown in Fig. 35a, load control mode refers to a force F_s being applied by the shaker to the stator in the $-Y$ direction with no force being applied through the X-axis (refer to Fig. 8) to achieve a specified ε_0. Alternatively, as shown in Fig. 35b to achieve a specified ε_0, the shaker heads are used directly to position the stator along the Y axis by applying forces from both shaker heads. The basic aim is to get the same ε_0 by two different schemes. Most of the seals can be tested in the load control mode as the seal-rotor system achieves an equilibrium position at a certain ε_0 and F_s. For some seal clearances, loads, eccentricity ratios, and inlet swirl conditions, testing cannot be performed in the load control mode as the seal becomes statically unstable. However, such seals can be tested using the shakers in the position control mode. The shakers in the X and Y direction provide the force components that are required to keep the stator in a specified eccentric position.

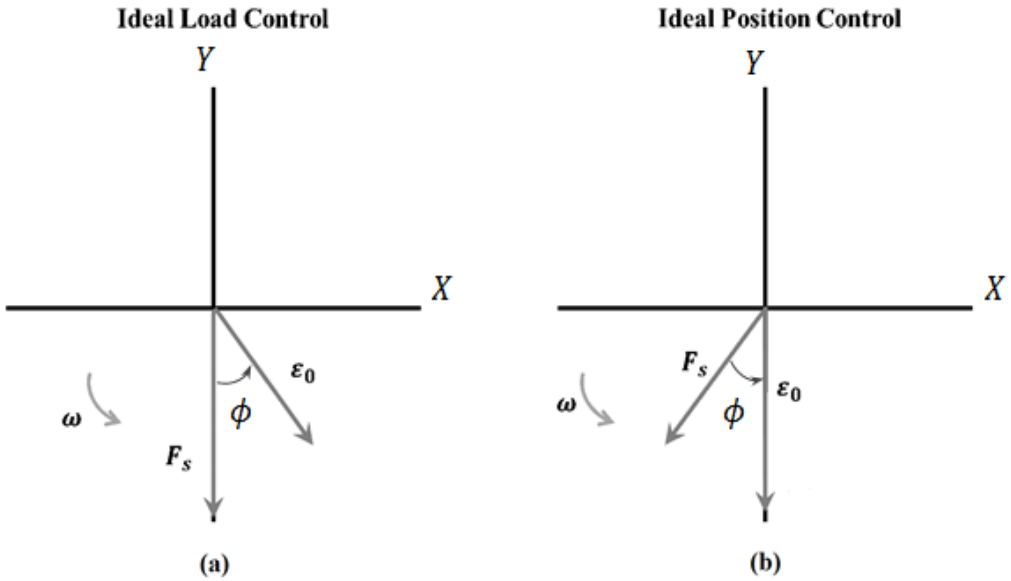

Figure 35. (a) Ideal load control, (b) Ideal position control.

The 1X and 2X clearance seals were tested in load-control mode. The 3X clearance seal was tested in the position control because, in some cases, the 3X clearance seal had no stable equilibrium position. To compare the 1X, 2X and 3X clearance seals, the author used the $\boldsymbol{\epsilon_r}$ and $\boldsymbol{\epsilon_t}$ coordinate system. As shown in Fig. 36, the eccentricity vector is always in the $\boldsymbol{\epsilon_r}$ direction.

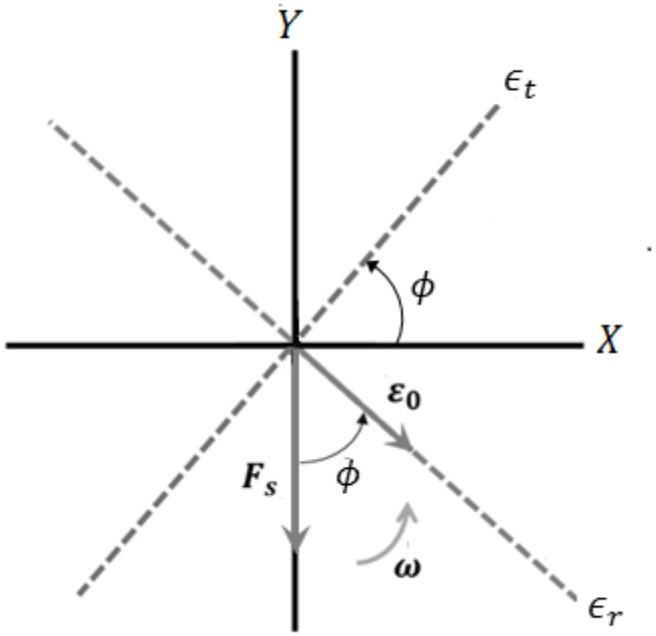

Figure 36. Coordinate transformation from cartesian coordinate system to r and t coordinate system.

The following similarity transformation is used to transform dynamic- coefficients in the X-Y cartesian coordinate system to the r-t system.

$$\begin{bmatrix} Z_{tt} & Z_{tr} \\ Z_{rt} & Z_{rr} \end{bmatrix} = \begin{bmatrix} \cos\phi & \sin\phi \\ -\sin\phi & \cos\phi \end{bmatrix} \begin{bmatrix} Z_{XX} & Z_{XY} \\ Z_{YX} & Z_{YY} \end{bmatrix} \begin{bmatrix} \cos\phi & -\sin\phi \\ \sin\phi & \cos\phi \end{bmatrix} \tag{24}$$

where ϕ, illustrated in Fig.36, is the angle between the $\boldsymbol{F_s}$ and $\boldsymbol{\varepsilon_0}$ vector. The transformation applies to the [K], [C], and [M] matrices.

The rotordynamic model using the $\boldsymbol{\epsilon_t}$ and $\boldsymbol{\epsilon_r}$ coordinate system is

$$-\begin{Bmatrix} f_t \\ f_r \end{Bmatrix} = \begin{bmatrix} K_{tt}(e_0) & K_{tr}(e_0) \\ K_{rt}(e_0) & K_{rr}(e_0) \end{bmatrix} \begin{Bmatrix} x_t \\ x_r \end{Bmatrix} + \begin{bmatrix} C_{tt}(e_0) & C_{tr}(e_0) \\ C_{rt}(e_0) & C_{rr}(e_0) \end{bmatrix} \begin{Bmatrix} \dot{x}_t \\ \dot{x}_r \end{Bmatrix}$$

$$+\begin{bmatrix} M_{tt}(e_0) & M_{tr}(e_0) \\ M_{rt}(e_0) & M_{rr}(e_0) \end{bmatrix} \begin{Bmatrix} \ddot{x}_t \\ \ddot{x}_r \end{Bmatrix} \quad (25)$$

7.5 Rotordynamic Coefficients

Stiffness Coefficients

Figure 37 shows measured K_{tt} and K_{rr} versus ε_0 at ΔP = 2.07 bar and ω = 4krpm. As expected, at higher ε_0 values, K_{rr} is greater than K_{tt}, since the rotor has been displaced in the ε_0 direction, and the rotor is closer to the seal wall in the r direction compared to the t direction. K_{tt} and K_{rr} increase as ε_0 increases for all clearances. K_{tt} and K_{rr} decrease as clearance increases. At the centered location, K_{tt} and K_{rr} are expected to coincide, but the measurements are slightly different for the 3X clearance seal as previously shown in Fig. 34c. The difference in stiffness coefficients might arise because the rotor is not exactly at the center location while measurements are being taken.

Interestingly, K_{tt} and K_{rr} are negative at all eccentricity ratios for the 3X clearance seal. This seems to be a prime reason why it was difficult to hold the 3X clearance seal in the load-control mode. A negative stiffness would mean that the pump rotor would be "sucked in" towards the stator wall.

For the 3X seal, recall that F_s was negative at ε_0 = 0.27, 0.53, ΔP = 2.07 bar and ω = 8krpm. This implied that K_{rr} would also be negative. Measured K_{rr} is negative at these conditions. However, $\phi < 90°$ for Fig. 31a at ε_0 = 0.80 implying a positive K_{rr} versus the negative K_{rr} shown in Fig. 37.

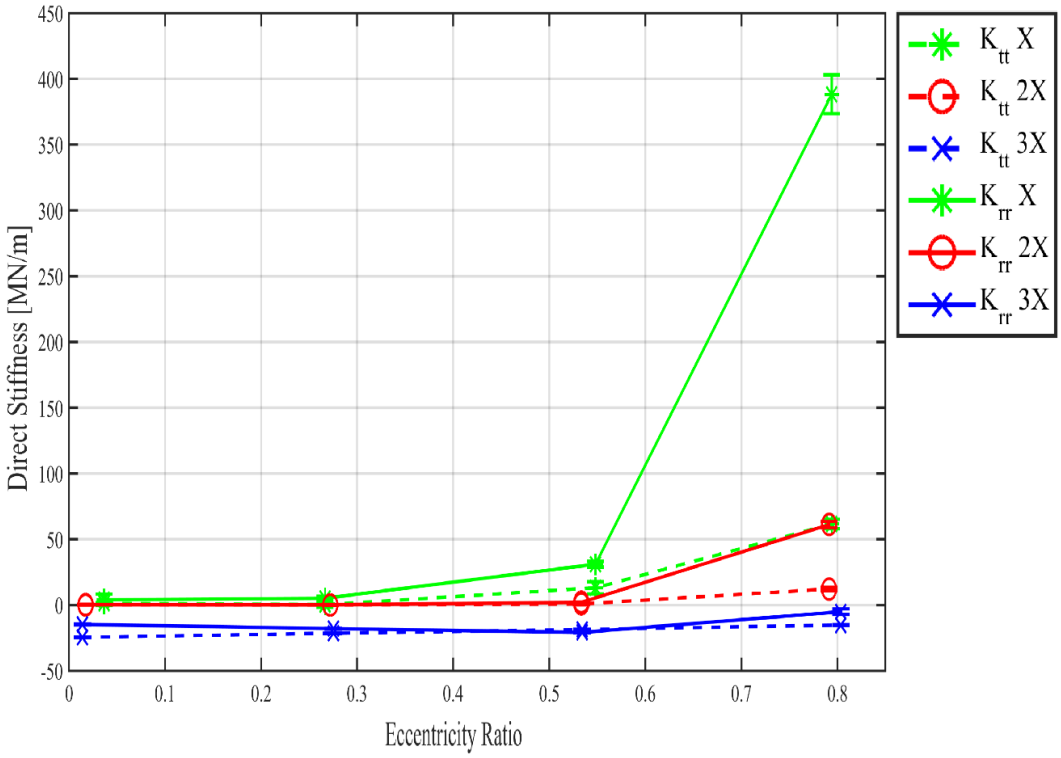

Figure 37. Measured K_{tt} and K_{rr} versus ε_0 at ΔP = 2.07 bar and ω = 4krpm.

Figure 38a shows K_{rr} versus ε_0 at ΔP = 2.07 bar and ω = 4krpm. K_{rr} is well predicted for the 1X and 2X clearance seal up to ε_0 = 0.53. At ε_0 = 0.80, K_{rr} is 20% greater than predicted for the 1X clearance seal.

Figure 38b shows K_{tt} versus ε_0. K_{tt} is well predicted for the 1X and 2X clearance seal up to ε_0 = 0.53. At ε_0 = 0.80, K_{tt} is 20% greater than predicted for the 3X clearance seal. Also, at ε_0 = 0.80, measured K_{tt} is 50% greater than predicted for the 2X clearance seal.

Most importantly, The model [16] predicts positive K_{tt} and K_{rr} for the 3X clearance seal while the measured data shows otherwise. Predicted K_{tt} and K_{rr} are slightly positive for the 3X clearance at all eccentricity ratios. Negative direct stiffness would drop the natural frequency of the pump and can destabilize the pump.

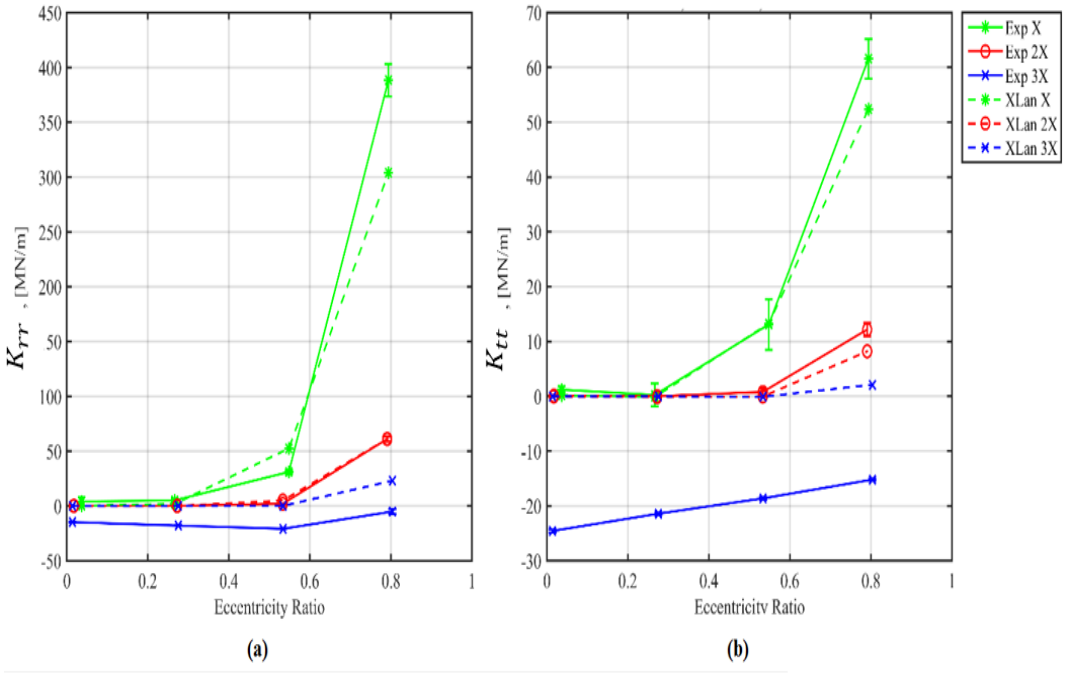

Figure 38. ΔP = 2.07 bar and ω = 4krpm (a) Measured and predicted K_{rr} versus ε_0. (b) Measured and predicted K_{tt} versus ε_0.

Figure 39 shows measured K_{tt} and K_{rr} versus ΔP at ε_0 = 0.80 and ω = 4 krpm. For the 1X clearance seal, K_{tt} and K_{rr} increase as ΔP increases, and their magnitudes are comparable. K_{tt} and K_{rr} are generally independent of ΔP at 2X and 3X clearances. Note that the magnitude of K_{rr} is generally 6 times that of K_{tt} for the 2X and 3X clearance seals.

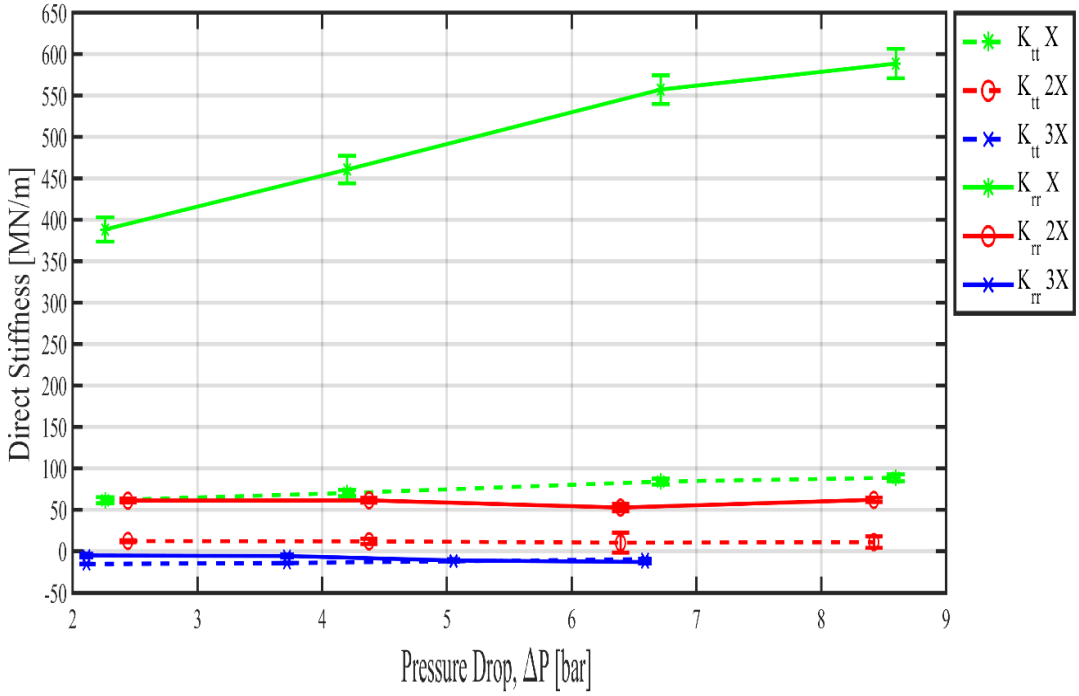

Figure 39. Measured K_{tt} and K_{rr} versus ΔP at ε_0 = 0.80 and ω = 4 krpm.

Figure 40 shows measured and predicted K_{tt} and K_{rr} versus ΔP at ε_0 = 0.80 and ω = 4 krpm. Figure 40a shows that K_{rr} is under predicted by about 25% for the 1X clearance seal. Predictions match measurements for the 2X clearance seal. As mentioned in Fig. 37, K_{rr} is predicted to be positive while measurements show that it is negative for the 3X clearance seal.

Figure 40b shows that K_{tt} is under predicted by about 30% for 1X clearance seal and by about 10% for the 2X clearance seal. For the 3X clearance seal, K_{tt} is predicted to be positive while it is measured to be negative.

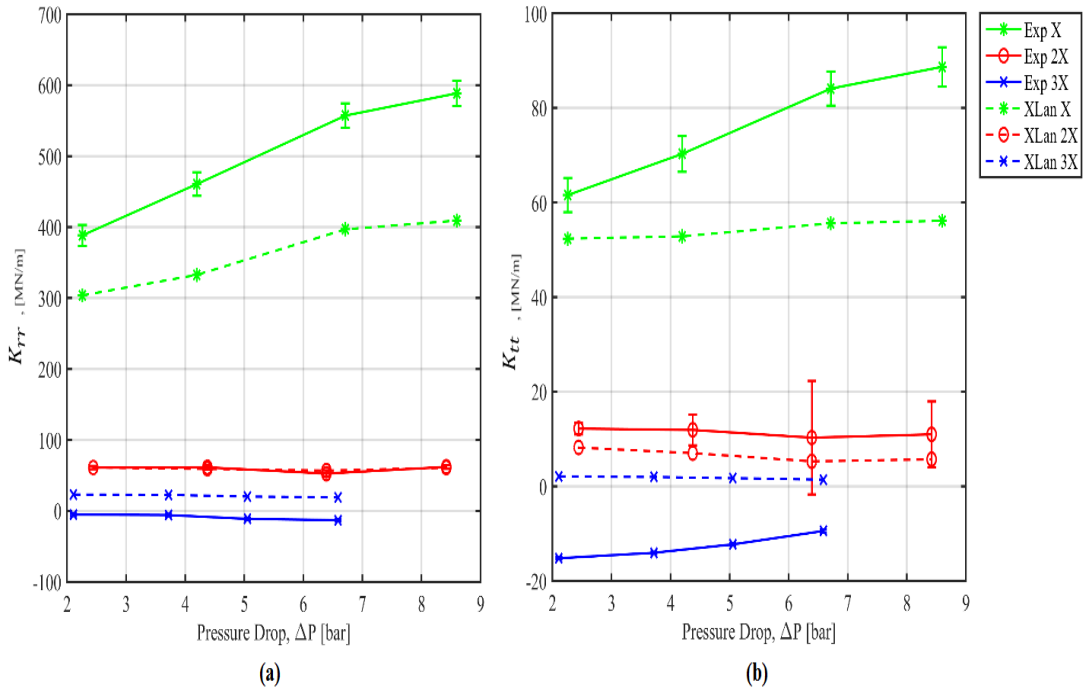

Figure 40. ε_0 = 0.80 and ω = 4 krpm (a) Measured and predicted K_{rr} versus ΔP. (b) Measured and predicted K_{tt} versus ΔP.

Figure 41 shows measured K_{tt} and K_{rr} versus ω at ε_0 = 0.00 and ΔP = 4.14 bar. For 1X clearance seal, K_{tt} and K_{rr} increase as ω increases. For 2X and 3X clearance seals, K_{tt} and K_{rr} are independent of ω. As previously stated, K_{tt} and K_{rr} are both negative for the 3X clearance seal.

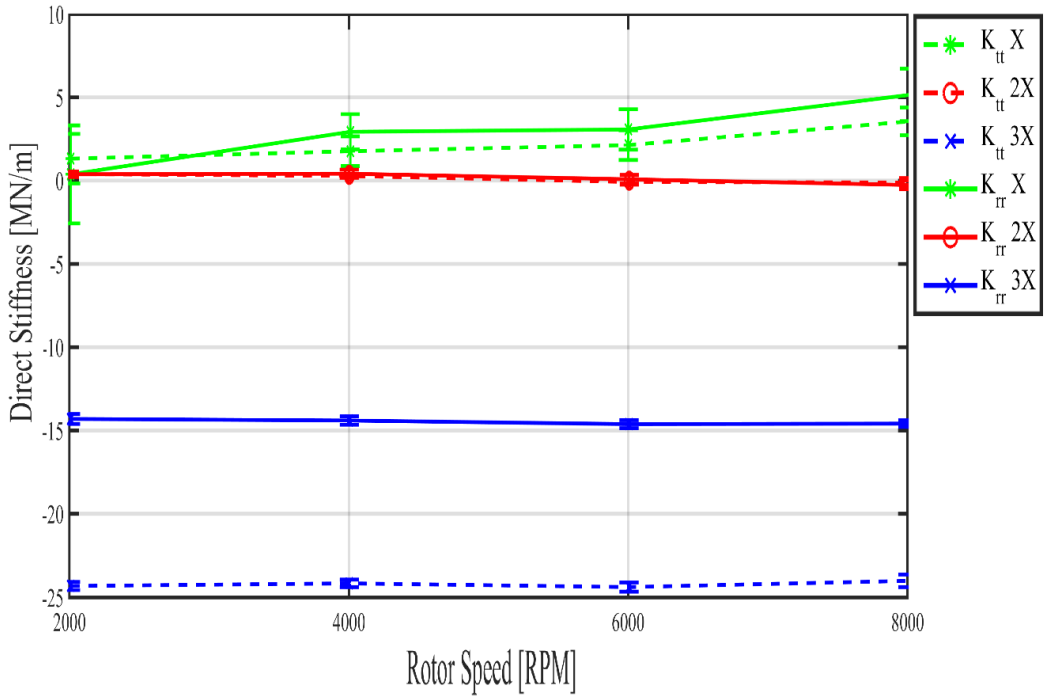

Figure 41. Measured K_{tt} and K_{rr} versus ω at ε_0 = 0.00 and ΔP = 4.14 bar.

Figure 42 shows measured and predicted K_{tt} and K_{rr} versus ω at ε_0 = 0.00 and ΔP = 4.14 bar. For the 1X clearance seal, Fig 42a shows that K_{rr} is under predicted by about 3-5 times. Predictions match measurements for the 2X clearance seal. As mentioned in Fig. 42, K_{rr} is predicted to be negative while measurements show comparatively large negative values. Note that at ω = 2krpm, the uncertainty value of measured K_{rr} is of the same order of magnitude; hence, the point is not shown in the figure.

Figure 42b shows that K_{tt} is under predicted by about 2-4 times for 1X clearance seal. Predictions match measurements for the 2X clearance seal. As with K_{rr} , K_{tt} is predicted to be positive while measurements show large negative values.

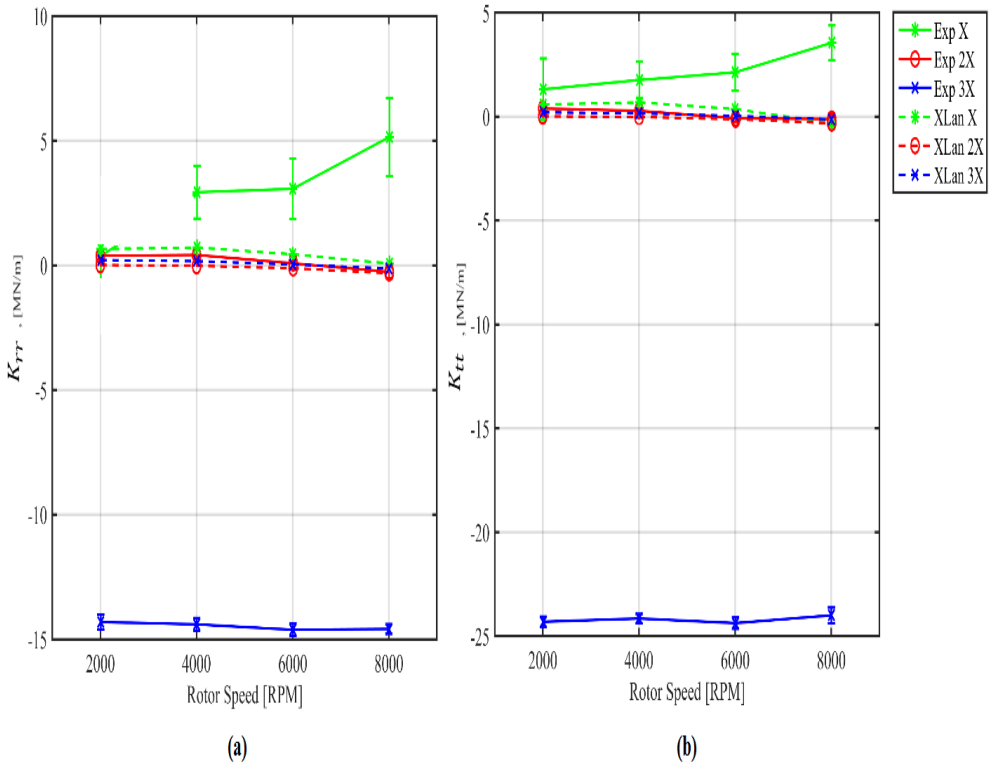

Figure 42. ε_0 = 0.00 and ΔP = 4.14 bar (a) Measured and predicted K_{rr} versus ω. (b) Measured and predicted K_{tt} versus versus ω.

Figure 43a shows measured K_{tr} and K_{rt} versus ε_0 at ΔP = 2.07 bar and ω = 4krpm. For 1X and 2X clearance seals, $K_{rt} \cong -K_{tr}$ indicating destabilizing characteristics. Increasing the clearance from 1X to 2X decreases the cross-coupled stiffness. Increasing from 2X to 3X causes K_{tr} and K_{rt} to both become positive and no longer destabilizing; hence, the SBs are effective at the 3X clearance.

Figure 43b shows predicted K_{tr} and K_{rt} versus ε_0. The predictions agree well with test data for 1X and 2X clearance seals. For the 3X clearance seal, the model predicts

different signs of K_{tr} and K_{rt} which could destabilize the pump. Measurements show that K_{tr} and K_{rt} are both positive, thus not destabilizing.

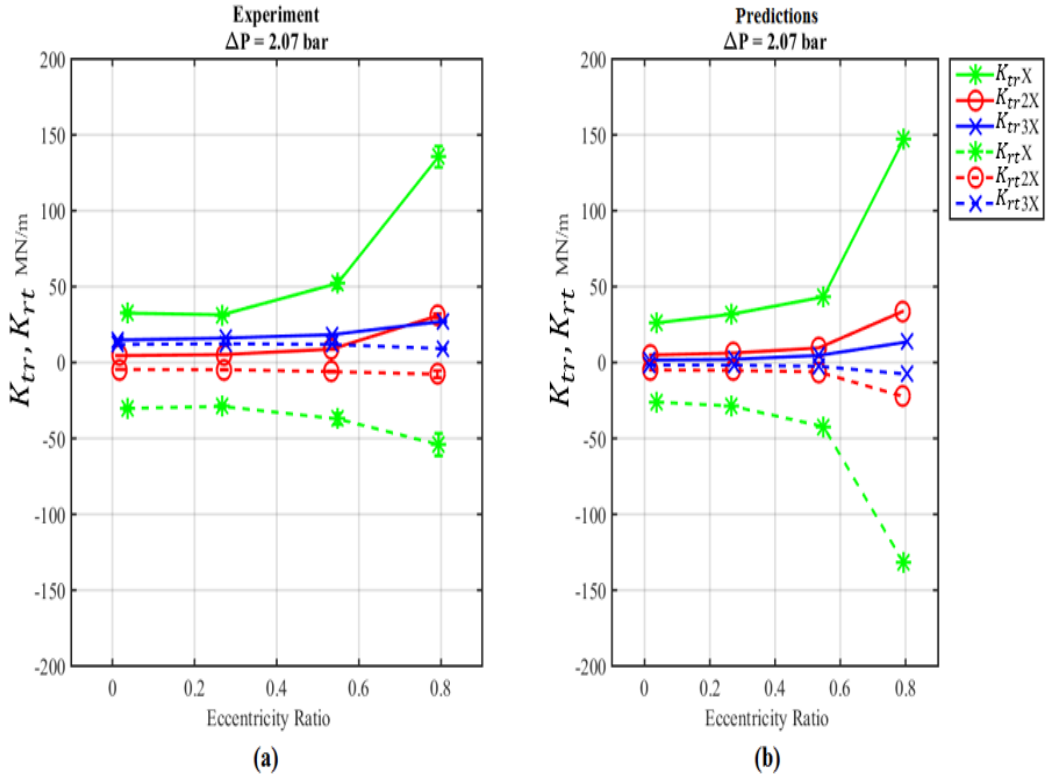

Figure 43. ΔP = 2.07 bar and ω = 4krpm (a) Measured K_{tr} and K_{rt} versus ε_0. (b) Predicted K_{tr} and K_{rt} versus ε_0.

Figure 44a shows measured K_{tr} and K_{rt} versus ΔP at ε_0 = 0.27 and ω = 6 krpm. For the 1X clearance seals, $K_{rt} \cong -K_{tr}$ and increases in magnitude as ΔP increases. K_{tr} and K_{rt} remain constant with increasing ΔP for the 2X and 3X clearance seals. Note for the 3X clearance seal, measured K_{tr} and K_{rt} differ in magnitude and are both positive as discussed in Fig. 43.

Figure 44b shows predicted K_{tr} and K_{rt} versus ΔP. For the 1X and 2X clearance seals, predicted K_{tr} and K_{rt} match the measured K_{tr} and K_{rt}. However, for the 3X clearance seal, K_{tr} and K_{rt} are predicted to have different signs while Fig. 44a shows them as positive.

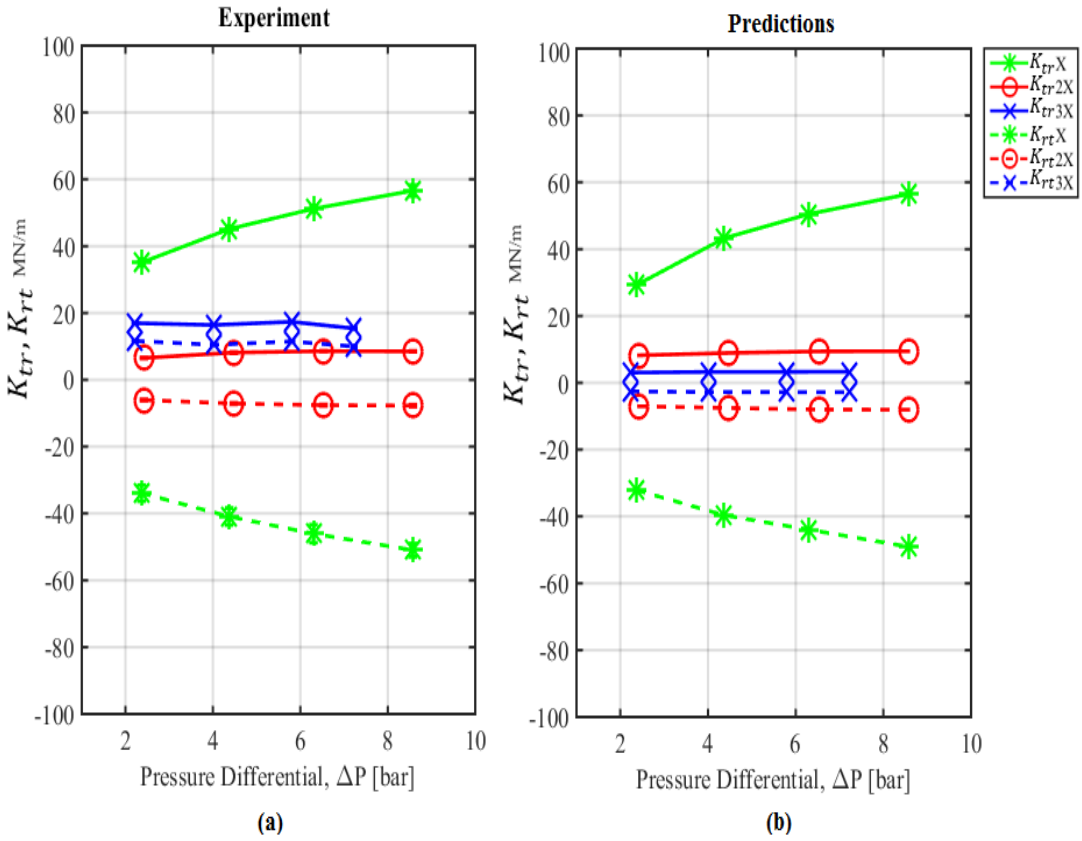

Figure 44. ε_0 = 0.27 and ω = 6 krpm (a) Measured K_{tr} and K_{rt} versus ΔP. (b) Predicted K_{tr} and K_{rt} versus ΔP.

Figure 45a shows measured K_{tr} and K_{rt} versus ω at ε_0 = 0.27 and ΔP = 4.14 bar. For all the clearances, K_{tr} and K_{rt} increase in magnitude with increasing ω. For the 1X

and 2X clearances seals, K_{tr} and K_{rt} have different signs. For the 3X clearance seal, K_{tr} and K_{rt} are both positive and no longer destabilizing.

Figure 45b shows predicted K_{tr} and K_{rt} versus ω. Predicted K_{tr} and K_{rt} match the test data very well for the 1X and 2X clearances. However, for the 3X clearance, predicted K_{tr} and K_{rt} have the same magnitude and opposite signs unlike measured K_{tr} and K_{rt} showing that SBs are working in minimizing circumferential fluid flow.

However, recall that measured K_{tt} and K_{rr} are negative at the 3X clearance. The 3X clearance seal 's negative direct stiffness coefficients would drop the pump's natural frequency, which would tend (by itself) to destabilize the pump rotor.

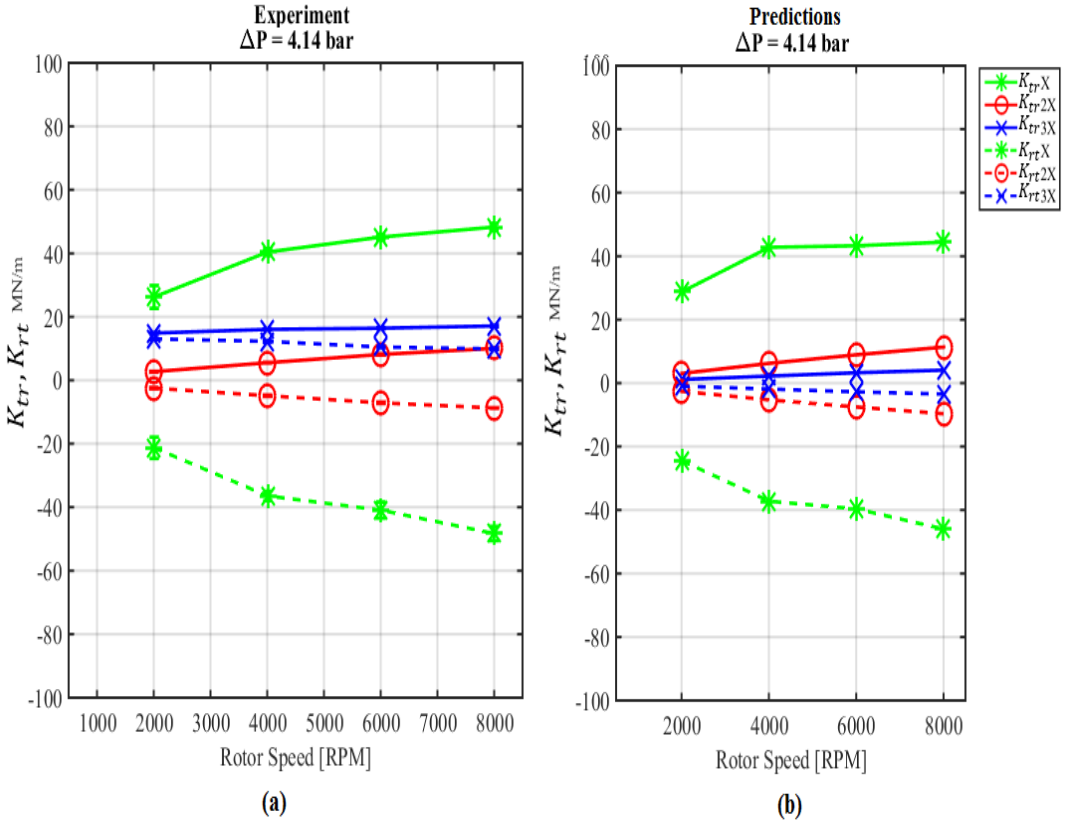

Figure 45. ε_0 = 0.27 and ΔP = 4.14 bar (a) Measured K_{tr} and K_{rt} versus ω. (b) Predicted K_{tr} and K_{rt} versus ω.

Damping

Figure 46 shows measured C_{tt} and C_{rr} versus ε_0 at ΔP = 2.07 bar and ω = 2 krpm for all clearances. C_{rr} increases as ε_0 increases and C_r decreases. Note that for ε_0 > 0.00, C_{rr} is greater than C_{tt} since the rotor is moving closer to the seal wall in the r direction compared to the t direction. C_{tt} and C_{rr} remain close to each other up to ε_0 = 0.27 and then start to diverge for all the three clearances.

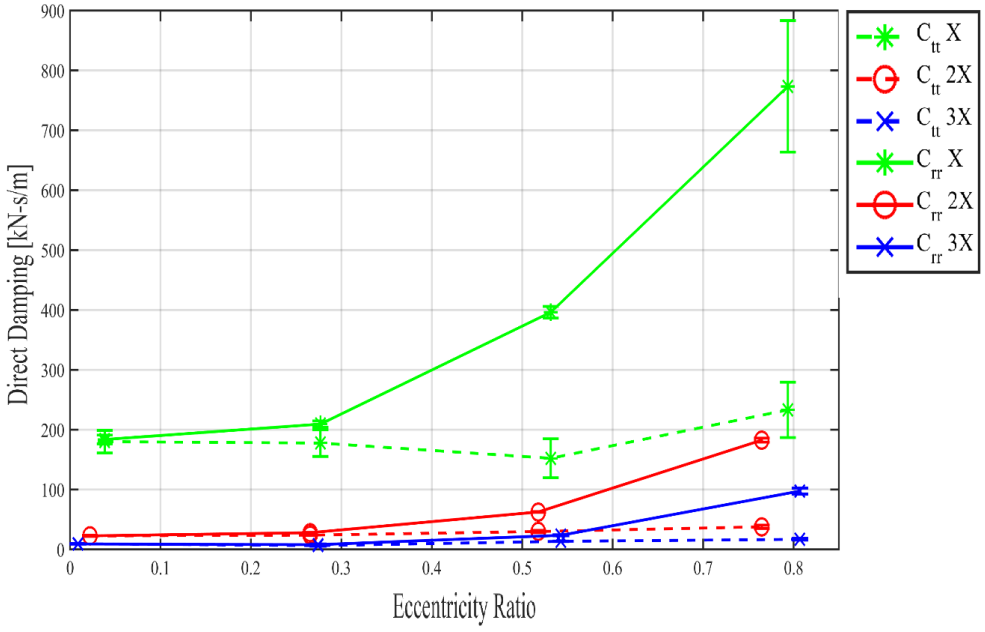

Figure 46. Measured C_{tt} and C_{rr} versus ε_0 at ΔP = 2.07 bar and ω = 2 krpm.

Figure 47a shows measured and predicted C_{rr} versus ε_0 at ΔP = 2.07 bar and ω = 2 krpm for all clearances. C_{rr} increases as ε_0 increases for all clearances. The predictions match the measurements very well for the 2X and 3X seals and the 1X seal out to $\varepsilon_0 \leq$ 0.57. However, for the 1X clearance seal, predicted damping is higher than measured at ε_0 = 0.80.

Figure 47b shows measured and predicted C_{tt} versus ε_0 at ΔP = 2.07 bar and ω = 2 krpm for all clearances. For the 1X clearance seal, C_{tt} decreases up to an ε_0 = 0.51 and then increases. The predictions follow the same trend but the predicted magnitude is higher. For the 2X and 3X clearance seals, C_{tt} increases as ε_0 increases, and the predictions closely match the measurements.

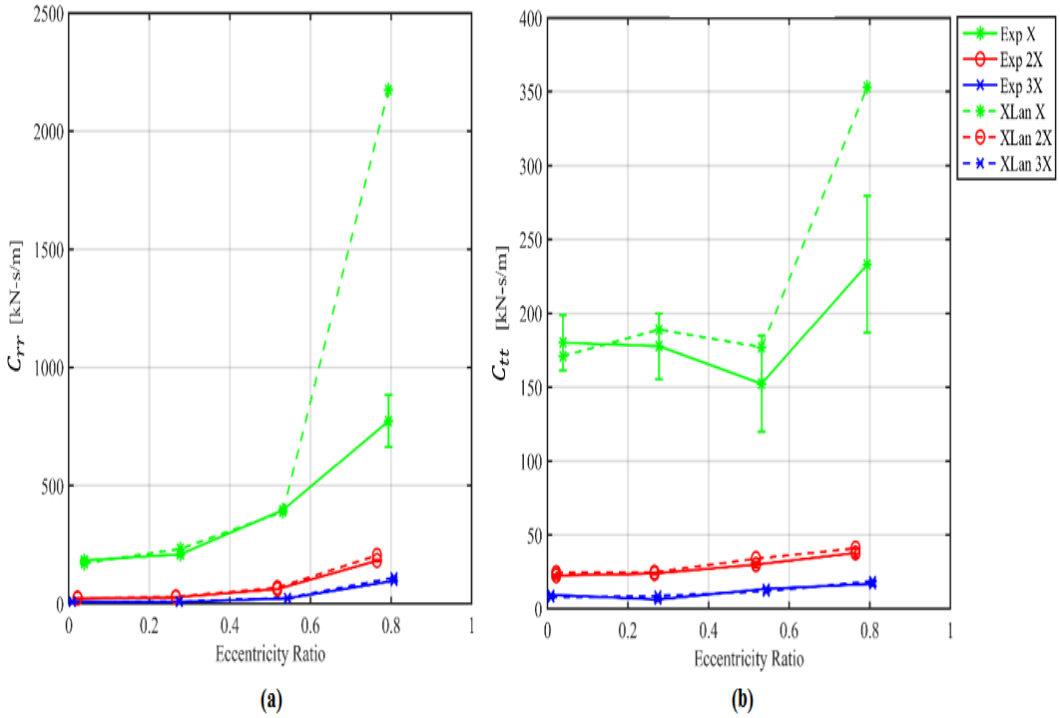

Figure 47. ΔP = 2.07 bar and ω = 2 krpm (a) Measured and Predicted C_{rr} versus ε_0. (b) Measured and Predicted C_{tt} versus ε_0.

At ε_0 = 0.00, C_{tt} and C_{rr} are both measured and predicted to be nearly equal. Figure 48 shows measured and predicted C_{rr} versus ΔP for all clearances at ε_0 = 0.00 and ω = 6 krpm. It decreases as clearance increases. C_{rr} is independent of ΔP for 2X and 3X clearance seals. For the 1X clearance seal, C_{rr} increases as ΔP increases. The model under predicts C_{rr} by about 30 kN-s/m at all eccentricity ratios. The predictions agree well with test data for the 2X and 3X clearance seals.

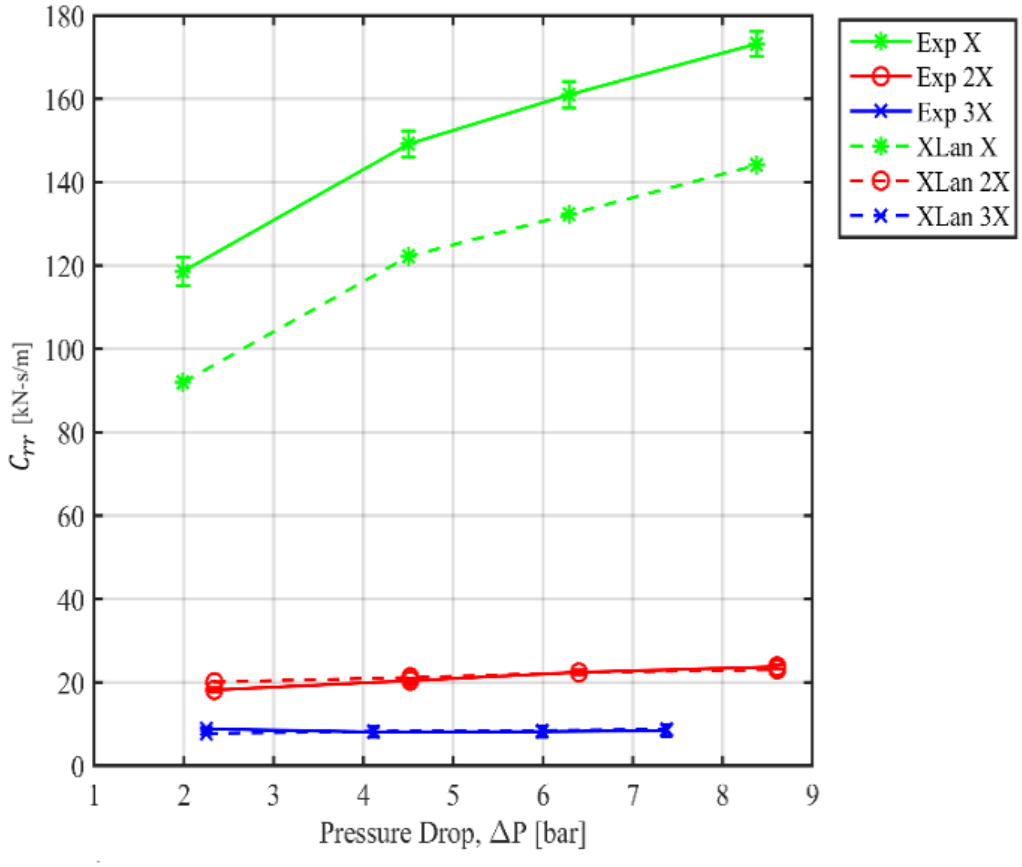

Figure 48. Measured and Predicted C_{rr} versus ΔP at ε_0 = 0.00 and ω = 6 krpm.

Figure 49 shows measured and predicted C_{rr} versus ω for all clearances at ε_0 = 0.00 and ΔP = 8.28 bar. C_{rr} decreases as clearance increases. C_{rr} decreases as ω increases for the 1X clearance seal. For 2X and 3X clearance seals, C_{rr} is independent of ω. The model agrees well with test data for 2X and 3X clearance seals. For the 1X clearance seal measured C_{rr} is larger than predicted. For speeds above 2 krpm, measured C_{rr} is larger than predicted by roughly 25%.

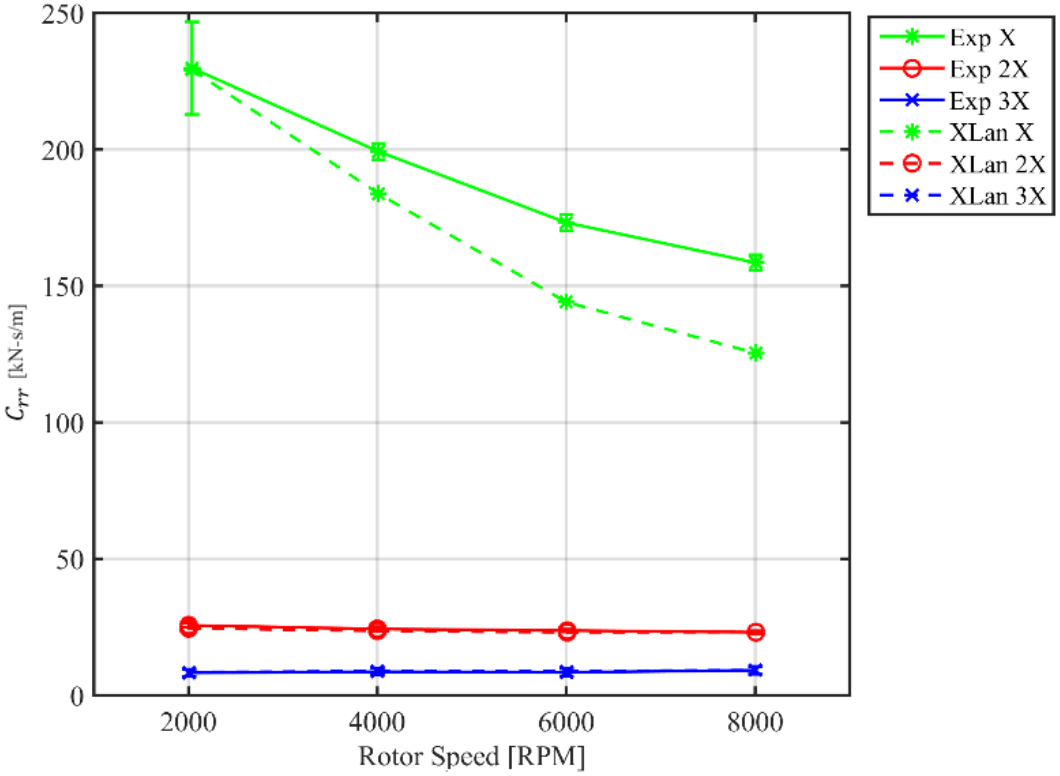

Figure 49. Measured and Predicted C_{rr} versus versus ω at ε_0 = 0.00 and ΔP = 8.28 bar.

Figure 50a shows measured and predicted C_{tr} versus ε_0 for all clearances at ΔP = 6.21 bar and ω = 4 krpm. Measured and predicted C_{tr} remains close to zero up to ε_0 = 0.53 and increases at ε_0 = 0.80 for all clearances. For the 1X clearance seal, predicted C_{tr} is larger than measured by about 5 times. For the 2X clearance seal at ε_0 > 0.27, predicted C_{tr} is larger than measured by about 10%. Predictions match measurements well for the 3X clearance seal.

Figure 50b shows C_{rt} versus ε_0. Measured and predicted C_{rt} remains close to zero up to ε_0 = 0.53 and increases at ε_0 = 0.80 for all the three clearance seals. For the 1X

clearance seal, predicted C_{tr} is larger than measured by about 2 times. For the 2X clearance seal at $\varepsilon_0 > 0.27$ predicted C_{tr} is larger than measured by about 10%. Predictions match measurements well for the 3X clearance seal.

Note that both C_{tr} and C_{rt} have large positive values for the 1X clearance seal at $\varepsilon_0 = 0.80$. Figure 51 shows $Im(\boldsymbol{H}_{XY})$ and $Im(\boldsymbol{H}_{YX})$ versus Ω at $\varepsilon_0 = 0.8$, $\Delta P = 6.21$ bar and ω = 4 krpm for the 1X clearance seal. $Im(\boldsymbol{H}_{XY})$ and $Im(\boldsymbol{H}_{YX})$ are both negative and decreasing as Ω increases. Curvefitting these functions produces C_{XX} = 217.5 kNs/m, C_{XY} = -213.2 kNs/m, C_{YX} =-85.0 kNs/m C_{YY} = 681.5 kNs/m. After the coordinate transformation with ϕ = 33.2° (refer to Eq. (24)), C_{tr} = 89.1 kNs/m and $C_{rt} = 217.4$ kNs/m. Note that when C_{tr} and C_{rt} have the same sign, they act as real dissipative damping and not gyroscopic damping.

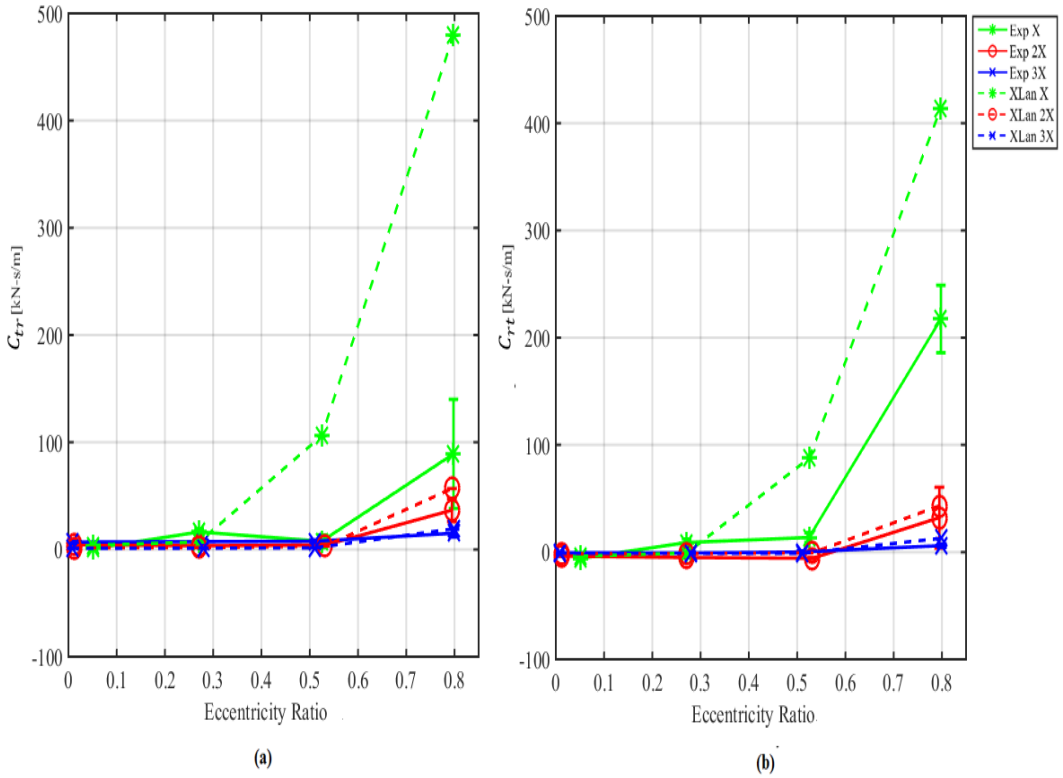

Figure 50. ΔP = 6.21 bar and ω = 4 krpm (a) Measured and predicted C_{tr} versus ε_0. (b) Measured and predicted C_{rt} versus ε_0.

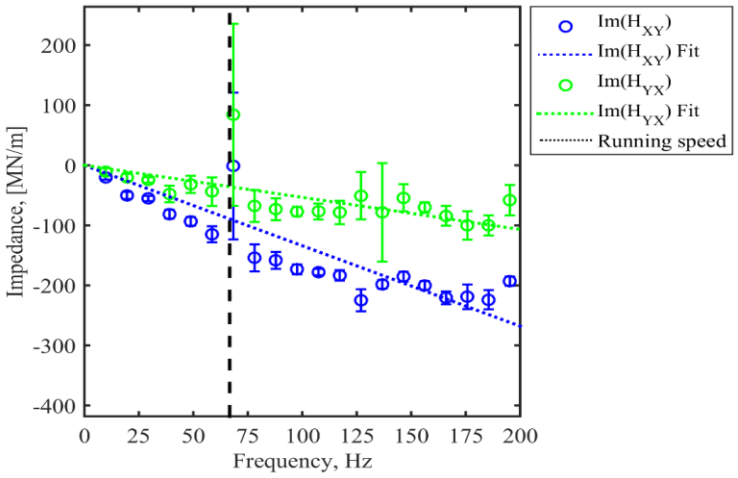

Figure 51. $Im(H_{XY})$ and $Im(H_{YX})$ versus Ω at ε_0= 0.8, ΔP = 6.21 bar and ω = 4 krpm for the 1X clearance seal .

Figure 52a shows C_{tr} versus ΔP for all clearances at ε_0 = 0.80 and ω = 4 krpm. Measured and predicted C_{tr} decrease as C_r increases. Measured C_{tr} is independent of ΔP for any of the clearances tested. However for the 1X clearance seal, predicted C_{tr} increases as ΔP increases. Predicted C_{tr} is about 4.5 times larger than measurements for the 1X clearance seal, 1.1 times for the 2X clearance seal and 1.05 times for the 3X clearance seal.

Figure 52b shows C_{rt} versus ΔP. Measured C_{rt} is higher than C_{tr} for the 1X clearance seal. For the 2X and 3X clearance seals, C_{rt} and C_{tr} have approximately equal values. Measured C_{rt} increases slightly as ΔP increases for the 1X clearance seal. Measured C_{rt} is independent of ΔP for the 2X and 3X clearance seals. C_{rt} is over predicted by 2 times for the 1X clearance seal, by 1.1 times for the 2X clearance seal and 1.05 times for the 3X clearance seal.

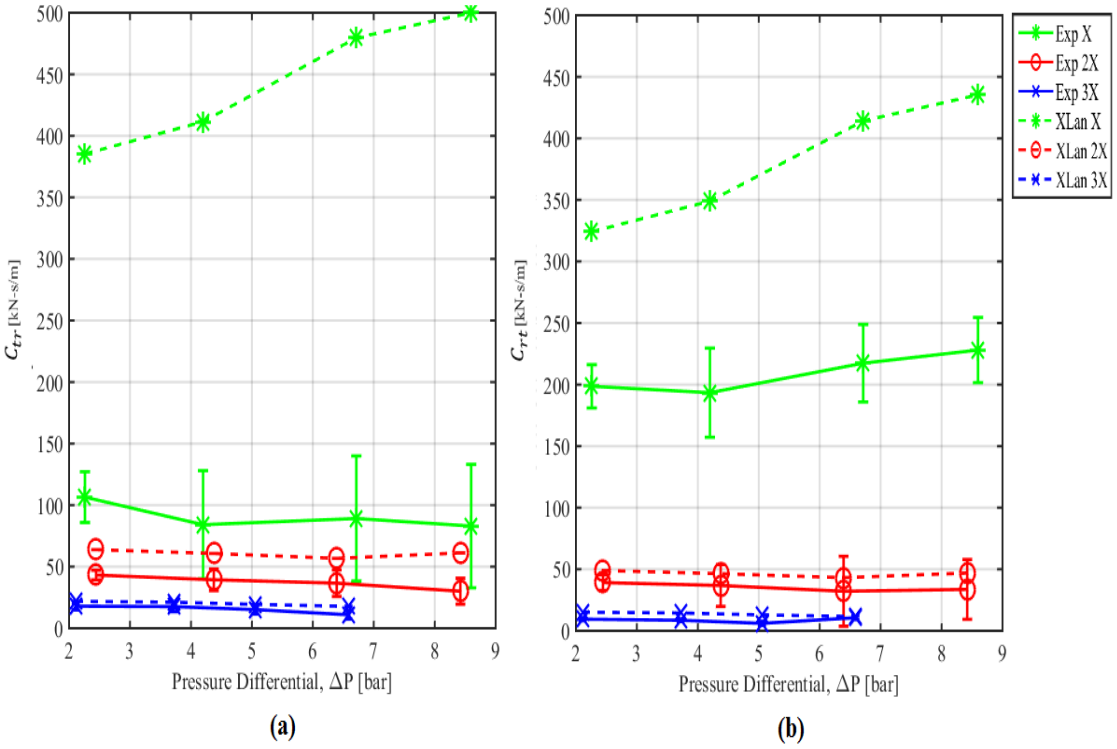

Figure 52. ε_0 = 0.80 and ω = 4 krpm (a) C_{tr} versus ΔP. (b) C_{rt} versus ΔP.

Figure 53a shows C_{tr} versus ω for all clearances at ε_0 = 0.00 and ΔP = 6.21 bar. C_{tr} generally decreases as clearance increases. C_{tr} increases as ω increases. Measured C_{tr} is about 4 times higher than predicted C_{tr} for the 2X and 3X clearance seals. Note that at ω = 2krpm, the uncertainty value of measured C_{tr} is of the same order of magnitude; hence, the point is not shown in the figure.

Figure 53b shows C_{rt} versus ω. C_{rt} generally decreases as clearance increases. It decreases as ω increases. Measured C_{rt} is negative at ω greater than 2 krpm. Measured C_{tr} is about 4 times lower than predicted C_{tr} for the 2X and 3X clearance seals. Note that

at $\omega = 2$krpm, the uncertainty value of measured C_{rt} is of the same order of magnitude; hence, the point is not shown in the figure. Opposite signs suggest that C_{tr} and C_{rt} would act as gyroscopic damping at these test conditions.

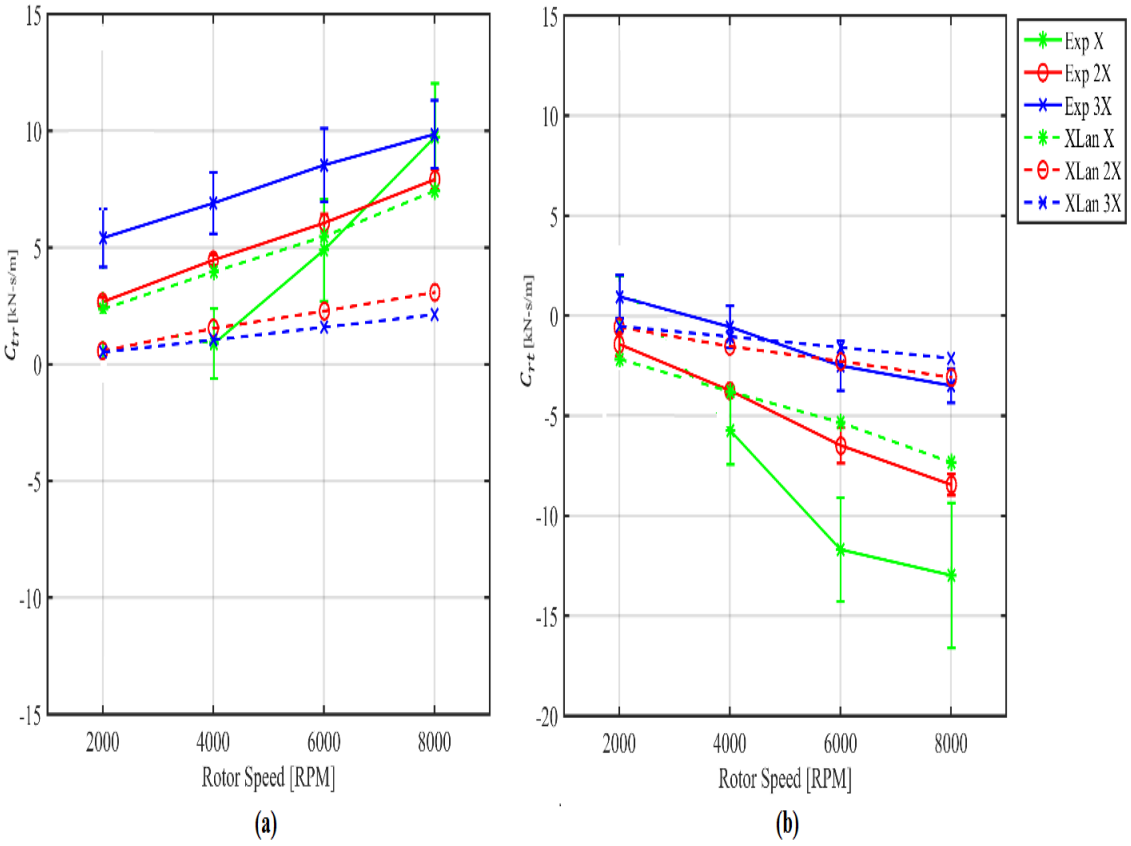

Figure 53. $\varepsilon_0 = 0.00$ and $\Delta P = 6.21$ bar (a) Measured and predicted C_{tr} versus ω. (b) Measured and predicted C_{rt} versus versus ω.

Virtual Mass Coefficients

Figure 54 shows measured M_{tt} and M_{rr} versus ε_0 for all clearances at $\Delta P = 2.07$ bar and ω = 4 krpm. M_{tt} and M_{rr} decrease as ε_0 increases for the 1X clearance seal. They

are largely independent of ε_0 for 2X and 3X clearance seals. For the 1X clearance seal, M_{rr} becomes negative with a large amplitude for ε_0 = 0.80. Recall that M_{tt} and M_{rr} are obtained as the curvature of $Re(\boldsymbol{H}_{ii})$ and $Re(\boldsymbol{H}_{jj})$ as shown in figures 33c, 34c. A negative value would suggest that the curve is directed upwards. Figure 55 shows $Re(\boldsymbol{H}_{XX})$ and $Re(\boldsymbol{H}_{YY})$ versus Ω at ε_0 =0.8, ΔP = 2.07 bar, ω = 4 krpm for the 1X clearance seal. As evident from the figure, the curves are moving upward, indicating a negative value for the direct virtual mass term in the X-Y coordinate system. After coordinate transformation (refer to Eq. (24)), M_{rr} is found to be negative. Note that the negative direct virtual mass term can increase the natural frequency of the rotordynamic system. For example, for the 1X clearance seal at ε_0 =0.8, ΔP = 2.07 bar and ω = 4 krpm, comparing $M_{rr}\,\omega^2$ to K_{rr}, the resultant K_{rr} increases by about 9%.

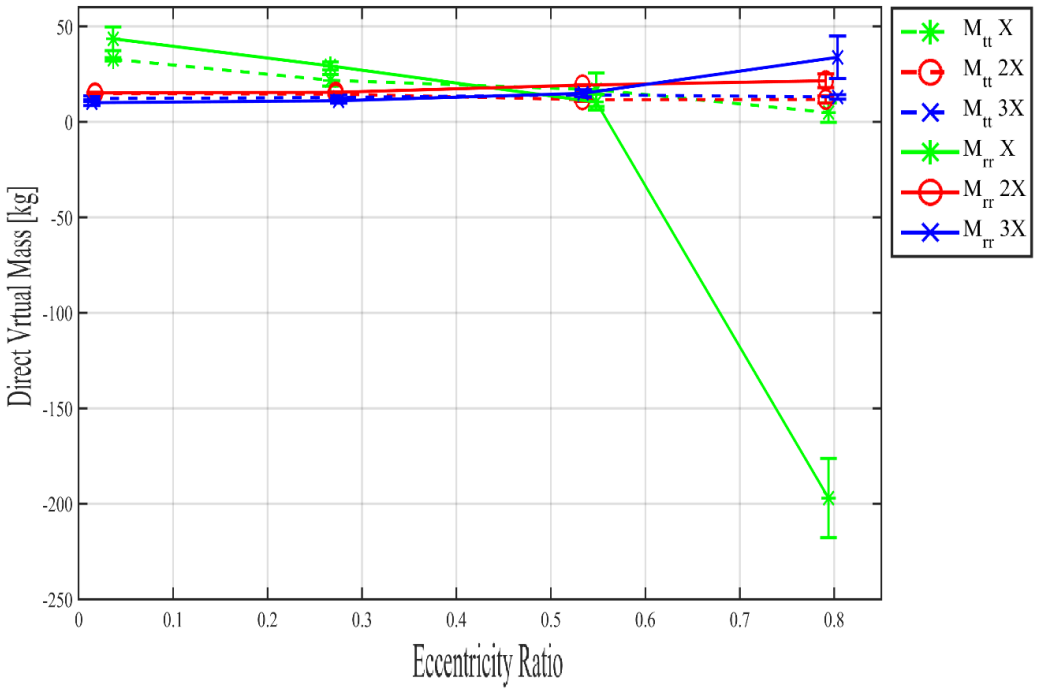

Figure 54. Measured M_{tt} and M_{rr} versus ε_0 at ΔP = 2.07 bar and ω = 4 krpm.

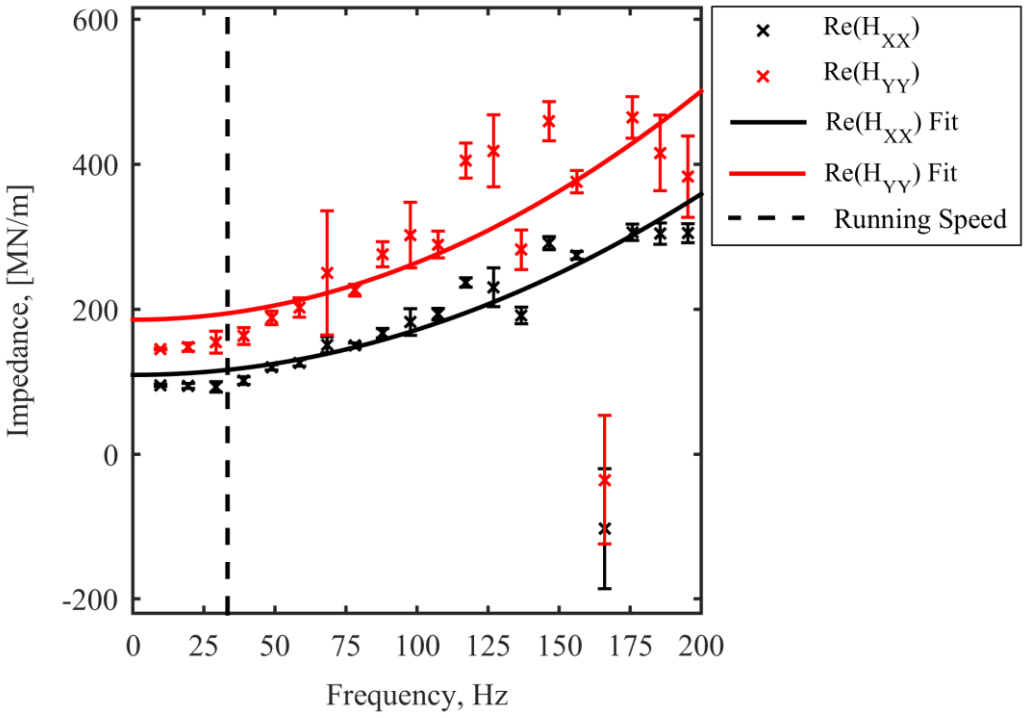

Figure 55. $Re(H_{XX})$ and $Re(H_{YY})$ versus Ω at ε_0 =0.8, ΔP = 2.07 bar, ω = 4 krpm for the 1X clearance seal.

Figure 56a shows measured and predicted M_{rr} versus ε_0 for all clearances at ΔP = 2.07 bar and ω = 4 krpm. For the 1X clearance seal, M_{rr} decreases with increasing ε_0. For the 2X and 3X clearance seals, measured M_{rr} is a weak function of ε_0 and increases as ε_0 increases. For the 1X seal, predicted M_{rr} is about 3 times lower than predicted M_{rr} for the 2X and 3X clearance seals and independent of ε_0. The model predicts a negative M_{rr} at ε_0 = 0.8, and the data agrees.

Figure 56b shows measured and predicted M_{tt} versus ε_0. For the 1X clearance seal, measured and predicted M_{tt} are positive and decrease with increasing ε_0. For the 2X and 3X clearance seals, measured M_{tt} is largely independent of ε_0. For the 2X and 3X clearance seals, predicted M_{tt} is about 3 times lower than measured. The model predicts a negative M_{tt} at ε_0 = 0.53, 0.8 while the data shows M_{tt} to be positive at all eccentricity ratios.

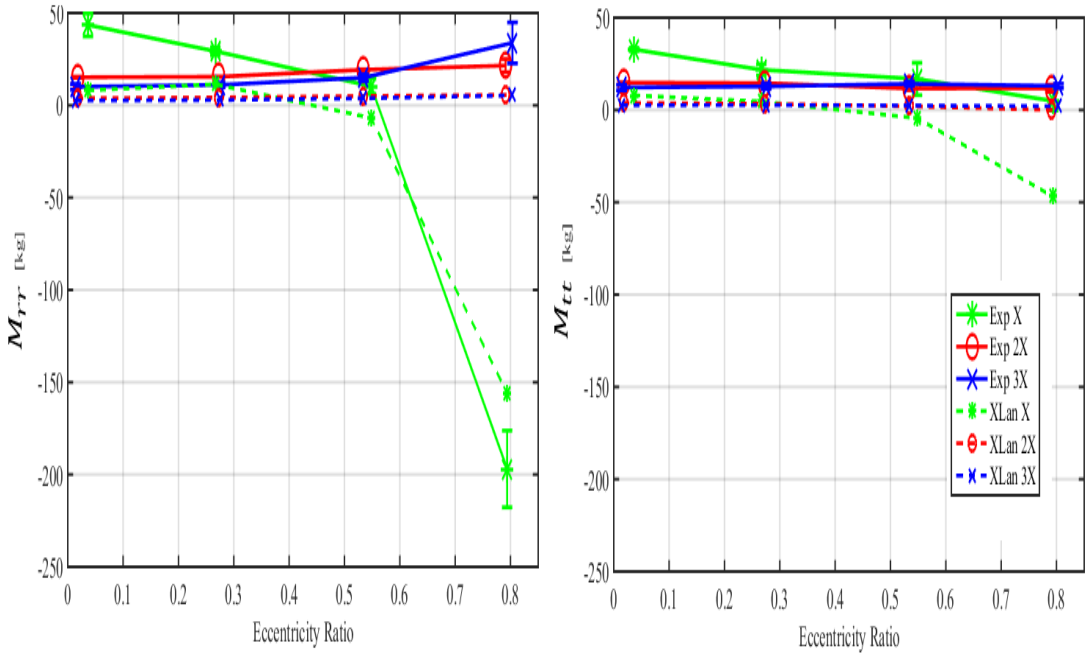

Figure 56. ΔP = 2.07 bar and ω = 4 krpm (a) Measured and predicted M_{rr} versus ε_0. (b) Measured and predicted M_{tt} versus ε_0.

Figure 57 shows measured M_{tt} and M_{rr} versus ΔP for all clearances at ε_0 = 0.00 and ω = 2 krpm. For the 1X clearance seal, M_{tt} decreases as ΔP increases. For the 2X and 3X clearance seals, M_{tt} slightly increases as ΔP increases. For the 1X clearance seal, M_{rr}

decreases as ΔP increases. For the 2X and 3X clearance seals, M_{rr} slightly increases as ΔP increases. M_{tt} is larger than M_{rr} for the 1X and 3X clearance seals while nearly the same for the 2X clearance seal.

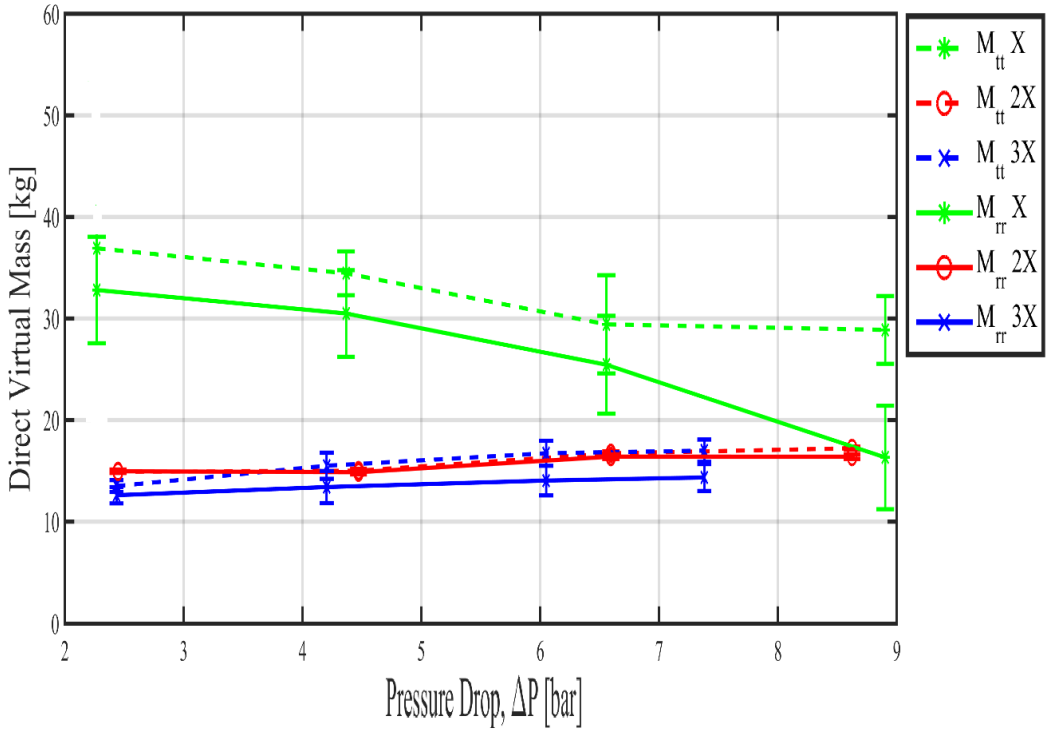

Figure 57. Measured M_{rr} and M_{tt} versus ΔP at ε_0 = 0.00 and ω = 2 krpm.

Figure 58 shows measured and predicted M_{tt} versus ΔP for all clearances at ε_0 = 0.00 and ω = 2 krpm. Measured M_{tt} decreases as ΔP increases for the 1X clearance. . Predicted M_{tt} increases with ΔP for the 1X clearance seal. For the 2X and 3X clearance seals, measured M_{tt} slightly increases with increasing ΔP while predicted M_{tt} slightly

decreases. Measured data is about 7 times larger than predicted data at all ΔPs. M_{rr} behaves similarly and is not shown here.

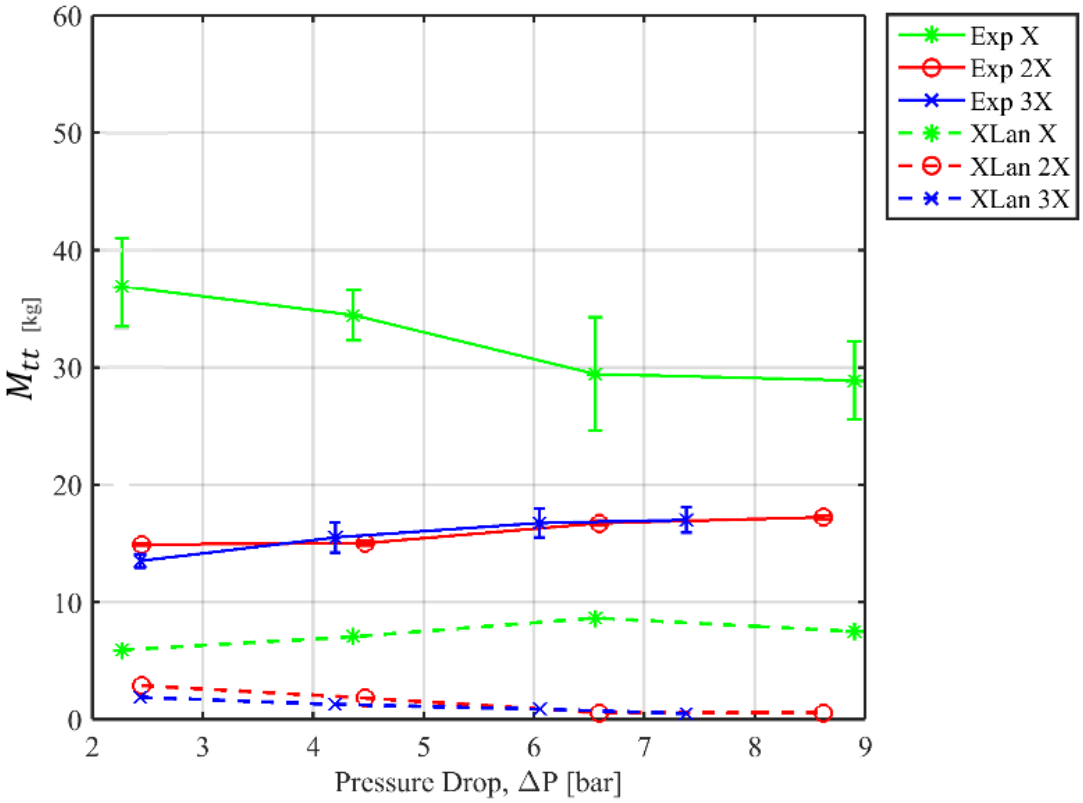

Figure 58. Measured and predicted M_{tt} versus ΔP at ε_0 = 0.00 and ω = 2 krpm.

Figure 59 shows measured M_{tr} and M_{rt} versus ε_0 for all clearances at ΔP = 6.21 bar and ω = 6 krpm. For $\varepsilon_0 \leq 0.53$, the error bars are the same order of magnitude and comparable to measured data at all the conditions tested. Therefore, these findings are not completely reliable. The magnitude and signs of M_{tr} and M_{rt} are difficult to view. Table 3 shows the stability impact of M_{tr} and M_{rt} versus ε_0 for all clearances at ΔP = 6.21 bar

and ω = 6 krpm. Note that (a) if M_{tr} and M_{rt} have the same signs, they do not impact the stability of the system (referred as 0), (b) if $M_{tr} > 0$ and $M_{rt} < 0$, they drive backward whirl (referred as Stabilizing FWD) and (c) if $M_{tr} < 0$ and $M_{rt} > 0$, they drive forward whirl (referred as Destabilizing FWD).

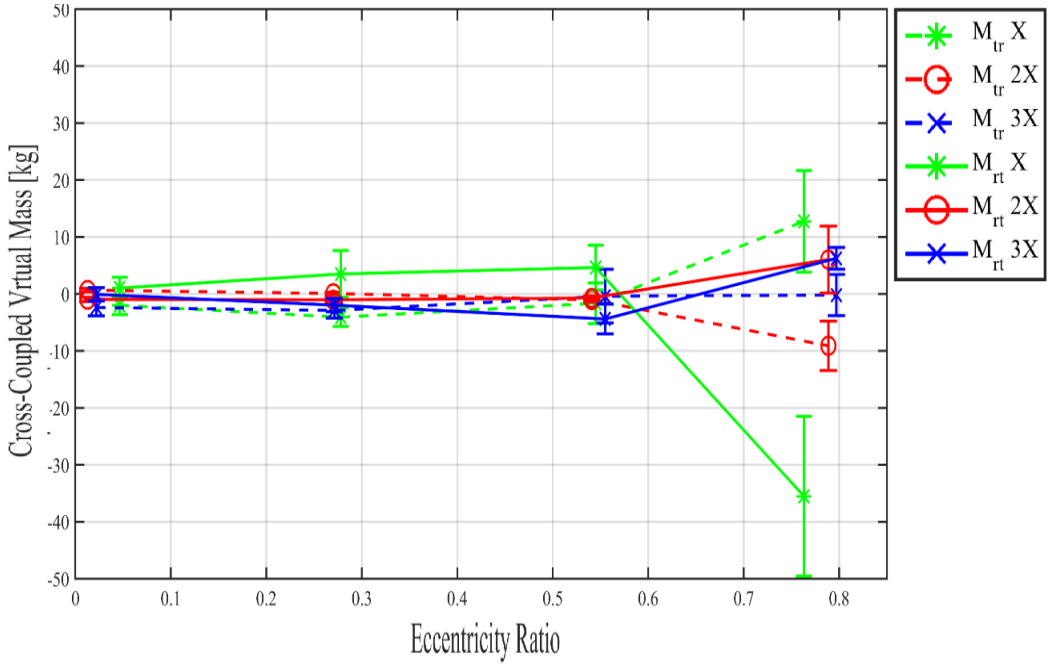

Figure 59. Measured M_{tr} and M_{rt} versus ε_0 at ΔP = 6.21 bar and ω = 6 krpm.

Table 3. Stability impact of M_{tr}, M_{rt} at ΔP = 6.21 bar and ω = 6krpm.

	ε_0			
Clearance	**0.00**	**0.27**	**0.53**	**0.80**
1X	Destabilizing FWD	Destabilizing FWD	Destabilizing FWD	Stabilizing FWD
2X	Stabilizing FWD	Stabilizing FWD	0	Destabilizing FWD
3X	0	0	0	Destabilizing FWD

7.6 Whirl Frequency Ratio

Figure 60 shows WFR [11] as function of ε_0 at ΔP = 4.14 bar and ω = 6 krpm. For the 1X and 2X clearance seals, WFR drops from approximately 0.5 to zero in moving from ε_0 =0.53 to ε_0 = 0.8. Note that this behavior resembles that of a plain journal bearing. For a clearance of 3X, since K_{tr} and K_{rt} have the same sign, WFR remains zero at all eccentricity ratios.

The model predicts well for 1X and 2X clearance. For the 3X clearance seal however, measured K_{tr} and K_{rt} have the same signs producing WFR = 0. The model predicts different signs for K_{tr} and K_{rt} netting WFR ≅ 0.5.

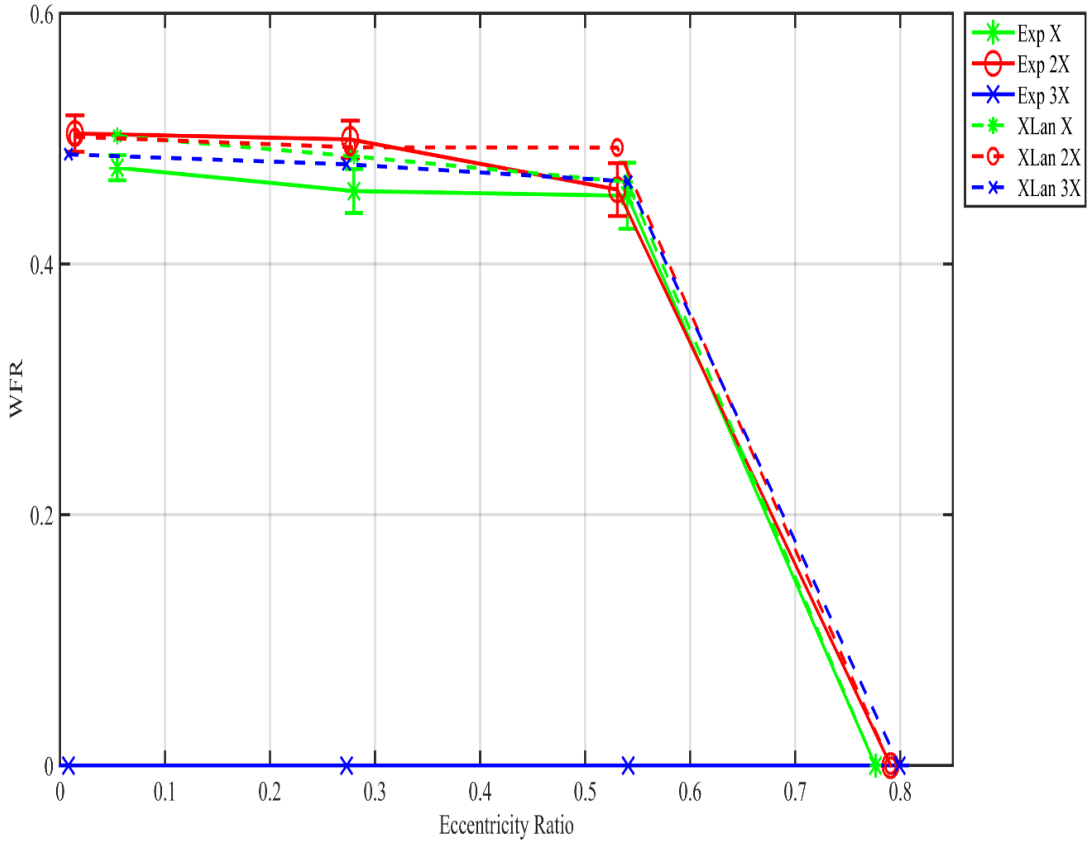

Figure 60. Measured and Predicted WFR versus ε_0 at ΔP = 4.14 bar and ω = 6 krpm.

WFR is independent of ΔP and ω for all the three clearances. Those results are not shown here. Note, as discussed in section 7.4, for the 3X clearance seal, K_{rr} and K_{tt} are negative for most of the test cases. The pump's first critical speed depends on the direct stiffness. Negative direct stiffness values would drop the natural frequency, thus worsening stability. For an ESP, a negative stiffness could cause the rotor to rub with the stator wall. However, unless there are different signs for K_{tr} and K_{rt}, a seal will not cause a dynamic instability.

8. SUMMARY & CONCLUSIONS

8.1 Summary

The study involved tests using a smooth seal with three radial clearances $C_r = 127\mu m, 254\mu m, 381\mu m$ (1X, 2X and 3X respectively), an axial length of 45.72 mm (1.80 in) and a diameter of 101.6 mm (4.00 in). An insert with 12 nozzles was used to induce pre-swirl upstream of the seal. Swirl brakes were used to reduce circumferential fluid flow at the seal inlet. Swirl brakes comprised 36 square cuts at the seal entrance with an axial depth of 5.08 mm (0.2 in), radial height of 6.35 mm (0.25 in) and circumferential width of 6.35 mm (0.25 in) each. The author conducted static and dynamic measurements at ω = 2, 4, 6, 8 krpm, ΔP = 2.07, 4.14, 6.21, 8.27 bar (30, 60, 90, 120 psi), and eccentricity ratios $\varepsilon_0 = e_0/C_r =$ 0.00, 0.27, 0.53, and 0.80. The test used ISO VG 46 oil at a range of 115-120 °F to keep fluid flow laminar (Total $Re \leq 650$). Dynamic measurements included components of the following vectors (a) stator-rotor relative displacements, (b) acceleration and (c) applied dynamic force in the X-Y coordinate system. Measurements were also compared to predictions by a code developed by Zirkelback and San Andrés [16].

8.2 Static Results

As expected, volumetric rate leakage $\dot{Q}$ increases as C_r increases. $\dot{Q}$ increases as ε_0 increases. $\dot{Q}$ increases as ΔP increases.

$\dot{Q}$ is independent of ω for the 2X and 3X clearance seal but increases with increasing ω for the 1X clearance seal. Measured $\dot{Q}$ is larger by about 23% than predicted for the 3X clearance seal.

Upstream circumferential velocity v_i is measured at one location with a pitot tube (refer to Fig. 22 and 23 for location of inlet pitot tube).As expected, v_i increases as C_r and ω increase.

Interestingly, v_i is influenced by the inlet velocity from the pre-swirl insert v_{insert} (refer Eq. (15)) to the extent that generally v_i (3X) > v_i (2X) > v_i (1X). As ΔP increases, v_i tends to trend more with v_{insert} and less with $R\omega$.

For the 1X clearance seal, the downstream circumferential v_o (refer to Fig. 22 and 24 for outlet pitot tube location) is independent of ω. At ΔP = 8.27 bar, for the 2X and 3X clearance seals, v_o increases as ω increases. There is no clear relation between v_o and ΔP for any of the clearances. Measured v_o is also less than the expected exit bulk fluid velocity ($R\omega/2$) for all the three clearance, but it is measured downstream of the seal exit.

Notably for the 1X clearance seal at ε_0 = 0.27, $\phi \geq 90°$ an indication that fluid inertia effects are important [21]. For the 3X clearance seal, $\phi \cong 180°$ at ε_0 = 0.27, 0.53, ΔP = 2.07 bar and ω = 8krpm. This implies that there is no forward destabilizing force and that the centering force is negative.

As expected, the applied static load F_s increases as ε_0 increases, and decreases C_r increases. For the 1X and 2X clearance seals, measured applied static load is positive at all test conditions. For the 3X clearance seal, F_s is negative at ε_0 = 0.27, 0.53, ΔP = 2.07 bar and ω = 8krpm. This result agrees with the ϕ = 180° results cited above.

8.3 Dynamic Results Summary

Rotordynamic coefficients are presented in the r-t system shown in Fig. 36 with $\boldsymbol{r}$ pointed along the static eccentricity vector $\boldsymbol{e_0}$. Eq. (25) shows the r-t rotordynamic model.

As expected, measured direct stiffness coefficients, K_{rr} and K_{tt} increase as ε_0 increases, bringing the rotor closer to the stator. K_{rr} and K_{tt} decrease as C_r increases. For the 1X clearance seal, measured K_{rr} and K_{tt} increase as ΔP increases. Notably, for the 1X clearance seal K_{rr} and K_{tt} increase as ω increases.

As expected, for the 2X and 3X clearance seal, measured K_{rr} and K_{tt} are independent of ΔP. K_{rr} and K_{tt} are also independent of ω.

Most importantly though, measured K_{rr} and K_{tt} are negative for the 3X clearance seal, an indication that the seal would fail to provide any support to the rotor and "suck" the rotor in. However, the model [16] fails to predict negative stiffness for the 3X clearance seal. The rest of the stiffness data matches well with predictions.

As expected, for the 1X and 2X clearance seals, $K_{tr} \cong -K_{rt}$. Thus they are destabilizing. They increase in magnitude as ε_0 increases. K_{tr} and K_{rt} increase in magnitude as ΔP and ω increase. They also increase as C_r decreases. Predicted K_{tr} and K_{rt} matches the measured data very well.

Interestingly, for the 3X clearance seal, swirl brakes were effective in making K_{tr} and K_{rt} both positive. Thus the seal's cross-coupled stiffness coefficients are no longer destabilizing. Note that the model predicts different signs for K_{tr} and K_{rt}.

As expected, for all clearances, measured C_{rr} increase as ε_0 increases. For the 1X and 2X clearance seals, measured C_{rr} and C_{tt} increase as ΔP increases. For the 2X clearance seal, measured C_{rr} and C_{tt} are independent of ω. For the 3X clearance seal, measured C_{rr} and C_{tt} are independent of ΔP and ω increase. Note that for the 1X clearance seal, C_{rr} and C_{tt} decreases as ω increases.

For the 1X clearance seal, the model predicts higher C_{rr} and C_{tt} than measured at some test conditions while lower for most of the test conditions. For the 2X and 3X clearance seals, predictions match well with test data.

As expected, the magnitude of measured C_{tr} and C_{rt} increases as ε_0 increases. C_{tr} and C_{rt} increase as C_r decreases. C_{tr} and C_{rt} also increases as ω increases. Measured and predicted C_{tr} and C_{rt} at most test conditions, are independent of ΔP. The model [16] predicts higher C_{tr} and C_{rt} values compared to measured data at most of the test conditions.

At most test conditions, surprisingly, measured and predicted C_{tr} and C_{rt} are both positive, an indication that they will act as direct damping as opposed to gyroscopic damping.

For the 1X clearance seal, measured M_{rr} and M_{tt} decrease as ε_0 increases and M_{rr} is negative only at ε_0 = 0.80. A negative direct virtual mass term could increase the first natural frequency of the pump.

For the 2X and 3X clearance seals, measured M_{rr} and M_{tt} increase as ΔP increases. Measured M_{rr} increases while M_{tt} remains constant as ε_0 increases for the 2X

and 3X clearance seals. The model predicts lower M_{rr} and M_{tt} than measurements at most of the test conditions tested.

For most of the test points, the error bars for M_{tr} and M_{rt} are the same order of magnitude and comparable to measured data. Therefore, these findings are not completely reliable.

As expected for the 1X and 2X clearance seals, Whirl frequency ratio WFR decreases and eventually goes to zero as ε_0 increases. For all three seals, WFR is independent of ΔP and ω. The model predicts WFR very well for the 1X and 2X clearance seals at all test conditions

Note that for the 3X clearance seal, WFR remains zero at all test conditions. The model fails to predict zero WFR for the 3X clearance seal.

8.4 Dynamic Results Conclusions and Recommendations

The following points serve to summarize the most important conclusions of the dynamic measurements:

- For the 1X and 2X clearance seals, dynamic measurement trends mostly meet expectations with some dependence on ω.
- For the 1X and 2X clearance seals, SBs have no impact on the rotordynamic coefficients.

- For the 3X clearance seal, measured direct stiffness coefficients are negative. Therefore the natural frequency of the pump would drop significantly, and the rotor could be sucked in to the stator.

- For the 3X clearance seal, swirl brakes were effective in making K_{tr} and K_{rt} both positive. Thus the seal's cross-coupled stiffness coefficients are no longer destabilizing. This result becomes less important, since direct stiffness coefficients are negative.

- Measured and predicted C_{tr} and C_{rt} are both positive for all clearances at most of the test conditions an indication that they will act as direct damping as opposed to gyroscopic damping.

- For the 1X clearance seal, measured virtual mass coefficients are negative at some test conditions, an indication that they could increase the natural frequency of the pump.

- Predictions generally agree well with measurements. Most important discrepancies pertain to stiffness coefficients for the 3X clearance seal. The model [16] fails to predict: (a) negative direct stiffness coefficients, and (b) same signs for the cross-coupled stiffness coefficients.

REFERENCES

[1] Childs, D.W., 2013, *Turbomachinery Rotordynamics with Case Studies*, Wellborn Texas: Minter Spring Publishing.

[2] Childs, D.W., 1983, "Finite-Length Solutions for Rotordynamic Coefficients of Turbulent Annular Seals," *ASME Journal of Lubrication,* **105**, pp. 437-444.

[3] Black, H.F., 1979, "Effects of Fluid-Filled Clearance Spaces on Centrifugal Pump and Submerged Motor Vibrations," in *Eighth Turbomachinery Symposium*, College Station, Texas, Texas A&M University, pp. 29-34.

[4] Black, H.F., 1969, "Effects of Hydraulic Forces in Annular Pressure Seals on the Vibrations of Centrifugal Pump Rotos," *Journal of Mechanical Engineering Science,* **11**, pp. 206-213.

[5] Lomakin, A., 1958, "Calculation of Critical Number of Revolutions and the Conditions Necessary for Dynamic Stability of Rotors in High-Pressure Hydraulic Machines When Taking Into Account Forces Originating in Sealings," *Journal for Power and Mechanical Engineering (In Russian),* **14**.

[6] Pinkus, O., and Sternlicht, B., 1961, *Theory of Hydrodynamic Lubrication*, New York: McGraw-Hill.

[7] Childs, D., Norrbin, C., and Phillips, S., 2014 “A lateral rotordynamics primer or electrical submersible pumps (ESP’s) for deep subsea applications,” in Proceedings of the *30th Pump User's Symposia*, .

[8] Nelson, C., and Nguyen, D., 1988, "Analysis of Eccentric Annular Incompressible Seals: Part 1 - A New Solution Using Fast Fourier Transforms for Determining Hydrodynamic Force," *Journal of Tribology,* **110**, pp. 354-359.

[9] Nelson, C., and Nguyen, D., 1988, "Analysis of Eccentric Annular Incompressible Seals: Part 2 - Effects of Eccentricity on Rotordynamic Coefficients," *Journal of Tribology,* **110**, pp. 361-366.

[10] Lund, J., 1966, *Self-excited, Stationary Whirl Orbits of a Journal in a Sleeve Bearing,* Rensselaer Polytechnic Institute.

[11] San Andres, L., 1991, “Effect of Eccentricity on the Force Response of a Hybrid Bearing,” *Tribology Transactions*, **34**, pp. 537–544.

[12] Black H.F., Allaire, P., and Barret, L., 1981, "Inlet Flow Swirl in Short Turbulent Annular Seal Dynamics," in *Ninth International Conference on Fluid Sealing*, Noordwijkerhout, Netherlands, pp. 141-152.

[13] Massey, I., (1985), "Subsynchronous Vibration Problems in High-Speed Multistage Centrifugal Pumps," Proceedings, 14th Turbomachinery Symposium, organized by Texas A&M University, pp. 11-16

[14] Benckert, H., and Wachter, J., 1980 "Flow Induced Spring Constants of Labyrinth Seals for Applications in Rotor Dynamics," in *Proceedings of the 1st Workshop on Rotordynamic Instability Problems in High-Performance Turbomachinery*, College Station, Texas, Texas A&M University, pp 189-212.

[15] Childs, D., Rodriguez. L., Cullotta, V., Al-Ghasem, A., and Graviss, M., "Rotordynamic-Coefficients, and Static Equilibrium Loci and Leakage Characteristics for Short, Laminar-Flow Annular Seals," ASME J. of Tribology, April 2006, 128, pp. 378-387

[16] Zirkelback, N., and San Andrés, L., (1996), "Bulk-Flow Model for the Transition to Turbulence Regime in Annular Seals," STLE Tribology Transactions, Vol 39 No 4, P. 835-842.

[17] Kaul, A., 1999, "Design and Development of a Test Setup for the Experimental Determination of the Rotordynamic and Leakage Characteristics of Annular Bushing Oil Seals", College Station, Texas: Texas A&M University.

[18] Kluitenberg, M., 2014, "Experimentally Determine the Impact of Inactive Jacking Ports on the Rotordynamic Characteristics of a Four-Pad, LBP, Tilting-Pad Journal Bearing," M.S. Thesis, Texas A&M University, College Station.

[19] Glienicke, J., 1966-67, "Experimental Investigation of the Stiffness and Damping Coefficients of Turbine Bearings and Their Application to Instability Prediction," in Proceedings of IMechE 1966-67, 181, pp. 116-129.

[20] Moreland, A. J., 2016, "Moreland - Effect of Eccentricity and Pre-swirl on Smooth Stator_Grooved Rotor Liquid Annular Seals, Measured Static and Dynamic Results," M.S. Thesis, Texas A&M University, College Station.

[21] You HI, Lu SS. The Effect of Fluid Inertia on the Operating Characteristics of a Journal Bearing. ASME. *J. Tribol.* 1988;110(3):499-502.

[22] Rouvas, C., and Childs, D.W., 1993, "A Parameter Identification Method for the Rotordynamic Coefficients of a High Reynolds Number Hydrostatic Bearing," Jounal of Vibration and Acoustics, 115, pp. 264-270.

[23] Childs, D.W., and Hale, K., 1994, "A Test Apparatus and Facility to Identify the Rotordynamic Coefficients of High-Speed Hydrostatic Bearings," *Journal of Tribology,* **116**, pp. 337-343.

[24] Beckwith, T., Marangoni, R., and Lienhard, V., 2007, *Mechanical Measurements*, Pearson Education, Inc, Upper Saddle River, NJ.

APPENDIX A

TABULATED RESULTS

Assembly 1 – 5 mil Clearance SB Seal with High Pre-Swirl

Table A.1. Static results of the 5 mil SB clearance seal with high pre-swirl.

Test Point	Target ω	Target ΔP	Target ε_0	Measured ω	Measured ΔP	Measured ε_0	ϕ	$\dot{Q}$	F_s
	[rpm]	[bar]	[-]	[rpm]	[bar]	[-]	[deg]	[LPM]	[N]
1	2000	2.07	0.00	2009.043	2.268	0.038	29.469	0.256	0
2	2000	2.07	0.27	2009.070	2.216	0.277	79.350	0.254	498
3	2000	2.07	0.53	2009.328	2.333	0.532	65.735	0.352	1067
4	2000	2.07	0.80	2008.389	2.164	0.794	38.569	0.328	3867
5	2000	4.14	0.00	2008.566	4.366	0.069	19.303	0.956	0
6	2000	4.14	0.27	2008.736	4.353	0.267	74.372	0.993	542
7	2000	4.14	0.53	2008.751	4.431	0.529	69.450	1.282	1318
8	2000	4.14	0.80	1996.949	4.223	0.788	44.152	1.378	4355
9	2000	6.21	0.00	2008.097	6.557	0.058	-3.347	1.552	0
10	2000	6.21	0.27	2008.264	6.544	0.278	76.054	1.668	665
11	2000	6.21	0.53	2008.128	6.631	0.536	73.524	2.092	1557
12	2000	6.21	0.80	2007.011	6.553	0.789	42.747	1.748	5327
13	2000	8.27	0.00	2038.000	8.902	0.065	61.121	2.021	0
14	2000	8.27	0.27	2008.279	8.596	0.271	81.623	2.142	629
15	2000	8.27	0.53	2007.890	8.560	0.535	78.931	2.705	1601
16	2000	8.27	0.80	1997.055	8.696	0.805	45.241	3.193	5552
17	4000	2.07	0.00	3976.397	2.192	0.037	87.860	0.350	0
18	4000	2.07	0.27	4038.030	2.151	0.267	96.467	0.374	0.42
19	4000	2.07	0.53	4009.139	2.301	0.548	67.117	0.469	1599
20	4000	2.07	0.80	4012.841	2.260	0.794	32.261	0.493	6414
21	4000	4.14	0.00	4010.315	4.244	0.015	100.89	1.180	0
22	4000	4.14	0.27	4009.543	4.378	0.291	82.579	1.080	973
23	4000	4.14	0.53	-	-	-	-	-	-
24	4000	4.14	0.80	4011.690	4.199	0.789	33.133	1.459	7800
25	4000	6.21	0.00	4012.219	6.547	0.052	91.286	1.757	0
26	4000	6.21	0.27	4012.025	6.519	0.271	86.572	1.797	921
27	4000	6.21	0.53	4012.033	6.454	0.525	74.703	2.050	2184
28	4000	6.21	0.80	4010.704	6.714	0.798	33.241	2.491	9497
29	4000	8.27	0.00	4012.485	8.749	0.069	85.957	2.244	0
30	4000	8.27	0.27	4012.122	8.532	0.268	85.465	2.247	910
31	4000	8.27	0.53	4012.228	8.744	0.532	75.175	2.668	2341
32	4000	8.27	0.80	4009.873	8.598	0.797	34.101	3.182	10003

Table A.2. Static results of the 5 mil SB clearance seal with high pre-swirl.

Test Point	Target ω	Target ΔP	Target ε_0	Measured ω	Measured ΔP	Measured ε_0	ϕ	$\dot{Q}$	F_s
	[rpm]	[bar]	[-]	[rpm]	[bar]	[-]	[deg]	[LPM]	[N]
33	6000	2.07	0.00	6003.20	2.07	0.08	116.81	0.48	0
34	6000	2.07	0.27	6004.26	2.45	0.30	94.49	0.58	763
35	6000	2.07	0.53	6000.91	2.63	0.54	57.70	0.75	1289
36	6000	2.07	0.80	-	-	-	-	-	-
37	6000	4.14	0.00	6001.25	4.58	0.05	115.98	1.49	0
38	6000	4.14	0.27	6002.54	4.49	0.28	95.47	1.50	967
39	6000	4.14	0.53	6002.66	4.45	0.54	75.86	1.64	2216
40	6000	4.14	0.80	5997.67	4.08	0.78	31.86	1.96	9227
41	6000	6.21	0.00	6002.57	6.37	0.05	134.53	2.12	0
42	6000	6.21	0.27	6003.07	6.40	0.28	95.69	2.18	1194
43	6000	6.21	0.53	5997.95	6.57	0.54	67.27	2.64	2950
44	6000	6.21	0.80	5992.71	6.44	0.76	33.36	2.92	10034
45	6000	8.27	0.00	6000.75	8.45	0.04	151.53	2.66	0
46	6000	8.27	0.27	6001.62	8.66	0.27	94.75	2.83	1388
47	6000	8.27	0.53	5999.60	8.44	0.54	65.63	3.18	3436
48	6000	8.27	0.80	5997.47	8.40	0.77	31.97	3.53	11412
49	8000	2.07	0.00	8013.71	1.74	0.09	28.85	0.40	0
50	8000	2.07	0.27	8019.78	2.21	0.30	109.67	0.69	742
51	8000	2.07	0.53	8021.60	2.12	0.53	78.47	0.59	1418
52	8000	2.07	0.80	8018.15	2.33	0.75	46.15	0.80	4806
53	8000	4.14	0.00	8012.30	4.53	0.11	-157.40	1.86	0
54	8000	4.14	0.27	7996.58	4.71	0.28	108.07	1.90	1785
55	8000	4.14	0.53	8019.37	4.27	0.53	76.59	1.73	2448
56	8000	4.14	0.80	8018.48	4.30	0.75	32.50	2.04	11423
57	8000	6.21	0.00	8010.17	6.50	0.04	97.85	2.38	0
58	8000	6.21	0.27	8012.57	6.29	0.28	92.74	2.39	1314
59	8000	6.21	0.53	8013.15	6.27	0.54	76.01	2.53	3424
60	8000	6.21	0.80	8016.11	6.40	0.72	34.59	2.88	11453
61	8000	8.27	0.00	8006.49	8.42	0.08	168.72	3.19	0
62	8000	8.27	0.27	8008.85	8.90	0.28	106.12	3.43	1559
63	8000	8.27	0.53	8015.19	8.59	0.55	76.05	3.44	4036
64	8000	8.27	0.80	8017.80	8.72	0.71	37.09	3.79	11482

Table A.3. Static results of the 5 mil SB clearance seal with high pre-swirl.

Test Point	PSR	OSR	Inlet Temperature	Average Outlet Temperature	Re_a	Re_c	Re_t
	[-]	[-]	[°C]	[°C]	[-]	[-]	[-]
1	0.291	0.125	47.738	44.938	0.970	42.942	42.952
2	0.302	0.101	47.637	45.745	0.978	43.547	43.558
3	0.288	0.088	47.654	45.486	1.347	43.343	43.364
4	0.189	0.080	44.641	44.043	1.142	39.426	39.442
5	0.409	0.143	44.473	44.177	3.324	39.401	39.541
6	0.284	0.169	44.222	44.895	3.489	39.799	39.952
7	0.307	0.247	44.480	44.112	4.453	39.356	39.607
8	0.272	0.317	43.332	43.736	4.634	37.862	38.145
9	0.410	0.164	45.503	43.381	5.430	39.615	39.985
10	0.437	0.213	44.678	43.642	5.762	39.121	39.543
11	0.501	0.251	45.163	43.800	7.328	39.666	40.337
12	0.000	0.246	40.802	41.170	5.249	33.993	34.396
13	0.000	0.246	44.983	42.639	6.881	39.136	39.736
14	0.067	0.269	44.564	43.332	7.331	38.772	39.459
15	0.125	0.273	44.837	43.252	9.299	38.929	40.025
16	0.000	0.300	45.454	45.718	11.716	41.324	42.952
17	0.338	0.071	47.191	47.263	1.374	88.066	88.077
18	0.334	0.085	47.605	48.499	1.518	92.486	92.498
19	0.331	0.087	44.790	46.096	1.711	82.483	82.500
20	0.303	0.069	45.643	49.012	1.946	89.369	89.390
21	0.328	0.084	48.931	51.906	5.270	100.984	101.121
22	0.328	0.083	44.922	46.716	4.001	83.817	83.912
23	-	-	-	-	-	-	-
24	0.285	0.133	47.097	51.050	6.183	95.895	96.094
25	0.324	0.089	47.311	51.670	7.572	97.545	97.838
26	0.322	0.113	46.559	50.435	7.444	93.716	94.011
27	0.316	0.124	46.048	49.795	8.295	91.562	91.937
28	0.207	0.203	45.597	49.885	10.010	90.917	91.466
29	0.315	0.121	45.636	49.703	8.989	90.672	91.117
30	0.311	0.110	45.241	49.219	8.844	89.046	89.484
31	0.303	0.188	44.437	48.628	10.205	86.561	87.161
32	0.000	0.249	44.539	48.910	12.271	87.215	88.074

Table A.4. Static results of the 5 mil SB clearance seal with high pre-swirl.

Test Point	PSR	OSR	Inlet Temperature	Average Outlet Temperature	Re_a	Re_c	Re_t
	[-]	[-]	[°C]	[°C]	[-]	[-]	[-]
33	0.302	0.069	50.306	56.851	2.412	171.106	171.123
34	0.298	0.058	50.709	56.851	2.928	172.325	172.350
35	0.298	0.045	54.243	59.016	4.213	190.721	190.768
36	-	-	-	-	-	-	-
37	0.317	0.037	47.125	56.659	7.121	161.434	161.591
38	0.313	0.048	50.318	58.774	7.886	177.832	178.007
39	0.315	0.072	47.261	55.567	7.672	158.172	158.358
40	0.288	0.108	50.252	57.206	9.978	172.012	172.302
41	0.316	0.061	47.766	57.141	10.302	164.867	165.189
42	0.314	0.063	50.047	57.935	11.214	174.099	174.460
43	0.286	0.072	47.316	55.010	12.210	156.361	156.837
44	0.289	0.207	47.608	55.045	13.568	157.133	157.718
45	0.327	0.069	47.085	56.181	12.573	159.691	160.185
46	0.322	0.077	48.440	55.837	13.545	162.291	162.855
47	0.247	0.155	47.947	55.604	15.047	160.093	160.798
48	0.241	0.236	46.068	53.931	15.586	149.518	150.328
49	0.280	0.034	53.237	58.804	2.232	249.408	249.418
50	0.280	0.028	56.393	62.445	4.317	281.376	281.409
51	0.274	0.000	50.738	56.265	2.981	227.681	227.701
52	0.267	0.041	52.555	57.512	4.247	240.634	240.671
53	0.298	0.058	48.851	60.203	9.844	238.633	238.836
54	0.282	0.061	50.774	65.359	11.495	272.219	272.462
55	0.284	0.000	47.209	59.710	8.804	230.359	230.527
56	0.278	0.036	50.029	61.597	11.278	250.286	250.540
57	0.228	0.054	47.726	62.331	12.899	245.053	245.392
58	0.242	0.046	50.993	66.659	14.831	280.822	281.213
59	0.298	0.054	45.758	60.905	12.921	230.878	231.239
60	0.282	0.099	47.563	62.424	15.603	245.108	245.604
61	0.220	0.072	47.480	61.361	16.900	239.114	239.710
62	0.210	0.075	51.032	65.726	20.933	275.674	276.468
63	0.297	0.070	48.391	62.105	18.773	246.515	247.228
64	0.272	0.119	47.989	64.726	21.685	258.842	259.749

Table A.5. Stiffness coefficients and uncertainties for the 5 mil SB clearance seal with high pre-swirl.

Test Point	K_{tt} [MN/m]	K_{tr} [MN/m]	K_{rt} [MN/m]	K_{rr} [MN/m]	$u_{K_{tt}}$ [MN/m]	$u_{K_{tr}}$ [MN/m]	$u_{K_{rt}}$ [MN/m]	$u_{K_{rr}}$ [MN/m]
1	0.749	17.930	-16.062	0.518	11.512	3.351	13.731	3.615
2	1.161	18.026	-17.925	3.456	2.798	-5.566	-2.494	3.683
3	8.865	38.771	-22.826	7.629	18.011	-9.312	-13.003	8.287
4	35.313	84.960	-39.793	222.784	35.846	14.879	10.837	5.423
5	1.318	19.371	-17.838	0.375	1.485	2.796	2.950	2.942
6	0.323	26.251	-21.279	1.916	6.368	-2.932	-3.155	2.989
7	7.362	28.978	-26.619	19.864	12.986	-20.110	-6.764	4.046
8	41.361	104.121	-34.252	253.847	58.644	13.355	13.840	4.195
9	0.563	19.905	-19.563	-0.943	3.336	2.846	2.157	3.322
10	-1.632	27.201	-19.763	-3.531	8.070	-8.871	-2.957	6.277
11	7.526	33.875	-29.476	13.546	10.093	-16.733	-6.917	1.496
12	44.879	106.924	-50.400	306.022	51.959	11.242	7.085	-0.207
13	0.806	23.401	-23.091	-1.137	2.273	5.247	3.959	3.472
14	-0.643	26.469	-25.309	1.774	14.027	-14.235	-4.898	5.148
15	9.262	45.582	-34.678	16.833	8.125	-14.897	-5.823	7.889
16	47.128	110.270	-37.144	345.766	57.907	13.574	-0.807	0.273
17	1.202	32.521	-30.232	3.970	0.570	1.765	1.169	4.222
18	0.242	31.451	-28.917	5.143	1.166	-1.441	-1.053	2.360
19	13.098	52.153	-37.174	31.010	5.075	-3.453	-3.194	1.742
20	61.561	135.660	-54.057	388.344	13.274	7.886	8.336	5.106
21	1.765	34.377	-32.753	2.931	0.890	1.286	0.910	1.057
22	0.550	40.408	-36.450	4.650	1.333	-1.726	-1.330	2.596
23	-	-	-	-	-	-	-	-
24	70.272	143.945	-63.014	460.623	14.188	7.385	10.143	6.205
25	2.905	37.146	-38.145	2.821	1.115	-1.031	-0.885	0.983
26	4.360	39.450	-45.096	0.850	2.786	1.880	1.353	1.058
27	12.526	62.379	-49.847	35.604	3.865	-2.416	-2.323	4.599
28	84.071	152.980	-69.746	557.147	15.018	9.938	8.974	5.888
29	3.077	40.119	-41.297	2.991	1.115	-1.394	-1.137	0.824
30	4.376	42.499	-49.490	0.501	2.226	1.532	1.612	1.384
31	13.259	69.976	-57.690	38.823	3.048	-3.100	-2.318	5.050
32	88.665	155.685	-71.699	588.513	16.735	9.508	9.755	5.186

Table A.6. Stiffness coefficients and uncertainties for the 5 mil SB clearance seal with high pre-swirl.

Test Point	K_{tt} [MN/m]	K_{tr} [MN/m]	K_{rt} [MN/m]	K_{rr} [MN/m]	$u_{K_{tt}}$ [MN/m]	$u_{K_{tr}}$ [MN/m]	$u_{K_{rt}}$ [MN/m]	$u_{K_{rr}}$ [MN/m]
33	0.751	34.415	-36.961	2.439	0.412	-0.937	-0.844	1.815
34	9.773	35.096	-33.907	3.657	2.472	1.066	2.432	1.632
35	11.875	53.064	-38.530	35.530	4.525	-2.772	-1.587	0.549
36	-	-	-	-	-	-	-	-
37	2.133	43.831	-45.764	3.070	0.279	-0.840	-0.771	1.826
38	0.757	45.114	-40.913	7.111	1.187	-2.485	-0.916	2.157
39	43.267	45.173	-76.934	17.739	6.556	3.071	4.409	1.838
40	87.413	168.608	-65.180	595.819	17.542	6.551	10.686	5.855
41	2.416	47.092	-48.095	3.653	-0.125	-0.167	0.018	2.202
42	1.406	51.177	-46.040	6.986	1.128	-2.552	-0.917	3.063
43	43.731	45.346	-87.255	26.007	7.576	2.652	2.904	3.309
44	95.066	159.108	-76.710	611.812	14.864	5.758	9.537	2.934
45	2.935	50.552	-51.064	4.863	0.282	0.577	0.477	1.863
46	1.565	56.597	-50.956	8.250	1.461	-1.913	-1.562	2.710
47	56.097	51.927	-95.755	33.087	5.411	2.476	2.263	2.923
48	102.119	159.001	-87.602	670.629	12.201	5.106	6.324	1.775
49	4.106	36.902	-37.882	5.912	3.162	0.952	1.354	0.664
50	9.441	29.083	-36.926	22.039	1.141	-1.109	-1.481	2.801
51	57.147	36.472	-47.591	16.773	3.199	1.416	4.608	4.558
52	49.990	109.997	-65.148	274.750	11.264	-0.971	3.061	0.712
53	3.557	53.630	-48.210	5.145	2.195	2.099	0.918	0.212
54	3.292	48.264	-48.281	14.248	0.553	-2.004	-0.948	2.328
55	62.966	44.916	-75.866	22.451	5.378	2.203	2.690	4.448
56	108.256	172.409	-68.042	734.425	14.644	5.843	7.812	5.203
57	5.058	53.969	-56.747	4.070	1.181	-1.260	-2.260	1.783
58	1.726	53.685	-51.877	8.964	1.179	-3.001	-1.191	1.816
59	80.258	57.101	-102.55	30.064	4.615	2.172	3.533	2.694
60	109.043	159.671	-98.244	696.916	16.118	5.573	8.948	4.315
61	4.054	60.427	-58.124	7.396	0.525	1.550	0.908	2.194
62	2.184	62.853	-58.158	12.084	0.593	-2.243	-1.509	2.599
63	97.781	56.447	-115.09	30.864	6.471	2.427	5.054	4.519
64	281.246	-115.92	-385.70	475.368	4.872	7.953	9.183	13.322

Table A.7. Damping coefficients and uncertainties for the 5 mil SB clearance seal with high pre-swirl.

Test Point	C_{tt} [kN-s/m]	C_{tr} [kN-s/m]	C_{rt} [kN-s/m]	C_{rr} [kN-s/m]	$u_{C_{tt}}$ [kN-s/m]	$u_{C_{tr}}$ [kN-s/m]	$u_{C_{rt}}$ [kN-s/m]	$u_{C_{rr}}$ [kN-s/m]
1	179.983	5.208	-6.303	183.629	18.905	7.501	14.916	7.254
2	177.636	-14.916	-17.373	209.311	8.350	-11.056	-7.922	19.211
3	152.231	13.337	17.769	396.101	25.692	-22.699	-15.773	16.539
4	233.088	109.013	186.562	773.428	139.201	55.515	37.580	16.816
5	192.703	8.267	-0.847	192.266	4.109	4.591	5.308	4.600
6	206.005	-13.701	-16.167	240.100	14.853	-1.938	-11.276	1.122
7	185.353	-14.555	25.528	369.619	120.629	-166.423	-90.565	133.654
8	247.639	64.094	158.745	735.010	173.435	38.130	14.764	10.197
9	197.801	1.863	1.870	204.503	6.786	11.915	8.429	13.006
10	225.059	-11.589	-13.263	266.139	11.748	-17.773	-8.838	11.782
11	212.258	-5.038	8.379	421.012	104.435	-151.840	-89.032	141.923
12	296.956	105.815	208.656	796.401	215.357	63.376	29.607	17.900
13	221.901	4.614	2.274	229.815	6.339	9.646	4.684	16.982
14	231.410	-10.435	-14.336	279.263	16.398	-13.743	-23.874	24.480
15	231.196	-55.859	18.848	441.214	57.889	-157.450	-68.106	211.576
16	286.870	54.690	174.183	747.226	194.757	38.258	7.194	4.716
17	152.808	9.507	-3.853	159.956	1.723	1.913	2.408	4.301
18	135.283	-10.811	-19.531	167.903	2.009	-4.197	-2.372	4.460
19	129.702	11.180	16.476	335.475	14.150	-8.660	-9.391	7.136
20	179.671	106.510	198.589	703.174	39.081	26.556	23.513	20.644
21	162.047	7.995	-3.729	165.397	1.606	1.837	1.524	3.066
22	176.283	-15.125	-21.891	211.702	2.515	-3.795	-3.276	3.821
23	-	-	-	-	-	-	-	-
24	196.313	84.127	193.412	673.580	75.957	51.002	43.291	29.904
25	186.796	0.882	-5.752	184.699	1.826	-1.698	-1.507	1.419
26	233.236	16.352	8.896	192.514	4.640	3.054	3.390	3.923
27	178.454	7.631	13.655	412.824	7.249	-5.272	-6.754	7.044
28	220.214	89.149	217.367	678.740	76.867	58.512	39.142	29.617
29	201.835	-0.971	-7.722	199.247	3.315	-1.622	-2.420	1.703
30	249.957	9.777	9.130	211.606	4.626	3.899	3.105	3.210
31	197.799	3.256	18.865	461.324	5.685	-4.953	-4.368	8.932
32	231.147	83.040	228.051	691.870	74.006	56.290	32.608	27.024

Table A.8. Damping coefficients and uncertainties for the 5 mil SB clearance seal with high pre-swirl.

Test Point	C_{tt}	C_{tr}	C_{rt}	C_{rr}	$u_{C_{tt}}$	$u_{C_{tr}}$	$u_{C_{rt}}$	$u_{C_{rr}}$
	[kN-s/m]	[kN-s/m]	[kN-s/m]	[kN-s/m]	[kN-s/m]	[kN-s/m]	[kN-s/m]	[kN-s/m]
33	121.705	4.005	-16.742	118.618	1.316	-1.841	-2.154	3.730
34	135.730	19.400	5.481	96.906	3.408	2.528	5.020	4.707
35	99.972	22.968	15.811	246.584	11.717	-5.340	-5.069	1.774
36	-	-	-	-	-	-	-	-
37	149.994	3.525	-14.927	149.156	1.339	-2.448	-1.226	3.288
38	133.646	-7.456	-23.338	167.321	2.717	-5.702	-2.452	4.936
39	308.374	-58.004	-44.541	144.046	13.785	8.726	8.175	6.091
40	155.391	71.529	173.096	561.626	68.613	44.598	53.713	37.550
41	156.181	4.894	-11.689	160.996	0.057	-1.012	-0.600	4.823
42	149.782	-5.607	-21.105	188.837	2.669	-5.378	-2.119	5.160
43	301.023	-64.423	-55.916	177.352	14.550	6.417	5.081	7.105
44	174.889	73.352	179.585	562.241	34.628	22.715	18.371	10.499
45	165.949	5.994	-9.546	173.214	0.143	0.216	0.965	4.436
46	166.439	-5.385	-17.603	207.663	3.291	-4.575	-3.662	6.306
47	309.628	-80.743	-63.491	199.272	9.582	4.439	4.114	7.068
48	184.423	74.022	189.661	583.812	27.862	20.110	12.018	8.382
49	87.735	13.719	-12.135	97.136	5.238	1.528	1.723	2.364
50	58.344	-0.125	-8.557	112.607	2.458	-3.933	-4.222	5.698
51	152.878	-24.503	-29.994	76.358	4.756	2.931	8.038	9.242
52	105.532	62.667	88.891	345.300	18.224	-5.013	4.152	-1.424
53	122.097	13.084	-6.333	145.452	5.409	4.356	2.230	0.454
54	108.625	-1.411	-22.038	148.451	1.789	-4.328	-1.345	6.606
55	206.935	-41.018	-41.004	113.715	9.280	3.986	5.902	5.376
56	145.219	74.690	156.528	460.277	23.366	8.864	9.559	5.450
57	140.041	9.735	-12.981	133.600	2.637	-3.686	-2.355	3.029
58	127.467	-0.357	-25.861	154.001	2.341	-7.140	-1.910	6.104
59	291.893	-62.789	-53.684	145.258	8.533	4.684	8.101	4.733
60	159.896	58.427	155.223	468.062	36.644	15.873	18.946	11.227
61	141.429	7.413	-11.787	158.514	1.345	2.493	2.704	3.981
62	138.314	-2.427	-23.364	183.530	2.065	-6.026	-1.654	8.765
63	302.031	-65.844	-61.656	161.854	10.740	5.690	10.101	6.152
64	186.518	-180.797	-77.806	479.044	22.707	18.944	15.640	21.254

Table A.9. Virtual mass coefficients and uncertainties for the 5 mil SB clearance seal with high pre-swirl.

Test Point	M_{tt}	M_{tr}	M_{rt}	M_{rr}	$u_{M_{tt}}$	$u_{M_{tr}}$	$u_{M_{rt}}$	$u_{M_{rr}}$
	[kg]	[kg]	[kg]	[kg]	[kg]	[kg]	[kg]	[kg]
1	36.912	-7.018	3.747	32.802	16.681	4.855	19.897	5.238
2	24.359	-14.720	-4.079	34.909	4.054	-8.065	-3.614	5.337
3	22.280	13.772	-7.058	-11.034	26.097	-13.493	-18.842	12.007
4	6.747	0.334	-45.219	-368.104	50.453	20.942	15.254	7.633
5	34.447	-7.614	2.739	30.493	2.152	4.051	4.274	4.263
6	24.296	3.002	-4.061	32.633	9.226	-4.248	-4.571	4.331
7	15.482	-47.447	-17.155	30.392	24.596	-38.090	-12.811	7.664
8	14.208	30.400	-60.645	-371.808	82.541	18.798	19.479	5.904
9	29.424	-9.526	-0.735	25.447	4.834	4.124	3.125	4.813
10	20.158	10.975	15.582	23.387	11.855	-13.033	-4.344	9.222
11	13.553	-34.916	-22.035	-0.905	19.116	-31.693	-13.101	2.834
12	4.820	32.549	-79.372	-407.488	73.133	15.823	9.973	-0.291
13	28.875	-2.252	-5.289	16.323	3.340	7.709	5.817	5.100
14	16.286	4.056	5.837	35.350	20.608	-20.913	-7.197	7.562
15	14.351	-12.607	-30.065	0.767	15.389	-28.216	-11.029	14.943
16	0.423	25.033	-67.045	-390.525	81.505	19.106	-1.136	0.385
17	32.789	1.074	3.006	43.508	0.838	2.594	1.718	6.202
18	21.773	-0.709	0.902	29.303	1.712	-2.117	-1.547	3.467
19	16.814	0.736	2.256	10.332	9.613	-6.539	-6.049	3.300
20	4.862	8.550	-34.153	-197.011	18.684	11.100	11.733	7.186
21	31.173	2.113	0.323	35.337	1.215	1.755	1.242	1.443
22	23.985	-1.325	2.216	27.086	1.820	-2.356	-1.815	3.542
23	-	-	-	-	-	-	-	-
24	10.647	28.665	-47.567	-205.042	19.970	10.394	14.276	8.733
25	27.902	1.315	3.471	30.370	1.522	-1.408	-1.207	1.342
26	28.971	-4.920	0.805	22.730	3.801	2.565	1.847	1.444
27	16.809	-11.032	-7.495	6.763	5.860	-3.662	-3.522	6.972
28	10.016	24.137	-75.552	-239.081	21.139	13.988	12.631	8.287
29	27.040	0.958	3.090	30.641	1.521	-1.903	-1.551	1.125
30	27.203	-6.706	-1.694	19.791	3.038	2.091	2.200	1.889
31	12.563	-11.707	-14.008	-2.517	4.620	-4.699	-3.514	7.655
32	10.908	30.210	-74.381	-233.678	23.554	13.382	13.731	7.300

Table A.10. Virtual mass coefficients and uncertainties for the 5 mil SB clearance seal with high pre-swirl.

Test Point	M_{tt}	M_{tr}	M_{rt}	M_{rr}	$u_{M_{tt}}$	$u_{M_{tr}}$	$u_{M_{rt}}$	$u_{M_{rr}}$
	[kg]	[kg]	[kg]	[kg]	[kg]	[kg]	[kg]	[kg]
33	29.426	-0.957	1.762	26.757	0.625	-1.420	-1.279	2.751
34	26.162	-0.469	-2.661	14.996	3.748	1.615	3.687	2.474
35	13.289	-5.179	1.891	17.618	6.860	-4.203	-2.406	0.832
36	-	-	-	-	-	-	-	-
37	31.896	-1.254	1.805	27.968	0.423	-1.273	-1.169	2.768
38	23.172	-2.390	3.974	25.688	1.800	-3.766	-1.389	3.270
39	24.742	-6.293	4.078	8.714	9.938	4.656	6.684	2.787
40	15.261	22.922	-32.414	-84.707	24.691	9.220	15.041	8.241
41	31.935	-1.999	1.022	27.854	-0.189	-0.253	0.028	3.338
42	25.356	-4.075	3.507	25.845	1.709	-3.868	-1.390	4.643
43	12.769	-1.641	4.629	13.881	10.218	3.576	3.917	4.464
44	19.822	12.743	-35.510	-100.552	20.048	7.767	12.864	3.958
45	31.683	-3.161	0.146	27.877	0.427	0.875	0.723	2.824
46	23.791	-3.444	5.944	28.501	2.214	-2.900	-2.368	4.108
47	4.494	9.205	4.223	11.253	7.298	3.339	3.053	3.943
48	16.464	20.038	-42.110	-103.384	16.456	6.887	8.529	2.394
49	26.382	0.827	0.159	35.566	4.793	1.443	2.053	1.007
50	7.010	4.747	0.104	18.178	1.730	-1.681	-2.244	4.246
51	12.297	-3.545	-3.106	4.071	4.452	1.970	6.413	6.343
52	5.660	20.340	-5.576	-9.665	15.676	-1.351	4.260	0.991
53	22.219	-8.365	-0.315	27.672	3.327	3.181	1.391	0.321
54	20.105	-1.155	3.015	23.892	0.774	-2.805	-1.326	3.258
55	4.938	0.027	-8.637	15.151	7.484	3.066	3.744	6.191
56	15.355	33.285	-20.721	-16.185	20.379	8.131	10.871	7.240
57	31.404	-1.395	0.174	26.837	1.653	-1.764	-3.163	2.496
58	25.133	-5.853	1.808	28.099	1.651	-4.200	-1.667	2.542
59	3.558	2.971	0.153	9.847	6.423	3.023	4.916	3.749
60	13.455	23.630	-28.693	-45.997	22.430	7.755	12.452	6.006
61	29.246	-5.628	-0.570	25.757	0.735	2.169	1.271	3.070
62	25.580	-5.674	3.493	27.695	0.830	-3.139	-2.112	3.638
63	15.771	2.574	1.208	11.920	9.005	3.377	7.034	6.289
64	-11.861	66.351	7.718	-25.968	6.781	11.068	12.780	18.540

Table A.11. WFR, C_{eff}, and uncertainties for the 5 mil SB clearance seal with high pre-swirl.

Test Point	WFR	u_{WFR}	C_{eff}	$u_{C_{eff}}$
			[kN-s/m]	[kN-s/m]
1	0.444	0.196	101.023	35.084
2	0.444	0.079	108.035	17.883
3	0.577	0.185	127.796	40.961
4	0.000	0.000	206.676	82.643
5	0.459	0.051	104.031	10.142
6	0.506	0.051	110.076	12.659
7	0.496	0.269	145.335	103.185
8	0.000	0.000	160.479	98.288
9	0.466	0.045	107.309	11.220
10	0.451	0.083	133.942	23.738
11	0.501	0.204	166.008	98.059
12	0.000	0.000	172.406	112.579
13	0.482	0.071	116.936	17.869
14	0.484	0.142	132.237	38.705
15	0.592	0.194	145.352	116.084
16	0.000	0.000	164.603	102.690
17	0.481	0.018	81.032	3.440
18	0.474	0.016	80.213	3.230
19	0.497	0.040	126.205	9.704
20	0.000	0.000	215.689	25.977
21	0.488	0.012	83.798	2.552
22	0.475	0.015	102.469	3.459
23	-	-	-	-
24	0.000	0.000	188.627	43.462
25	0.482	0.009	96.149	1.988
26	0.474	0.015	112.258	4.102
27	0.481	0.019	162.081	6.438
28	0.000	0.000	184.327	44.165
29	0.483	0.012	103.660	2.838
30	0.475	0.013	121.309	3.864
31	0.493	0.018	177.636	7.017
32	0.000	0.000	190.756	42.602

Table A.12. WFR, C_{eff}, and uncertainties for the 5 mil SB clearance seal with high pre-swirl.

Test Point	WFR	u_{WFR}	C_{eff}	$u_{C_{eff}}$
			[kN-s/m]	[kN-s/m]
33	0.473	0.012	63.392	2.217
34	0.479	0.023	61.447	3.592
35	0.448	0.032	100.400	6.447
36	-	-	-	-
37	0.477	0.008	78.292	1.994
38	0.458	0.016	82.054	3.518
39	0.454	0.026	129.083	8.663
40	0.000	0.000	172.394	40.361
41	0.478	0.007	82.873	2.415
42	0.460	0.015	91.985	3.618
43	0.449	0.022	133.631	8.680
44	0.000	0.000	180.678	20.153
45	0.477	0.007	88.728	2.298
46	0.460	0.013	101.486	4.063
47	0.472	0.018	136.921	6.524
48	0.000	0.000	187.794	15.922
49	0.482	0.019	47.878	3.038
50	0.473	0.021	46.177	3.292
51	0.423	0.045	64.581	5.937
52	0.000	0.000	121.121	9.338
53	0.455	0.014	73.086	3.038
54	0.452	0.015	70.893	3.669
55	0.448	0.024	88.412	5.748
56	0.000	0.000	159.570	13.329
57	0.482	0.013	70.826	2.532
58	0.450	0.017	77.830	3.793
59	0.447	0.017	123.450	5.469
60	0.000	0.000	160.356	20.165
61	0.472	0.010	79.274	2.359
62	0.452	0.015	88.779	4.782
63	0.426	0.022	129.758	7.032
64	0.000	0.000	34.061	17.152

Assembly 2 – 10 mil Clearance SB Seal with High Pre-Swirl

Table A.13. Static results of the 10 mil SB clearance seal with high pre-swirl.

Test Point	Target ω	Target ΔP	Target ε_0	Measured ω	Measured ΔP	Measured ε_0	ϕ	$\dot{Q}$	F_s
	[rpm]	[bar]	[-]	[rpm]	[bar]	[-]	[deg]	[LPM]	[N]
1	2000	2.068	0.00	1996.352	2.447	0.022	85.597	3.840	0.00
2	2000	2.068	0.27	1997.550	2.471	0.265	81.908	4.357	143.56
3	2000	2.068	0.53	1998.466	2.457	0.518	82.146	5.215	382.10
4	2000	2.068	0.80	1998.215	2.406	0.765	53.967	7.077	933.10
5	2000	4.137	0.00	1999.177	4.472	0.030	105.87	8.863	0.00
6	2000	4.137	0.27	1999.168	4.537	0.263	81.646	9.677	144.04
7	2000	4.137	0.53	1998.758	4.519	0.520	81.446	11.863	392.40
8	2000	4.137	0.80	1998.006	4.442	0.786	62.065	15.363	1050.1
9	2000	6.205	0.00	1999.018	6.594	0.027	117.95	13.581	0.00
10	2000	6.205	0.27	1998.621	6.566	0.263	76.825	14.463	152.87
11	2000	6.205	0.53	1998.159	6.469	0.529	77.899	17.619	423.54
12	2000	6.205	0.80	1997.871	6.422	0.780	67.297	23.746	1117.6
13	2000	8.274	0.00	2002.578	8.623	0.013	178.55	15.179	0.00
14	2000	8.274	0.27	2002.401	8.533	0.277	70.284	17.006	191.91
15	2000	8.274	0.53	2002.764	8.660	0.521	72.616	22.087	455.80
16	2000	8.274	0.80	2002.175	8.359	0.794	67.323	29.961	1289.9
17	4000	2.068	0.00	4000.678	2.466	0.017	65.247	4.027	0.00
18	4000	2.068	0.27	4001.823	2.480	0.272	86.579	4.495	288.90
19	4000	2.068	0.53	4002.345	2.359	0.533	81.452	5.425	665.59
20	4000	2.068	0.80	3999.868	2.443	0.791	53.367	5.379	2223.8
21	4000	4.137	0.00	4002.314	4.468	0.015	114.06	9.060	0.00
22	4000	4.137	0.27	4001.324	4.469	0.268	86.096	9.588	297.68
23	4000	4.137	0.53	4001.007	4.601	0.526	84.640	12.297	768.34
24	4000	4.137	0.80	3998.394	4.375	0.793	59.674	13.288	2335.4
25	4000	6.205	0.00	4001.290	6.534	0.013	124.70	12.674	0.00
26	4000	6.205	0.27	4001.472	6.520	0.271	84.675	14.111	332.88
27	4000	6.205	0.53	4001.375	6.358	0.532	83.763	17.984	814.07
28	4000	6.205	0.80	3997.617	6.392	0.795	64.091	22.625	2408.5
29	4000	8.274	0.00	4001.231	8.601	0.025	177.82	18.487	0.00
30	4000	8.274	0.27	4001.092	8.483	0.270	84.190	18.968	353.42
31	4000	8.274	0.53	4000.288	8.636	0.525	82.536	23.581	883.76
32	4000	8.274	0.80	3996.207	8.421	0.795	67.662	28.668	2613.3

Table A.14. Static results of the 10 mil SB clearance seal with high pre-swirl.

Test Point	Target ω	Target ΔP	Target ε_0	Measured ω	Measured ΔP	Measured ε_0	ϕ	$\dot{Q}$	F_s
	[rpm]	[bar]	[-]	[rpm]	[bar]	[-]	[deg]	[LPM]	[N]
33	6000	2.068	0.00	6006.199	2.340	0.019	58.48	4.057	0.00
34	6000	2.068	0.27	6006.821	2.419	0.268	89.33	4.643	366.78
35	6000	2.068	0.53	6007.001	2.464	0.539	77.82	5.833	881.62
36	6000	2.068	0.80	6003.628	2.329	0.793	49.60	7.677	3271.2
37	6000	4.137	0.00	6008.146	4.524	0.014	114.68	9.417	0.00
38	6000	4.137	0.27	6007.854	4.477	0.276	88.97	9.820	441.42
39	6000	4.137	0.53	6006.978	4.519	0.531	86.52	12.258	1089.7
40	6000	4.137	0.80	6003.671	4.291	0.791	56.10	16.078	3272.3
41	6000	6.205	0.00	6008.627	6.401	0.013	129.01	13.528	0.00
42	6000	6.205	0.27	6008.228	6.533	0.270	87.24	14.531	469.56
43	6000	6.205	0.53	6007.900	6.391	0.541	85.89	18.511	1182.9
44	6000	6.205	0.80	6004.091	6.317	0.789	61.02	25.536	3273.1
45	6000	8.274	0.00	6008.666	8.611	0.017	150.55	18.664	0.00
46	6000	8.274	0.27	6009.032	8.575	0.275	86.31	19.860	491.44
47	6000	8.274	0.53	6008.161	8.341	0.531	85.14	23.601	1220.7
48	6000	8.274	0.80	6003.912	8.197	0.794	62.11	35.336	3568.5
49	8000	2.068	0.00	8005.732	2.525	0.010	-38.37	5.030	0.00
50	8000	2.068	0.27	8007.430	2.314	0.273	91.09	4.717	450.81
51	8000	2.068	0.53	8006.378	2.438	0.537	77.88	6.471	1044
52	8000	2.068	0.80	8004.817	2.492	0.788	51.29	6.611	3522.7
53	8000	4.137	0.00	8007.097	4.433	0.004	-81.08	9.708	0.00
54	8000	4.137	0.27	8008.063	4.545	0.274	91.15	10.611	568.81
55	8000	4.137	0.53	8007.559	4.577	0.530	84.47	12.945	1339.9
56	8000	4.137	0.80	8001.731	4.376	0.791	56.67	14.829	3841.1
57	8000	6.205	0.00	8006.938	6.494	0.008	123.32	14.650	0.00
58	8000	6.205	0.27	-	-	-	-	-	-
59	8000	6.205	0.53	8006.574	6.570	0.523	86.36	18.434	1438.0
60	8000	6.205	0.80	7999.828	6.268	0.792	58.40	23.974	4142.0
61	8000	8.274	0.00	8007.375	8.496	0.008	161.08	18.686	0.00
62	8000	8.274	0.27	8006.640	8.387	0.277	87.40	20.432	625.91
63	8000	8.274	0.53	8005.397	8.451	0.531	86.32	24.820	1518.8
64	8000	8.274	0.80	7998.895	8.531	0.787	61.17	32.670	4324.9

Table A.15. Static results of the 10 mil SB clearance seal with high pre-swirl.

Test Point	PSR	OSR	Inlet Temperature	Average Outlet Temperature	Re_a	Re_c	Re_t
	[-]	[-]	[°C]	[°C]	[-]	[-]	[-]
1	0.476	0.253	45.362	43.658	13.449	85.365	86.418
2	0.588	0.283	47.163	45.795	16.572	92.768	94.237
3	0.655	0.174	46.297	46.467	19.753	92.414	94.501
4	0.423	0.195	47.856	48.016	28.564	98.470	102.529
5	0.603	0.261	48.284	47.600	35.783	98.549	104.844
6	0.520	0.245	47.973	47.103	38.438	96.950	104.292
7	0.409	0.232	47.489	47.275	46.818	96.306	107.083
8	0.241	0.000	46.997	47.199	59.929	95.160	112.458
9	0.462	0.229	47.341	47.015	53.151	95.520	109.312
10	0.433	0.152	47.106	46.817	56.104	94.657	110.035
11	0.475	0.202	46.905	46.690	67.888	94.001	115.953
12	0.462	0.263	47.871	48.170	96.174	98.791	137.874
13	0.506	0.221	45.869	45.983	56.411	90.866	106.952
14	0.515	0.234	46.543	46.613	64.937	93.352	113.716
15	0.502	0.275	46.379	46.802	84.383	93.416	125.886
16	0.554	0.410	47.004	47.533	117.698	96.026	151.901
17	0.353	0.091	44.903	48.116	15.356	186.236	186.868
18	0.363	0.121	45.893	48.785	17.728	192.689	193.502
19	0.379	0.229	47.338	50.543	22.828	205.615	206.878
20	0.277	0.096	44.680	50.032	21.285	193.237	194.406
21	0.424	0.310	48.012	49.633	37.907	204.441	207.926
22	0.459	0.237	47.328	49.216	39.246	199.958	203.773
23	0.537	0.209	47.077	49.044	49.908	198.254	204.439
24	0.316	0.227	46.208	48.987	52.956	194.547	201.626
25	0.530	0.236	45.137	46.568	46.974	181.054	187.049
26	0.565	0.215	46.072	47.371	54.212	187.696	195.368
27	0.491	0.233	47.440	48.870	73.252	198.991	212.045
28	0.296	0.279	47.189	49.582	93.059	200.749	221.269
29	0.561	0.218	47.303	48.542	74.593	197.106	210.749
30	0.528	0.209	46.402	47.783	73.995	190.568	204.429
31	0.449	0.251	45.882	47.352	90.209	186.840	207.477
32	0.323	0.264	45.361	47.548	108.975	185.466	215.113

Table A.16. Static results of the 10 mil SB clearance seal with high pre-swirl.

Test Point	PSR	OSR	Inlet Temperature	Average Outlet Temperature	Re_a	Re_c	Re_t
	[-]	[-]	[°C]	[°C]	[-]	[-]	[-]
33	0.316	0.000	46.932	54.077	18.240	329.687	330.192
34	0.316	0.114	46.302	55.247	21.164	334.311	334.980
35	0.316	0.145	45.737	54.260	25.781	324.144	325.168
36	0.364	0.140	45.267	52.292	32.250	307.929	309.613
37	0.326	0.129	47.670	52.604	41.607	324.104	326.764
38	0.328	0.189	46.625	51.874	41.916	313.105	315.898
39	0.325	0.156	46.596	51.536	51.926	310.673	314.982
40	0.443	0.255	45.373	51.041	65.874	300.324	307.464
41	0.337	0.308	47.081	50.663	56.785	307.928	313.120
42	0.333	0.181	46.051	50.122	59.135	298.516	304.317
43	0.324	0.216	47.593	51.042	79.077	313.347	323.171
44	0.320	0.264	46.974	51.265	108.318	310.941	329.268
45	0.349	0.198	47.021	50.113	77.359	304.073	313.759
46	0.339	0.197	46.945	50.083	82.146	303.458	314.380
47	0.328	0.231	46.496	49.566	95.741	297.568	312.591
48	0.288	0.227	45.856	49.786	142.240	295.072	327.566
49	0.306	0.000	48.022	61.237	26.755	519.851	520.540
50	0.307	0.098	45.739	61.646	24.449	506.689	507.278
51	0.315	0.121	46.303	59.948	32.619	492.696	493.775
52	0.312	0.113	46.486	58.533	32.422	479.308	480.404
53	0.316	0.117	47.533	56.227	46.137	464.622	466.908
54	0.320	0.222	46.257	55.727	48.831	449.932	452.574
55	0.326	0.161	46.148	55.048	58.605	442.619	446.482
56	0.441	0.177	46.346	54.794	66.997	441.390	446.446
57	0.324	0.231	47.137	53.825	65.759	438.805	443.705
58	-	-	-	-	-	-	-
59	0.326	0.180	45.537	52.554	78.262	415.008	422.323
60	0.340	0.244	47.124	53.738	107.389	437.504	450.491
61	0.330	0.263	45.992	51.849	78.791	412.234	419.697
62	0.334	0.196	47.296	52.869	90.155	431.340	440.661
63	0.325	0.229	47.014	52.376	107.834	424.643	438.121
64	0.289	0.230	46.496	52.531	141.063	421.676	444.645

Table A.17. Stiffness coefficients and uncertainties for the 10 mil SB clearance seal with high pre-swirl.

Test Point	K_{tt} [MN/m]	K_{tr} [MN/m]	K_{rt} [MN/m]	K_{rr} [MN/m]	$u_{K_{tt}}$ [MN/m]	$u_{K_{tr}}$ [MN/m]	$u_{K_{rt}}$ [MN/m]	$u_{K_{rr}}$ [MN/m]
1	0.242	2.335	-2.359	0.213	0.067	0.077	0.071	0.123
2	0.069	2.818	-2.425	0.009	0.119	-0.145	-0.140	0.244
3	0.152	5.471	-3.275	0.122	0.245	-0.545	-0.336	1.075
4	3.413	13.148	-6.116	17.648	4.884	-1.661	-0.899	0.159
5	0.392	2.233	-2.216	0.382	0.138	0.100	0.103	0.163
6	0.190	2.694	-2.486	0.319	0.127	-0.275	-0.173	0.379
7	0.166	5.661	-3.274	0.542	0.262	-0.588	-0.370	1.153
8	3.639	15.686	-7.743	18.077	5.575	-4.029	-2.786	1.752
9	0.564	2.333	-2.394	0.478	0.145	0.078	0.118	0.155
10	0.355	2.922	-2.609	0.573	0.149	-0.102	-0.183	0.242
11	0.371	5.910	-3.365	0.316	0.356	-0.727	-0.348	0.676
12	3.023	16.893	-8.013	17.015	3.953	-3.374	-2.748	2.578
13	0.795	2.573	-2.577	0.689	0.102	0.075	0.129	0.151
14	0.690	3.109	-2.736	0.697	0.210	-0.173	-0.155	0.217
15	0.687	6.058	-3.546	0.645	0.333	-0.385	-0.417	0.911
16	3.477	19.232	-8.798	20.950	2.302	-2.391	-2.886	2.840
17	0.121	4.546	-4.589	0.197	0.110	0.092	0.082	0.227
18	0.001	5.230	-4.729	0.103	0.129	-0.194	-0.120	0.212
19	0.800	8.800	-6.006	2.063	0.223	-0.357	-0.242	0.539
20	12.186	30.758	-7.703	61.112	3.683	-0.488	0.454	-0.141
21	0.280	4.538	-4.472	0.415	0.104	0.130	0.099	0.245
22	0.132	5.516	-4.876	0.308	0.156	-0.195	-0.105	0.161
23	0.272	10.649	-6.457	0.826	0.230	-0.461	-0.271	0.595
24	11.918	32.794	-10.210	61.389	5.643	-2.442	-0.860	0.504
25	0.564	5.136	-5.138	0.538	0.164	0.090	0.082	0.195
26	0.325	5.972	-5.353	0.520	0.143	-0.192	-0.075	0.160
27	0.302	11.425	-6.648	1.066	0.276	-0.332	-0.226	0.532
28	10.284	33.268	-13.525	52.662	12.009	-7.856	-7.504	4.550
29	0.845	4.916	-4.869	0.838	0.188	0.103	0.108	0.213
30	0.621	5.987	-5.348	0.688	0.135	-0.199	-0.120	0.175
31	0.591	11.984	-7.126	1.068	0.378	-0.882	-0.348	0.619
32	10.978	37.786	-13.004	62.045	6.959	-6.147	-4.213	2.708

Table A.18. Stiffness coefficients and uncertainties for the 10 mil SB clearance seal with high pre-swirl.

Test Point	K_{tt} [MN/m]	K_{tr} [MN/m]	K_{rt} [MN/m]	K_{rr} [MN/m]	$u_{K_{tt}}$ [MN/m]	$u_{K_{tr}}$ [MN/m]	$u_{K_{rt}}$ [MN/m]	$u_{K_{rr}}$ [MN/m]
33	-0.310	6.012	-5.975	-0.130	0.194	0.218	0.219	0.220
34	-0.311	6.535	-6.046	0.090	0.144	-0.214	-0.166	0.396
35	0.874	10.575	-6.977	6.037	0.456	-0.717	-0.435	0.690
36	16.248	44.312	-12.458	100.589	5.032	-0.398	0.308	-0.371
37	-0.077	6.437	-6.464	0.080	0.167	0.210	0.222	0.260
38	-0.112	8.141	-7.106	0.039	0.153	-0.225	-0.187	0.310
39	0.042	14.765	-9.129	1.519	0.365	-0.575	-0.403	1.290
40	15.286	43.339	-13.573	94.773	6.223	-2.001	-0.312	-0.441
41	0.204	7.030	-7.042	0.400	0.189	0.214	0.243	0.281
42	0.138	8.582	-7.594	0.300	0.151	-0.223	-0.144	0.254
43	0.110	16.232	-9.678	1.422	0.319	-0.343	-0.321	1.262
44	13.352	43.015	-15.166	82.990	5.730	-2.265	-1.272	0.194
45	0.440	7.363	-7.296	0.760	0.182	0.160	0.230	0.264
46	0.520	8.502	-7.722	0.662	0.166	-0.317	-0.155	0.369
47	0.298	17.206	-10.202	0.952	0.343	-0.407	-0.382	1.207
48	14.951	47.338	-16.244	89.934	6.119	-3.506	-2.490	1.326
49	-0.550	6.718	-7.030	-0.620	0.342	0.185	0.315	0.226
50	-0.497	7.387	-6.710	0.144	0.132	-0.349	-0.136	0.243
51	1.349	11.714	-8.160	8.213	0.427	-0.608	-0.331	0.690
52	16.539	45.987	-9.867	102.288	5.692	-0.322	-0.367	0.128
53	-0.117	7.873	-8.271	-0.263	0.270	0.212	0.235	0.260
54	-0.516	10.056	-8.746	-0.139	0.171	-0.078	-0.212	0.454
55	0.802	14.929	-11.014	7.281	0.314	-0.792	-0.322	0.620
56	16.678	49.945	-14.792	94.836	4.189	-1.511	-0.503	0.465
57	0.374	8.707	-8.857	0.056	0.230	0.136	0.164	0.179
58	-	-	-	-	-	-	-	-
59	0.242	17.628	-12.004	5.277	0.286	-0.491	-0.282	0.688
60	17.702	50.578	-17.926	112.131	4.759	-2.162	0.181	-0.330
61	0.669	9.507	-9.488	0.357	0.079	0.144	0.125	0.253
62	0.569	9.670	-10.953	0.211	0.246	0.143	0.280	0.102
63	2.347	12.793	-20.337	1.014	0.913	0.382	0.308	0.281
64	75.246	-13.772	-83.049	53.407	6.929	2.411	6.483	3.285

Table A.19. Damping coefficients and uncertainties for the 10 mil SB clearance seal with high pre-swirl.

Test Point	C_{tt}	C_{tr}	C_{rt}	C_{rr}	$u_{C_{tt}}$	$u_{C_{tr}}$	$u_{C_{rt}}$	$u_{C_{rr}}$
	[kN-s/m]	[kN-s/m]	[kN-s/m]	[kN-s/m]	[kN-s/m]	[kN-s/m]	[kN-s/m]	[kN-s/m]
1	22.534	2.418	-1.513	22.665	0.802	0.222	0.383	0.849
2	23.830	1.541	-2.747	27.906	0.691	-0.401	-0.240	0.532
3	29.913	1.447	-2.234	62.543	0.870	-1.268	-0.806	1.618
4	37.730	31.159	27.807	182.535	5.574	-0.444	-0.640	0.447
5	21.678	2.415	-1.449	21.935	0.638	0.238	0.437	0.792
6	24.503	1.492	-2.701	27.895	0.570	-0.321	-0.300	0.553
7	32.554	1.420	-3.282	60.734	0.665	-0.811	-0.877	2.232
8	44.578	30.972	29.007	229.286	9.068	-6.338	-6.284	3.206
9	23.197	2.672	-1.422	23.287	0.720	0.188	0.593	0.841
10	25.315	1.654	-2.891	28.541	0.928	-0.315	-0.272	0.791
11	34.197	1.352	-3.837	65.067	0.943	-0.765	-0.865	1.192
12	47.178	23.711	22.030	237.020	18.317	-16.240	-13.195	11.778
13	25.130	2.683	-1.443	25.679	0.876	0.222	0.476	0.753
14	27.299	1.807	-2.899	30.697	0.790	-0.442	-0.249	0.650
15	35.157	1.990	-3.343	63.636	0.971	-0.519	-0.593	1.507
16	53.202	23.994	22.905	262.541	4.061	-3.813	-3.400	3.274
17	21.069	4.369	-3.916	21.347	0.701	0.164	0.155	0.697
18	22.290	3.657	-4.969	26.086	0.592	-0.295	-0.232	0.692
19	24.719	6.111	-1.628	51.713	0.825	-0.609	-0.542	0.950
20	40.103	43.225	39.167	193.965	9.582	-1.562	0.772	-0.923
21	21.113	4.282	-3.913	21.428	0.754	0.197	0.108	0.683
22	23.509	3.783	-4.899	27.120	0.544	-0.371	-0.241	0.779
23	30.407	4.404	-5.010	58.927	0.525	-0.718	-0.741	1.812
24	44.450	39.379	36.788	211.061	21.510	-12.588	-4.399	1.465
25	24.811	4.462	-3.737	24.783	0.642	0.207	0.214	0.787
26	26.055	3.445	-5.074	29.700	0.478	-0.232	-0.293	0.784
27	32.464	4.077	-5.788	60.946	0.696	-0.777	-0.781	1.596
28	46.572	36.636	32.109	237.076	29.786	-25.881	-8.279	6.799
29	24.243	4.198	-3.698	24.327	0.676	0.199	0.276	0.853
30	26.585	3.473	-4.991	30.574	0.716	-0.341	-0.290	0.629
31	35.181	3.332	-5.846	64.256	0.817	-1.333	-0.642	1.145
32	50.191	30.096	33.618	232.212	25.328	-24.141	-10.363	10.613

Table A.20. Damping coefficients and uncertainties for the 10 mil SB clearance seal with high pre-swirl.

Test Point	C_{tt}	C_{tr}	C_{rt}	C_{rr}	$u_{C_{tt}}$	$u_{C_{tr}}$	$u_{C_{rt}}$	$u_{C_{rr}}$
	[kN-s/m]	[kN-s/m]	[kN-s/m]	[kN-s/m]	[kN-s/m]	[kN-s/m]	[kN-s/m]	[kN-s/m]
33	18.265	6.071	-6.567	18.191	0.574	0.427	0.777	0.511
34	18.431	5.634	-6.561	21.986	0.515	-0.519	-0.318	0.838
35	21.470	10.312	0.615	41.699	1.201	-1.248	-0.823	1.179
36	42.494	46.741	39.734	203.202	16.049	-1.570	2.112	0.632
37	20.266	6.025	-6.585	20.413	0.496	0.288	0.678	0.453
38	22.460	5.808	-7.166	26.121	0.651	-0.299	-0.328	0.860
39	28.511	7.016	-6.736	55.946	0.574	-1.117	-0.973	1.817
40	42.791	42.277	34.320	184.827	13.655	-4.356	-2.182	2.562
41	22.390	6.055	-6.486	22.429	0.674	0.383	0.886	0.571
42	24.213	5.749	-7.181	27.625	0.786	-0.347	-0.355	1.275
43	30.844	6.658	-7.739	59.505	0.686	-0.911	-0.975	0.862
44	44.924	38.738	30.686	196.152	21.118	-10.517	-4.596	2.719
45	23.751	5.846	-6.431	23.768	0.664	0.576	0.940	0.484
46	25.110	5.789	-7.323	28.606	0.614	-0.527	-0.570	0.803
47	32.803	6.187	-7.809	60.965	1.024	-1.045	-1.025	1.805
48	49.153	37.598	33.158	211.497	11.135	-5.371	-3.534	0.558
49	16.093	7.785	-8.520	15.956	0.704	0.417	0.493	0.663
50	15.554	7.336	-7.972	18.505	0.647	-0.473	-0.519	0.795
51	18.917	11.088	1.032	34.911	0.899	-1.209	-0.549	0.865
52	35.358	38.218	28.466	143.771	11.251	0.121	1.421	0.459
53	19.163	7.918	-8.586	19.059	0.628	0.399	0.557	0.617
54	20.729	7.781	-8.792	24.215	0.616	-0.403	-0.435	0.721
55	23.472	11.177	-2.373	43.037	0.883	-1.064	-0.669	1.220
56	39.035	35.711	28.495	169.394	14.210	-5.216	2.789	-0.855
57	21.072	7.916	-8.449	21.094	0.717	0.421	0.532	0.613
58	-	-	-	-	-	-	-	-
59	27.567	9.983	-5.397	48.643	0.780	-0.601	-0.781	1.101
60	42.662	34.506	30.463	177.464	10.317	-3.446	-2.308	0.883
61	23.269	7.902	-8.290	23.134	0.433	0.368	0.545	0.878
62	27.135	8.482	-7.525	23.456	0.725	0.422	0.573	0.728
63	53.263	6.912	-10.400	30.689	1.010	0.863	0.514	0.584
64	116.706	-68.975	-75.754	103.215	13.702	10.353	15.033	9.537

Table A.21. Virtual mass coefficients and uncertainties for the 10 mil SB clearance seal with high pre-swirl.

Test Point	M_{tt}	M_{tr}	M_{rt}	M_{rr}	$u_{M_{tt}}$	$u_{M_{tr}}$	$u_{M_{rt}}$	$u_{M_{rr}}$
	[kg]	[kg]	[kg]	[kg]	[kg]	[kg]	[kg]	[kg]
1	14.907	0.002	0.397	14.965	0.092	0.105	0.097	0.167
2	14.825	-0.617	-0.173	15.307	0.162	-0.197	-0.190	0.333
3	14.536	-1.441	-0.140	20.041	0.334	-0.743	-0.457	1.465
4	12.146	2.168	3.089	22.147	6.654	-2.263	-1.224	0.217
5	15.016	0.057	0.457	14.870	0.188	0.136	0.140	0.222
6	14.771	-0.860	-0.353	16.463	0.173	-0.374	-0.236	0.516
7	16.211	-1.418	-0.485	23.042	0.357	-0.801	-0.504	1.571
8	14.321	-1.946	2.031	1.731	7.594	-5.488	-3.795	2.386
9	16.721	0.092	0.478	16.401	0.216	0.116	0.176	0.231
10	16.376	-0.628	-0.481	17.830	0.223	-0.152	-0.273	0.361
11	18.374	-2.306	-0.297	23.129	0.532	-1.084	-0.520	1.009
12	15.658	-1.997	2.014	7.618	5.900	-5.036	-4.102	3.848
13	17.225	0.023	0.668	16.396	0.152	0.112	0.193	0.226
14	17.152	-0.866	-0.398	17.883	0.314	-0.258	-0.231	0.325
15	18.879	-1.675	-0.422	23.544	0.497	-0.575	-0.623	1.359
16	16.658	-2.777	1.464	13.571	3.436	-3.568	-4.308	4.239
17	14.793	0.441	0.096	15.195	0.157	0.132	0.118	0.324
18	14.524	-0.779	-0.900	15.473	0.185	-0.278	-0.171	0.303
19	11.635	-0.084	0.108	19.243	0.319	-0.509	-0.345	0.769
20	11.753	-4.566	6.515	21.520	5.717	-0.757	0.705	-0.220
21	14.629	0.620	0.136	15.092	0.145	0.182	0.138	0.343
22	14.772	-0.436	-0.689	15.566	0.218	-0.272	-0.147	0.225
23	14.893	-1.147	-0.236	20.640	0.322	-0.644	-0.378	0.831
24	11.205	-7.039	5.932	17.204	8.760	-3.791	-1.334	0.783
25	15.499	0.469	0.000	15.152	0.229	0.126	0.115	0.272
26	14.982	-0.565	-0.859	16.053	0.200	-0.268	-0.105	0.224
27	15.731	-1.106	-0.713	21.805	0.386	-0.464	-0.315	0.743
28	10.225	-9.196	3.550	12.827	18.645	-12.197	-11.651	7.064
29	15.210	0.304	0.106	14.907	0.262	0.144	0.150	0.296
30	14.822	-0.492	-0.742	15.896	0.188	-0.277	-0.167	0.244
31	16.137	-0.850	-0.897	21.394	0.525	-1.226	-0.483	0.861
32	13.357	-5.797	3.760	23.028	10.805	-9.543	-6.540	4.205

Table A.22. Virtual mass coefficients and uncertainties for the 10 mil SB clearance seal with high pre-swirl.

Test Point	M_{tt}	M_{tr}	M_{rt}	M_{rr}	$u_{M_{tt}}$	$u_{M_{tr}}$	$u_{M_{rt}}$	$u_{M_{rr}}$
	[kg]	[kg]	[kg]	[kg]	[kg]	[kg]	[kg]	[kg]
33	14.248	0.726	-0.820	14.719	0.266	0.298	0.301	0.301
34	13.117	-0.724	-1.245	14.249	0.198	-0.294	-0.227	0.543
35	9.100	1.493	1.599	15.575	0.625	-0.984	-0.596	0.946
36	9.253	-11.094	8.772	15.169	7.812	-0.618	0.478	-0.575
37	14.182	0.686	-0.790	14.956	0.229	0.289	0.304	0.356
38	14.433	-0.010	-0.870	15.318	0.210	-0.308	-0.256	0.425
39	13.927	-0.887	-0.035	19.902	0.500	-0.788	-0.552	1.770
40	11.141	-5.636	5.377	23.039	9.661	-3.106	-0.484	-0.685
41	14.438	0.673	-0.961	15.239	0.279	0.316	0.358	0.415
42	14.643	0.083	-1.031	15.543	0.223	-0.330	-0.212	0.375
43	15.040	-1.056	-0.712	21.238	0.471	-0.507	-0.474	1.864
44	8.890	-9.107	6.030	21.936	8.896	-3.516	-1.974	0.301
45	14.370	0.879	-0.934	15.191	0.249	0.219	0.315	0.362
46	14.773	-0.360	-1.102	15.819	0.228	-0.434	-0.213	0.506
47	15.511	-0.654	-1.178	20.207	0.470	-0.559	-0.524	1.655
48	10.177	-8.185	5.642	21.166	9.500	-5.443	-3.866	2.058
49	13.930	0.417	-0.945	14.148	0.469	0.254	0.432	0.310
50	12.819	0.039	-1.452	14.140	0.181	-0.479	-0.187	0.334
51	9.521	1.962	1.436	13.272	0.586	-0.834	-0.454	0.946
52	9.720	-1.595	7.152	20.436	8.837	-0.500	-0.570	0.198
53	14.416	0.506	-0.979	14.792	0.377	0.297	0.328	0.364
54	13.992	0.515	-1.140	15.056	0.239	-0.109	-0.296	0.635
55	10.933	3.316	1.019	17.064	0.439	-1.106	-0.450	0.867
56	8.778	-5.416	5.363	16.266	6.504	-2.345	-0.782	0.722
57	14.706	1.006	-0.946	14.757	0.321	0.191	0.229	0.250
58	-	-	-	-	-	-	-	-
59	12.285	2.303	0.701	18.821	0.399	-0.685	-0.394	0.961
60	8.846	-10.020	4.482	18.745	7.389	-3.357	0.281	-0.513
61	14.623	1.136	-1.045	14.860	0.110	0.201	0.175	0.353
62	15.390	1.403	-0.869	14.150	0.344	0.199	0.391	0.142
63	18.837	1.142	-1.560	14.924	1.276	0.533	0.430	0.393
64	19.225	-9.972	4.429	10.444	10.758	3.743	10.066	5.101

Table A.23. WFR, C_{eff}, and uncertainties for the 10 mil SB clearance seal with high pre-swirl.

Test Point	WFR	u_{WFR}	C_{eff}	$u_{C_{eff}}$
			[kN-s/m]	[kN-s/m]
1	0.497	0.017	11.374	0.635
2	0.485	0.021	13.336	0.649
3	0.468	0.035	25.331	1.785
4	0.476	0.109	64.102	5.309
5	0.487	0.019	11.181	0.613
6	0.473	0.030	13.827	0.872
7	0.462	0.037	25.300	2.027
8	0.498	0.157	80.944	12.655
9	0.486	0.019	11.953	0.648
10	0.490	0.022	13.716	0.789
11	0.452	0.037	27.469	2.070
12	0.496	0.171	82.577	15.056
13	0.483	0.018	13.125	0.679
14	0.481	0.021	15.060	0.753
15	0.467	0.032	26.498	1.624
16	0.479	0.109	91.027	9.310
17	0.514	0.014	10.305	0.516
18	0.492	0.014	12.307	0.531
19	0.482	0.017	20.553	0.812
20	0.170	0.255	71.123	4.878
21	0.505	0.015	10.523	0.545
22	0.490	0.014	12.914	0.544
23	0.467	0.016	24.253	1.139
24	0.261	0.297	76.403	11.214
25	0.494	0.012	12.538	0.528
26	0.485	0.012	14.365	0.521
27	0.467	0.013	25.139	0.994
28	0.392	0.319	85.935	20.043
29	0.481	0.013	12.608	0.573
30	0.474	0.012	15.054	0.552
31	0.464	0.022	26.909	1.332
32	0.345	0.274	80.518	16.365

Table A.24. WFR, C_{eff}, and uncertainties for the 10 mil SB clearance seal with high pre-swirl.

Test Point	WFR	u_{WFR}	C_{eff}	$u_{C_{eff}}$
			[kN-s/m]	[kN-s/m]
33	0.523	0.017	8.699	0.456
34	0.496	0.016	10.208	0.537
35	0.437	0.027	17.633	1.073
36	0.000	0.000	77.700	8.041
37	0.504	0.015	10.088	0.415
38	0.499	0.015	12.173	0.587
39	0.459	0.016	23.236	1.104
40	0.000	0.000	68.548	7.131
41	0.499	0.015	11.228	0.511
42	0.496	0.016	13.065	0.778
43	0.463	0.011	24.583	0.665
44	0.140	0.384	74.271	10.845
45	0.490	0.013	12.111	0.467
46	0.481	0.014	13.967	0.578
47	0.470	0.015	25.102	1.128
48	0.161	0.218	79.760	6.540
49	0.512	0.020	7.826	0.530
50	0.494	0.020	8.624	0.559
51	0.429	0.021	15.062	0.748
52	0.000	0.000	56.249	5.638
53	0.504	0.015	9.485	0.479
54	0.499	0.012	11.262	0.493
55	0.463	0.019	17.785	0.909
56	0.097	0.393	65.586	7.181
57	0.497	0.013	10.609	0.489
58	-	-	-	-
59	0.463	0.012	20.434	0.754
60	0.000	0.000	69.177	5.337
61	0.488	0.011	11.875	0.502
62	0.486	0.012	12.998	0.547
63	0.474	0.010	22.216	0.653
64	0.000	0.000	52.166	9.313

Assembly 3 – 15 mil Clearance SB Seal with High Pre-Swirl

Table A.25. Static results of the 15 mil SB clearance seal with high pre-swirl.

Test Point	Target ω	Target ΔP	Target ε_0	Measured ω	Measured ΔP	Measured ε_0	ϕ	$\dot{Q}$	F_s
	[rpm]	[bar]	[-]	[rpm]	[bar]	[-]	[deg]	[LPM]	[N]
1	2000	2.068	0.00	2006.73	2.435	0.009		18.223	0.00
2	2000	2.068	0.27	2006.89	2.292	0.274	66.68	18.304	91.42
3	2000	2.068	0.53	2007.18	2.147	0.543	72.09	22.321	229.17
4	2000	2.068	0.80	2006.87	2.067	0.807	65.02	28.632	665.92
5	2000	4.137	0.00	2008.15	4.202	0.051		31.586	0.00
6	2000	4.137	0.27	2007.74	4.102	0.271	76.38	31.569	118.69
7	2000	4.137	0.53	2007.45	3.944	0.547	70.44	38.829	291.66
8	2000	4.137	0.80	2006.94	3.865	0.801	71.94	46.152	756.67
9	2000	6.205	0.00	2008.15	6.051	0.009		42.942	0.00
10	2000	6.205	0.27	2008.15	5.869	0.271	42.62	45.721	163.93
11	2000	6.205	0.53	2008.17	5.611	0.529	53.29	54.947	345.83
12	2000	6.205	0.80	2007.76	5.096	0.801	69.76	65.399	822.30
13	2000	8.274	0.00	2008.31	7.381	0.010		59.758	0.00
14	2000	8.274	0.27	2008.02	7.571	0.272	37.62	59.780	215.38
15	2000	8.274	0.53	2008.07	7.079	0.532	46.29	67.935	424.28
16	2000	8.274	0.80	2007.67	6.481	0.792	63.47	79.668	874.70
17	4000	2.068	0.00	4002.12	2.245	0.014		18.249	0.00
18	4000	2.068	0.27	4002.20	2.325	0.275	78.19	18.936	175.94
19	4000	2.068	0.53	4002.44	2.228	0.534	82.23	23.734	435.67
20	4000	2.068	0.80	4002.72	2.110	0.804	64.58	31.012	1207.8
21	4000	4.137	0.00	4002.63	4.268	0.004		34.149	0.00
22	4000	4.137	0.27	4002.46	3.952	0.278	70.54	34.345	195.34
23	4000	4.137	0.53	4002.63	3.752	0.547	76.66	41.532	478.82
24	4000	4.137	0.80	4001.28	3.718	0.805	66.88	49.859	1379.5
25	4000	6.205	0.00	4002.76	5.836	0.008		47.361	0.00
26	4000	6.205	0.27	4002.91	5.676	0.280	62.71	51.290	237.89
27	4000	6.205	0.53	4002.57	5.645	0.510	70.79	55.356	510.40
28	4000	6.205	0.80	4001.20	5.053	0.800	68.79	66.066	1401.9
29	4000	8.274	0.00	4002.34	7.657	0.022		57.952	0.00
30	4000	8.274	0.27	4002.91	7.258	0.278	51.68	61.238	270.16
31	4000	8.274	0.53	4002.28	6.861	0.537	60.13	70.452	574.35
32	4000	8.274	0.80	4000.76	6.587	0.800	67.59	80.350	1516.5

Table A.26. Static results of the 15 mil SB clearance seal with high pre-swirl.

Test Point	Target ω	Target ΔP	Target ε_0	Measured ω	Measured ΔP	Measured ε_0	ϕ	$\dot{Q}$	F_s
	[rpm]	[bar]	[-]	[rpm]	[bar]	[-]	[deg]	[LPM]	[N]
33	6000	2.068	0.00	6007.03	2.250	0.007		17.217	0.00
34	6000	2.068	0.27	6006.82	2.221	0.273	86.35	18.946	240.06
35	6000	2.068	0.53	6006.41	2.203	0.542	87.57	22.761	656.04
36	6000	2.068	0.80	6005.79	2.049	0.792	58.95	28.446	1617.7
37	6000	4.137	0.00	6006.40	4.115	0.008		31.912	0.00
38	6000	4.137	0.27	6006.13	4.014	0.273	83.66	34.154	261.40
39	6000	4.137	0.53	6006.13	3.837	0.541	84.24	41.913	646.30
40	6000	4.137	0.80	6004.49	3.501	0.799	66.53	50.616	1694.0
41	6000	6.205	0.00	6005.22	5.989	0.022		48.335	0.00
42	6000	6.205	0.27	6005.23	5.801	0.271	67.84	48.435	313.00
43	6000	6.205	0.53	6005.40	5.370	0.555	76.80	56.456	752.45
44	6000	6.205	0.80	6002.56	5.084	0.797	80.64	66.919	2481.3
45	6000	8.274	0.00	6003.20	7.374	0.021		60.757	0.00
46	6000	8.274	0.27	6003.65	7.224	0.278	66.47	65.102	331.22
47	6000	8.274	0.53	6003.03	7.138	0.524	73.96	69.944	757.15
48	6000	8.274	0.80	6000.10	6.397	0.808	66.42	82.533	2105.3
49	8000	2.068	0.00	7999.27	2.321	0.017		18.213	0.00
50	8000	2.068	0.27	8000.18	2.277	0.274	-87.81	18.188	333.00
51	8000	2.068	0.53	8000.73	2.243	0.537	-89.55	21.519	876.37
52	8000	2.068	0.80	7999.16	2.113	0.794	57.81	27.700	2220.5
53	8000	4.137	0.00	8002.10	3.950	0.019		32.570	0.00
54	8000	4.137	0.27	8002.47	4.104	0.277	84.56	35.380	328.99
55	8000	4.137	0.53	8000.99	4.080	0.534	86.77	41.355	871.18
56	8000	4.137	0.80	8000.00	3.759	0.795	64.13	50.784	2365.3
57	8000	6.205	0.00	8002.48	5.739	0.001		46.823	0.00
58	8000	6.205	0.27	8001.87	5.666	0.273	75.88	52.552	322.17
59	8000	6.205	0.53	8001.25	5.570	0.535	83.56	57.158	872.36
60	8000	6.205	0.80	7998.92	5.308	0.794	66.32	66.572	2387.0
61	8000	8.274	0.00	8001.93	7.448	0.024		57.049	0.00
62	8000	8.274	0.27	8002.01	7.214	0.281	71.23	63.401	413.71
63	8000	8.274	0.53	8001.11	7.156	0.523	79.21	69.448	938.24
64	8000	8.274	0.80	7998.68	6.625	0.790	68.98	79.201	2519.7

Table A.27. Static results of the 15 mil SB clearance seal with high pre-swirl.

Test Point	PSR	OSR	Inlet Temperature	Average Outlet Temperature	Re_a	Re_c	Re_t
	[-]	[-]	[°C]	[°C]	[-]	[-]	[-]
1	0.332	0.276	47.258	46.807	70.822	139.512	156.459
2	0.285	0.257	46.186	45.901	68.287	133.932	150.336
3	0.304	0.316	46.254	46.720	84.822	136.442	160.658
4	0.445	0.401	47.074	48.007	113.616	142.454	182.214
5	0.670	0.208	46.241	46.757	120.090	136.580	181.867
6	0.529	0.332	46.026	45.659	116.794	132.872	176.906
7	0.639	0.476	46.791	47.134	150.473	139.160	204.957
8	0.408	0.572	46.651	46.418	175.725	136.694	222.631
9	0.703	0.330	46.661	45.990	162.105	135.606	211.346
10	0.590	0.367	46.296	46.499	173.093	135.998	220.129
11	0.456	0.499	45.959	45.715	203.231	132.868	242.810
12	0.421	0.550	46.149	46.536	247.039	135.669	281.841
13	0.761	0.338	46.789	47.303	232.375	139.700	271.135
14	0.578	0.383	45.885	45.027	217.630	130.769	253.896
15	0.474	0.452	44.698	45.224	242.182	128.055	273.953
16	0.465	0.548	46.036	46.641	300.906	135.647	330.068
17	0.389	0.000	47.511	48.760	74.185	291.034	300.340
18	0.295	0.031	46.899	46.714	72.911	275.663	285.142
19	0.254	0.180	45.884	47.104	90.231	272.196	286.761
20	0.265	0.235	46.511	48.294	122.411	282.631	308.001
21	0.391	0.228	47.181	47.224	133.644	280.215	310.453
22	0.333	0.250	46.666	47.017	132.434	276.082	306.203
23	0.354	0.289	46.997	48.126	164.949	284.373	328.749
24	0.381	0.359	46.703	46.738	191.301	274.628	334.689
25	0.495	0.244	46.445	47.321	182.945	276.587	331.616
26	0.464	0.312	47.167	48.237	204.879	286.030	351.836
27	0.447	0.352	46.615	46.286	210.035	271.670	343.394
28	0.415	0.363	46.431	47.319	255.121	276.395	376.139
29	0.602	0.234	46.173	45.618	214.883	265.473	341.542
30	0.550	0.331	45.734	46.459	228.974	267.739	352.297
31	0.446	0.354	46.560	47.598	274.354	278.802	391.153
32	0.376	0.362	46.765	46.568	307.603	273.980	411.928

Table A.28. Static results of the 15 mil SB clearance seal with high pre-swirl.

Test Point	PSR	OSR	Inlet Temperature	Average Outlet Temperature	Re_a	Re_c	Re_t
	[-]	[-]	[°C]	[°C]	[-]	[-]	[-]
33	0.485	0.167	46.170	48.071	67.184	419.306	424.654
34	0.409	0.154	46.737	49.233	76.598	434.436	441.137
35	0.294	0.206	47.306	48.714	92.067	434.611	444.256
36	0.248	0.243	46.298	49.006	113.483	428.604	443.373
37	0.346	0.179	46.181	46.643	120.897	407.044	424.619
38	0.289	0.222	45.693	47.122	129.393	407.032	427.104
39	0.285	0.253	46.297	48.608	165.813	425.047	456.245
40	0.298	0.282	47.341	49.930	210.080	445.805	492.824
41	0.373	0.122	47.168	47.820	191.438	425.465	466.551
42	0.326	0.188	46.376	46.670	184.332	408.830	448.464
43	0.329	0.243	45.751	47.445	215.592	410.239	463.440
44	0.359	0.348	47.451	48.227	268.774	431.264	508.162
45	0.423	0.202	46.674	48.119	239.726	423.714	486.829
46	0.395	0.273	47.368	48.909	264.724	436.701	510.673
47	0.383	0.309	46.512	46.915	268.281	411.888	491.555
48	0.467	0.334	46.511	48.410	326.557	424.680	535.717
49	0.423	0.115	47.052	49.657	74.742	587.233	591.971
50	0.444	0.166	46.476	49.216	73.132	575.440	580.069
51	0.404	0.212	45.781	48.908	84.809	564.066	570.407
52	0.285	0.269	45.766	50.042	111.800	577.539	588.260
53	0.345	0.237	46.978	50.288	135.232	594.348	609.539
54	0.301	0.259	47.448	49.817	146.798	593.965	611.836
55	0.270	0.265	46.819	48.710	165.662	573.330	596.784
56	0.268	0.296	46.017	48.047	197.461	556.438	590.435
57	0.336	0.223	45.787	48.286	182.144	556.874	585.905
58	0.317	0.252	47.232	50.118	218.504	595.161	634.003
59	0.296	0.247	47.305	48.592	230.620	577.490	621.836
60	0.302	0.276	46.131	47.955	258.945	556.568	613.857
61	0.356	0.206	44.947	46.553	210.318	527.708	568.075
62	0.332	0.249	45.862	48.458	247.899	559.687	612.131
63	0.319	0.256	45.984	47.370	266.040	548.286	609.422
64	0.326	0.287	45.299	47.004	296.910	536.397	613.088

Table A.29. Stiffness coefficients and uncertainties for the 15 mil SB clearance seal with high pre-swirl.

Test Point	K_{tt} [MN/m]	K_{tr} [MN/m]	K_{rt} [MN/m]	K_{rr} [MN/m]	$u_{K_{tt}}$ [MN/m]	$u_{K_{tr}}$ [MN/m]	$u_{K_{rt}}$ [MN/m]	$u_{K_{rr}}$ [MN/m]
1	0.091	0.875	-0.881	0.023	0.110	0.096	0.107	0.152
2	-22.489	14.833	13.146	-16.839	0.265	0.196	0.204	0.256
3	0.071	2.315	-1.285	-0.129	0.129	0.146	0.179	0.194
4	-18.538	21.840	11.456	-13.018	0.476	0.844	0.759	1.524
5	-24.311	14.092	12.511	-14.306	0.244	0.191	0.259	0.299
6	-22.204	14.864	13.037	-16.476	0.254	0.212	0.195	0.245
7	-22.016	16.142	12.785	-16.931	0.290	0.272	0.224	0.327
8	-17.796	23.182	11.280	-16.111	0.463	0.756	0.463	1.165
9	-23.507	14.331	12.351	-13.833	0.234	0.230	0.223	0.277
10	-24.197	14.197	12.110	-13.474	0.214	0.191	0.219	0.254
11	-20.729	16.310	12.744	-17.584	0.299	0.254	0.242	0.308
12	-17.726	25.696	11.334	-20.052	0.701	0.905	0.999	1.947
13	-22.860	14.383	12.315	-13.194	0.207	0.231	0.248	0.251
14	-20.968	15.219	12.781	-15.786	0.273	0.231	0.256	0.231
15	-17.501	16.550	12.774	-20.101	0.365	0.191	0.234	0.228
16	-15.161	24.107	11.077	-22.746	0.574	0.725	0.442	0.957
17	-24.574	14.814	11.902	-14.752	0.277	0.186	0.264	0.290
18	-21.425	16.132	12.391	-17.934	0.314	0.199	0.213	0.197
19	-18.624	18.339	11.898	-20.813	0.318	0.255	0.200	0.251
20	-15.208	27.103	9.136	-5.104	0.536	0.901	0.688	1.792
21	-24.155	14.958	11.809	-14.400	0.226	0.183	0.209	0.252
22	-21.657	16.032	12.246	-17.095	0.240	0.205	0.226	0.214
23	-19.832	18.309	12.029	-19.121	0.297	0.248	0.211	0.261
24	-14.049	28.626	8.470	-5.794	0.606	0.905	0.733	1.367
25	-23.484	15.026	11.731	-13.798	0.196	0.208	0.228	0.211
26	-23.425	15.293	11.687	-14.214	0.229	0.202	0.215	0.241
27	-18.418	18.223	11.750	-19.819	0.330	0.243	0.236	0.188
28	-12.276	28.508	7.891	-11.166	0.799	0.991	0.789	1.094
29	-22.899	15.345	11.541	-13.219	0.208	0.249	0.241	0.257
30	-19.728	16.283	12.205	-17.175	0.294	0.244	0.224	0.144
31	-17.761	18.490	11.813	-20.019	0.399	0.321	0.277	0.217
32	-9.444	29.297	7.392	-12.974	0.996	1.021	0.682	0.827

Table A.30. Stiffness coefficients and uncertainties for the 15 mil SB clearance seal with high pre-swirl.

Test Point	K_{tt} [MN/m]	K_{tr} [MN/m]	K_{rt} [MN/m]	K_{rr} [MN/m]	$u_{K_{tt}}$ [MN/m]	$u_{K_{tr}}$ [MN/m]	$u_{K_{rt}}$ [MN/m]	$u_{K_{rr}}$ [MN/m]
33	-0.083	2.641	-2.488	-0.031	0.109	0.143	0.145	0.142
34	-17.557	16.959	11.642	-22.021	0.343	0.194	0.141	0.191
35	0.081	6.410	-3.589	-0.221	0.283	0.206	0.183	0.075
36	-11.321	29.364	7.990	-0.626	1.299	0.973	0.475	0.703
37	-24.376	15.987	10.861	-14.618	0.275	0.214	0.193	0.243
38	-14.252	16.405	10.471	-24.880	0.358	0.136	0.165	0.114
39	-12.174	18.463	8.963	-27.027	0.438	0.235	0.143	0.143
40	-8.829	29.752	5.256	-1.820	1.028	1.091	0.694	0.733
41	-23.808	15.754	11.211	-14.003	0.387	0.280	0.224	0.219
42	-19.907	17.360	11.479	-18.277	0.326	0.244	0.205	0.169
43	-4.954	11.492	1.063	-32.888	1.354	-0.232	-0.629	-0.051
44	-9.543	33.084	6.755	-1.446	0.861	0.985	0.661	0.987
45	-23.072	15.699	11.109	-13.424	0.242	0.243	0.236	0.231
46	-11.296	15.383	9.980	-25.525	0.348	0.130	0.198	0.005
47	-10.382	17.888	8.203	-27.501	0.467	0.156	0.196	0.062
48	-6.551	32.317	2.987	0.605	1.731	1.261	0.644	0.502
49	-24.739	16.725	10.571	-14.890	0.290	0.505	0.238	0.351
50	-12.236	16.021	8.868	-27.602	0.439	0.142	0.090	0.150
51	-11.479	19.675	7.310	-27.940	0.501	0.166	0.116	0.142
52	-8.444	33.292	6.252	9.319	1.062	0.460	0.157	0.336
53	-24.002	16.520	10.408	-14.587	0.378	0.248	0.268	0.197
54	-14.025	17.103	9.876	-25.010	0.391	0.166	0.147	0.085
55	-11.970	20.307	7.569	-27.436	0.486	0.224	0.254	0.135
56	-7.463	34.997	3.725	5.585	1.413	0.853	0.425	0.129
57	-23.900	16.693	10.086	-14.261	0.327	0.271	0.191	0.261
58	-13.938	17.065	10.151	-24.329	0.457	0.223	0.151	0.109
59	0.690	8.403	-4.623	-0.310	0.421	0.379	0.097	0.090
60	-6.844	34.679	2.598	6.154	1.172	1.248	0.620	0.549
61	-23.422	16.784	10.202	-13.915	0.256	0.255	0.320	0.273
62	-13.003	17.086	9.785	-24.507	0.552	0.256	0.134	0.060
63	-11.373	20.486	7.770	-26.842	0.523	0.219	0.144	0.039
64	-5.927	34.780	1.215	3.144	1.537	1.213	0.433	0.218

Table A.31. Damping coefficients and uncertainties for the 15 mil SB clearance seal with high pre-swirl.

Test Point	C_{tt} [kN-s/m]	C_{tr} [kN-s/m]	C_{rt} [kN-s/m]	C_{rr} [kN-s/m]	$u_{C_{tt}}$ [kN-s/m]	$u_{C_{tr}}$ [kN-s/m]	$u_{C_{rt}}$ [kN-s/m]	$u_{C_{rr}}$ [kN-s/m]
1	9.457	2.058	-1.678	9.098	0.284	0.159	0.386	0.248
2	6.364	5.012	1.442	7.908	1.228	1.370	1.024	1.088
3	13.507	2.143	-1.871	23.594	0.391	0.393	0.338	0.697
4	16.902	14.490	11.115	97.478	2.223	2.976	1.992	4.089
5	5.594	5.299	1.511	7.038	1.564	1.253	1.671	1.175
6	7.253	5.441	1.020	8.697	1.102	1.310	1.013	0.996
7	9.938	5.791	0.910	21.421	1.179	1.266	1.140	1.141
8	20.230	9.822	6.893	103.782	2.522	3.646	2.464	5.754
9	6.759	5.413	0.953	7.921	0.945	1.248	1.077	1.233
10	7.171	5.700	0.736	9.912	0.852	1.260	1.022	1.274
11	11.009	6.117	0.613	21.007	1.223	1.341	1.034	1.079
12	24.203	4.461	0.077	124.178	2.385	2.236	2.867	3.475
13	7.108	5.689	0.687	8.272	0.876	1.446	1.054	1.306
14	8.705	5.933	0.568	10.381	1.077	1.358	0.977	1.035
15	12.283	6.240	0.182	21.089	1.379	1.325	1.012	0.902
16	24.157	5.333	-0.372	107.715	2.419	2.071	2.463	1.666
17	4.944	5.993	0.383	5.803	1.081	1.333	1.225	1.280
18	7.093	6.264	0.156	7.797	1.302	1.352	1.015	1.006
19	10.475	6.784	-0.217	18.556	1.317	1.434	0.765	0.894
20	16.116	17.947	9.468	81.043	2.402	4.393	2.591	6.046
21	6.043	6.723	-0.345	7.109	0.928	1.295	0.990	1.286
22	7.576	6.933	-0.461	8.422	1.089	1.281	0.932	1.065
23	10.228	7.814	-0.582	19.339	1.252	1.286	1.004	1.025
24	18.583	17.589	8.555	92.075	3.100	5.581	2.515	5.821
25	6.586	6.903	-0.560	7.559	0.746	1.313	1.056	1.173
26	7.344	7.277	-0.804	9.436	0.827	1.244	1.164	1.206
27	11.880	7.676	0.135	18.310	1.376	1.354	1.028	1.019
28	19.837	15.161	6.032	89.761	3.565	5.026	3.102	4.770
29	7.505	7.076	-0.745	8.663	0.693	1.378	1.296	1.258
30	8.990	7.588	-1.064	9.700	1.028	1.318	1.156	0.971
31	11.864	8.295	-1.390	19.485	1.684	1.332	1.045	1.016
32	22.425	10.943	10.612	91.729	4.045	4.470	2.464	3.274

Table A.32. Damping coefficients and uncertainties for the 15 mil SB clearance seal with high pre-swirl.

Test Point	C_{tt}	C_{tr}	C_{rt}	C_{rr}	$u_{C_{tt}}$	$u_{C_{tr}}$	$u_{C_{rt}}$	$u_{C_{rr}}$
	[kN-s/m]	[kN-s/m]	[kN-s/m]	[kN-s/m]	[kN-s/m]	[kN-s/m]	[kN-s/m]	[kN-s/m]
33	9.556	4.362	-4.136	8.846	0.380	0.487	0.380	0.400
34	7.086	7.390	-1.234	5.825	1.536	1.449	0.844	0.664
35	13.554	5.254	-4.574	22.151	0.951	0.236	0.333	0.234
36	16.696	20.159	10.842	61.766	6.407	5.528	3.141	3.385
37	7.177	7.853	-1.543	8.093	0.966	1.476	0.909	1.239
38	9.765	7.704	-2.469	7.405	1.525	1.097	0.721	0.546
39	12.306	8.587	-2.959	17.619	1.988	1.107	0.764	0.263
40	17.726	20.139	6.821	72.974	5.731	6.747	3.288	3.852
41	7.072	8.535	-2.503	8.190	1.148	1.571	1.243	1.339
42	8.798	8.778	-2.423	9.073	1.558	1.184	0.962	0.955
43	13.049	7.427	-4.928	17.510	4.463	-0.392	-0.919	0.253
44	20.158	20.956	9.200	75.206	4.607	6.099	2.945	3.740
45	7.625	8.802	-2.517	8.442	0.914	1.462	1.383	1.403
46	10.192	8.252	-3.076	7.503	1.753	1.050	1.201	0.055
47	13.451	9.127	-3.686	17.551	2.089	0.796	0.785	0.117
48	21.032	19.926	4.816	86.401	8.551	6.617	3.311	1.944
49	4.197	8.802	-2.562	5.453	1.047	1.802	0.834	2.028
50	7.914	8.119	-3.038	4.605	1.981	0.945	0.614	0.333
51	11.453	9.140	-2.945	15.142	2.220	1.164	0.487	0.167
52	16.159	22.227	11.361	57.069	5.552	3.137	1.156	1.521
53	5.930	8.004	-1.795	6.851	1.878	1.521	1.004	1.254
54	8.918	8.274	-2.490	6.777	2.166	1.301	0.739	0.193
55	12.930	9.835	-3.193	17.102	2.037	1.169	1.000	0.242
56	19.648	22.694	7.126	67.170	8.025	6.672	2.167	1.224
57	7.862	9.855	-3.492	8.521	1.642	1.458	0.860	1.445
58	9.853	9.970	-4.204	7.324	2.173	1.149	0.567	0.469
59	15.078	8.912	-7.975	23.015	1.031	0.742	0.591	0.252
60	19.620	22.665	3.805	67.827	7.032	7.123	1.879	1.053
61	8.353	10.470	-4.064	9.194	1.115	1.456	1.587	1.428
62	10.662	10.152	-4.525	8.094	2.664	1.234	0.562	0.387
63	13.563	11.398	-5.282	17.481	2.006	1.159	0.922	0.231
64	21.286	22.024	1.770	70.602	7.468	6.074	1.354	0.549

Table A.33. Virtual mass coefficients and uncertainties for the 15 mil SB clearance seal with high pre-swirl.

Test Point	M_{tt}	M_{tr}	M_{rt}	M_{rr}	$u_{M_{tt}}$	$u_{M_{tr}}$	$u_{M_{rt}}$	$u_{M_{rr}}$
	[kg]	[kg]	[kg]	[kg]	[kg]	[kg]	[kg]	[kg]
1	13.505	-0.214	0.432	12.605	0.582	0.505	0.566	0.804
2	14.708	-1.998	-1.500	12.634	1.397	1.035	1.079	1.352
3	14.912	-0.462	0.322	15.824	0.681	0.768	0.947	1.025
4	13.731	6.030	5.024	20.723	2.510	4.455	4.005	8.044
5	15.505	-1.520	-1.599	13.408	1.289	1.006	1.365	1.577
6	15.913	-2.155	-1.487	13.823	1.340	1.117	1.029	1.292
7	17.194	-1.976	-1.548	16.454	1.531	1.433	1.182	1.727
8	15.607	7.597	4.508	20.699	2.441	3.991	2.443	6.147
9	16.736	-1.407	-1.449	14.047	1.233	1.216	1.175	1.462
10	17.005	-1.602	-1.256	14.152	1.130	1.006	1.156	1.341
11	17.712	-1.757	-1.613	16.783	1.576	1.341	1.275	1.624
12	20.034	-2.301	-2.310	32.670	3.697	4.776	5.270	10.275
13	16.992	-1.786	-1.117	14.349	1.092	1.221	1.306	1.325
14	17.154	-1.665	-1.638	15.145	1.438	1.222	1.350	1.221
15	17.583	-1.854	-1.558	17.738	1.928	1.008	1.236	1.202
16	20.536	-1.956	-1.865	31.114	3.029	3.825	2.330	5.052
17	12.178	-1.487	-1.863	10.038	1.463	0.979	1.395	1.531
18	12.759	-2.123	-2.326	11.058	1.658	1.052	1.121	1.041
19	14.165	-2.580	-2.125	14.935	1.678	1.344	1.054	1.327
20	13.034	2.062	5.607	33.813	2.828	4.754	3.631	9.458
21	15.668	-2.096	-1.171	13.160	1.193	0.967	1.103	1.331
22	15.848	-2.419	-1.668	13.843	1.265	1.080	1.193	1.128
23	16.748	-2.647	-1.660	16.575	1.567	1.311	1.111	1.377
24	14.406	2.400	5.935	33.085	3.196	4.774	3.868	7.213
25	16.556	-1.722	-1.170	13.930	1.033	1.100	1.203	1.116
26	17.041	-1.919	-1.534	14.076	1.208	1.064	1.133	1.272
27	16.854	-2.964	-1.615	15.480	1.741	1.284	1.244	0.992
28	15.507	2.957	4.672	30.709	4.217	5.231	4.161	5.774
29	17.306	-0.885	-1.652	14.897	1.097	1.314	1.271	1.359
30	16.948	-2.006	-1.803	14.730	1.550	1.286	1.184	0.760
31	16.813	-2.405	-1.906	17.311	2.105	1.693	1.463	1.143
32	15.964	4.492	2.704	24.002	5.255	5.387	3.600	4.364

Table A.34. Virtual mass coefficients and uncertainties for the 15 mil SB clearance seal with high pre-swirl.

Test Point	M_{tt}	M_{tr}	M_{rt}	M_{rr}	$u_{M_{tt}}$	$u_{M_{tr}}$	$u_{M_{rt}}$	$u_{M_{rr}}$
	[kg]	[kg]	[kg]	[kg]	[kg]	[kg]	[kg]	[kg]
33	10.703	0.720	-0.326	10.909	0.574	0.754	0.765	0.748
34	11.944	-1.632	-2.613	11.237	1.810	1.022	0.745	1.007
35	12.389	-0.531	-0.689	13.478	1.491	1.086	0.964	0.395
36	10.799	-1.228	2.088	19.505	6.857	5.135	2.505	3.708
37	14.298	-2.747	-0.707	12.308	1.449	1.127	1.021	1.282
38	13.284	-2.803	-1.651	14.399	1.888	0.719	0.870	0.604
39	14.240	-2.553	-0.835	17.102	2.312	1.238	0.756	0.754
40	13.054	-2.839	6.258	36.112	5.425	5.759	3.663	3.870
41	15.963	-2.376	-0.077	13.913	2.044	1.478	1.181	1.156
42	16.178	-2.895	-1.968	14.665	1.723	1.287	1.080	0.891
43	16.793	-0.383	-4.401	19.812	7.145	-1.224	-3.321	-0.270
44	14.118	-0.192	6.255	35.717	4.543	5.196	3.488	5.208
45	16.403	-2.128	-0.974	13.741	1.276	1.280	1.247	1.221
46	15.578	-2.382	-2.188	15.649	1.835	0.684	1.043	0.024
47	16.013	-2.368	-2.373	17.844	2.466	0.825	1.035	0.327
48	14.133	-0.418	6.357	44.539	9.136	6.654	3.400	2.647
49	11.626	0.681	-1.568	10.489	1.529	2.663	1.254	1.854
50	11.294	-1.033	-2.418	11.573	2.317	0.751	0.474	0.790
51	11.515	-1.830	-1.827	13.467	2.643	0.875	0.611	0.748
52	10.221	0.786	3.751	19.343	5.605	2.425	0.826	1.772
53	14.403	-1.335	-1.461	10.341	1.997	1.310	1.414	1.040
54	12.371	-2.788	-2.398	11.979	2.061	0.875	0.773	0.449
55	12.323	-3.685	-1.181	13.899	2.563	1.184	1.342	0.713
56	10.703	-3.455	7.261	30.080	7.455	4.502	2.244	0.678
57	15.913	-3.122	-0.421	13.697	1.723	1.430	1.006	1.378
58	14.216	-3.112	-0.776	14.445	2.410	1.177	0.799	0.577
59	15.022	-1.029	0.982	15.931	2.220	2.002	0.510	0.474
60	12.056	-2.843	8.215	41.125	6.187	6.587	3.269	2.900
61	17.008	-2.499	0.329	13.909	1.349	1.346	1.690	1.441
62	14.471	-2.397	-1.216	14.479	2.912	1.353	0.708	0.316
63	15.475	-2.736	-2.001	17.216	2.762	1.153	0.762	0.205
64	12.330	-4.935	7.573	44.650	8.113	6.402	2.287	1.148

Table A.35. WFR, C_{eff}, and uncertainties for the 15 mil SB clearance seal with high pre-swirl.

Test Point	WFR	u_{WFR}	C_{eff}	$u_{C_{eff}}$
			[kN-s/m]	[kN-s/m]
1	0.450	0.038	9.278	0.391
2	0.000	0.000	7.136	1.062
3	0.460	0.036	18.551	0.679
4	0.000	0.000	57.190	3.565
5	0.000	0.000	6.316	1.241
6	0.000	0.000	7.975	1.010
7	0.000	0.000	15.679	1.172
8	0.000	0.000	62.006	3.784
9	0.000	0.000	7.340	1.088
10	0.000	0.000	8.542	1.032
11	0.000	0.000	16.008	1.166
12	0.000	0.000	74.191	3.836
13	0.000	0.000	7.690	1.126
14	0.000	0.000	9.543	1.109
15	0.000	0.000	16.686	1.093
16	0.000	0.000	65.936	2.496
17	0.000	0.000	5.373	0.922
18	0.000	0.000	7.445	0.893
19	0.000	0.000	14.515	0.885
20	0.000	0.000	48.579	3.523
21	0.000	0.000	6.576	0.860
22	0.000	0.000	7.999	0.844
23	0.000	0.000	14.783	0.898
24	0.000	0.000	55.329	3.578
25	0.000	0.000	7.072	0.787
26	0.000	0.000	8.390	0.811
27	0.000	0.000	15.095	0.947
28	0.000	0.000	54.799	3.339
29	0.000	0.000	8.084	0.829
30	0.000	0.000	9.345	0.810
31	0.000	0.000	15.675	1.106
32	0.000	0.000	57.077	2.986

Table A.36. WFR, C_{eff}, and uncertainties for the 15 mil SB clearance seal with high pre-swirl.

Test Point	WFR	u_{WFR}	C_{eff}	$u_{C_{eff}}$
			[kN-s/m]	[kN-s/m]
33	0.443	0.022	9.201	0.320
34	0.000	0.000	6.455	0.858
35	0.441	0.020	17.853	0.536
36	0.000	0.000	39.231	3.724
37	0.000	0.000	7.635	0.818
38	0.000	0.000	8.585	0.828
39	0.000	0.000	14.963	1.026
40	0.000	0.000	45.350	3.603
41	0.000	0.000	7.631	0.927
42	0.000	0.000	8.935	0.948
43	0.000	0.000	15.279	2.298
44	0.000	0.000	47.682	3.113
45	0.000	0.000	8.033	0.879
46	0.000	0.000	8.847	0.897
47	0.000	0.000	15.501	1.065
48	0.000	0.000	53.716	4.527
49	0.000	0.000	4.825	1.189
50	0.000	0.000	6.260	1.009
51	0.000	0.000	13.298	1.120
52	0.000	0.000	36.614	2.893
53	0.000	0.000	6.391	1.150
54	0.000	0.000	7.847	1.095
55	0.000	0.000	15.016	1.045
56	0.000	0.000	43.409	4.099
57	0.000	0.000	8.192	1.112
58	0.000	0.000	8.588	1.123
59	0.401	0.017	19.047	0.580
60	0.000	0.000	43.724	3.651
61	0.000	0.000	8.774	0.938
62	0.000	0.000	9.378	1.357
63	0.000	0.000	15.522	1.021
64	0.000	0.000	45.944	3.822

APPENDIX B

UNCERTAINTY ANALYSIS

The author of this study is part of a turbo machinery research group headed by Dr. Dara Childs. Students from this group use the same testing instrumentation, apparatus testing procedure, and data analysis tools. The author therefore derives uncertainty analysis from an ex student, Alex J. Moreland [20] and changes it accordingly where necessary. The analysis is discussed as follows

"Instrument bias and precision error is assumed to be negligible and only repeatability is calculated for the uncertainty of measurements. A 95% confidence interval is used to calculate the uncertainties for static measurements and the dynamic stiffness values. The true mean, μ, of a set of sample measurements, x_i, lies within the confidence interval

$$\bar{x} - t_{\alpha/2,\nu}\frac{S_x}{\sqrt{n}} < \mu < \bar{x} + t_{\alpha/2,\nu}\frac{S_x}{\sqrt{n}} \tag{B.1}$$

where $\bar{x}$ is the sample mean, $t_{\alpha/2,\nu}$ is the Student's *t*-distribution value, the level of significance is $\alpha = 1 - c$, c = 0.95 is the confidence, the degrees of freedom are $\nu = 1 - n$, and n is the number of samples. The standard deviation is

$$S_x = \sqrt{\frac{(\sum_{i=1}^{n} x_i^2) - n\bar{x}^2}{n-1}} \tag{B.2}$$

Recalling Eqs. (17)-(20) of Section 4.5 used to calculated the rotordynamic coefficients from curve fits to the dynamic stiffness data, the confidence intervals on the rotordynamic

coefficients are determined using a statistical test described in [22]. The true slope of a least squares regression lies within the $c\%$ confidence interval

$$b \pm t_{\alpha/2,\nu} \frac{s_{y/x}}{S_{xx}} \tag{B.3}$$

where the standard error of the y-data about the curve fit is

$$s_{y/x} = \left(\frac{1}{n-2} \sum_{i=1}^{n} [y_i - y(x_i)]^2 \right)^{1/2} \tag{B.4}$$

and the total squared variation of the independent variable, x_i, is

$$S_{xx}^2 = \sum_{i=1}^{n} (x_i - \bar{x})^2 \tag{B.5}$$

Finally, the true intercept lies within the interval

$$a \pm t_{\alpha/2,\nu} s_{y/x} \sqrt{\frac{1}{n} + \frac{\bar{x}^2}{S_{xx}^2}} \tag{B.6}$$

Confidence intervals of the rotordynamic coefficients are propagated into the confidence intervals on the WFR and C_{eff} values. Uncertainty propagation is defined as"

$$u_y = \sqrt{\left(\frac{\partial y}{\partial x_1} u_1\right)^2 + \left(\frac{\partial y}{\partial x_2} u_2\right)^2 + \cdots + \left(\frac{\partial y}{\partial x_n} u_n\right)^2} \tag{B.7}$$

APPENDIX C

NON-DIMENSIONAL ROTORDYNAMIC COEFFICIENTS

Rotordynamic coefficients are non-dimensionalised using

$$\bar{C} = \frac{\mu LD}{2C_r^3} \cdot \pi \tag{C.1}$$

$$\overline{K} = \frac{\omega}{2} \cdot \bar{C} \tag{C.2}$$

where $\bar{C}$ and $\overline{K}$ are predicted bearing damping, and stiffness coefficients respectively. Non-dimensional stiffness and damping coefficients are discussed here to better understand the trends seen in the study.

Non-Dimensional Stiffness Coefficients

Figure C-1 shows measured non-dimensional direct stiffness K_d versus ε_0 at ω = 4krpm and ΔP = 2.07 bar. Solid lines represent positive values while dotted lines represent negative values plotted on a logarithmic scale. For the 1X and 2X clearance seals, K_d increases as ε_0 increases. For the 1X and 2X clearance seals, at $\varepsilon_0 < 0.80$, $\overline{K}$ gives a poor representation of the measured direct stiffness coefficients. For the 3X clearance seal, K_d is negative and not a function of ε_0.

Figure C-2 shows measured non-dimensional cross coupled stiffness k_d versus ε_0 at ω = 4krpm and ΔP = 2.07 bar. Same color lines represent non-dimensional K_{tr} and K_{rt}

values and dotted lines represent negative values plotted on a logarithmic scale. For the 1X and 2X clearance seals, k_d increases as ε_0 increases. At $\varepsilon_0 = 0.00$, $k_{d\,X} \cong k_{d\,2X}$. At $\varepsilon_0 > 0.00$, k_d values are close for the 1X and 2X clearance seals. For the 3X clearance seal, cross coupling stiffness coefficients have the same sign and are not destabilizing.

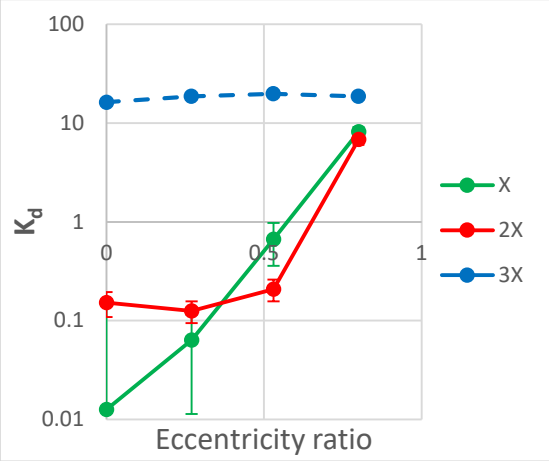

Figure C-1. K_d versus ε_0 at ω = 4krpm and ΔP = 2.07 bar.

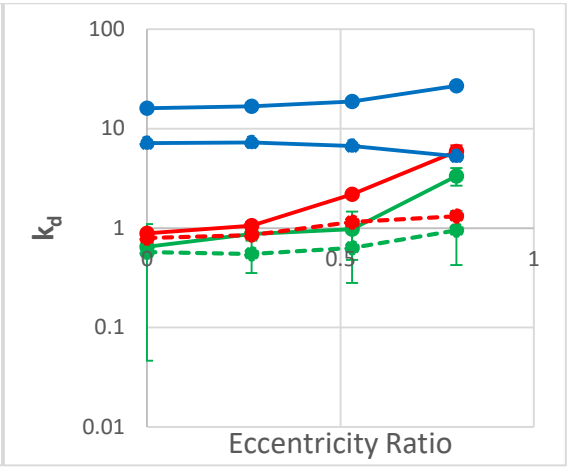

Figure C-2. k_d versus ε_0 at ω = 4krpm and ΔP = 2.07 bar.

Figure C-3 shows K_d versus ω at $\varepsilon_0 = 0.00$ and ΔP = 8.28 bar. Solid lines represent positive values while dotted lines represent negative values plotted on a logarithmic scale. For the 1X clearance seal, K_d increases as ω increases. For the 2X and 3X clearance seals, K_d decreases as ω increases. For the 3X clearance seal, K_d is negative and could suck the rotor into the stator.

Figure C-4 shows k_d versus ω at $\varepsilon_0 = 0.00$ and ΔP = 8.28 bar. Same color lines represent non-dimensional K_{tr} and K_{rt} values and dotted lines represent negative values

plotted on a logarithmic scale. k_d increases as C_r increases. For 1X and 3X clearance seals, k_d decreases as ω increases. For the 2X clearance seal, k_d is not a function of ω.

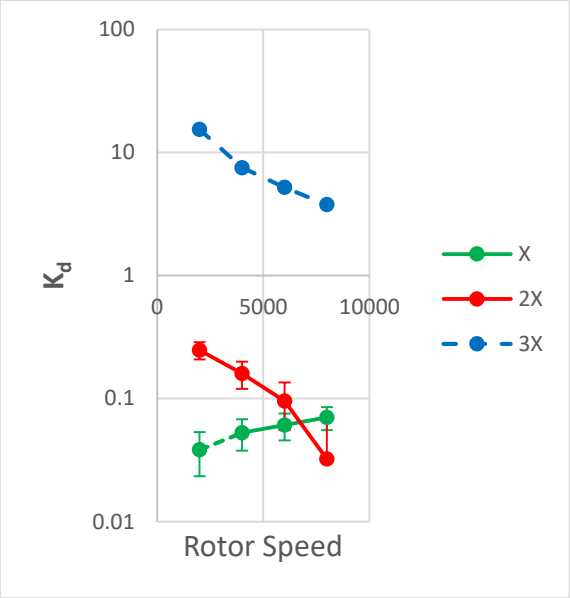

Figure C-3. K_d versus ω at ε_0 = 0.00 and ΔP = 8.28 bar

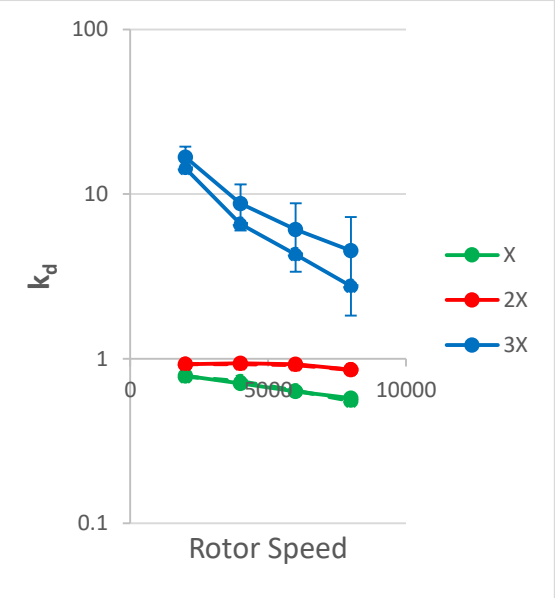

Figure C-4. k_d versus ω at ε_0 = 0.00 and ΔP = 8.28 bar

Non-Dimensional Damping

Figure C-5 shows non-dimensional direct damping C_d versus ε_0 at ω = 2krpm and ΔP = 2.07 bar plotted on a logarithmic scale. C_d increases as ε_0 and C_r increase. This result is expected; as C_r increases, the distance between the rotor and the annular seal wall increases at each ε_0.

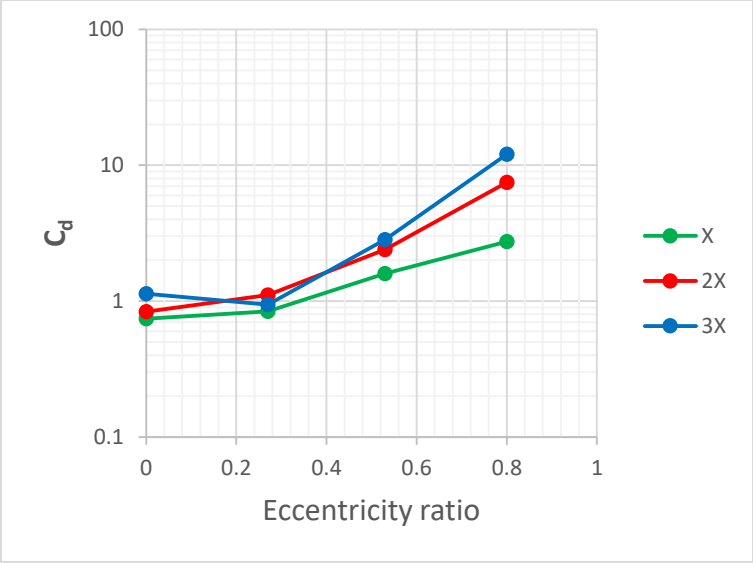

Figure C-5. C_d versus ε_0 at ω = 2krpm and ΔP = 2.07 bar.

Figure C-6 shows C_d versus ω at ε_0 = 0.00 and ΔP = 8.28 bar. C_d increases as ω increases. For the 1X and 2X clearance seals, C_d slightly decreases as ω increases. For the 3X clearance seal, C_d is not a function of ω.

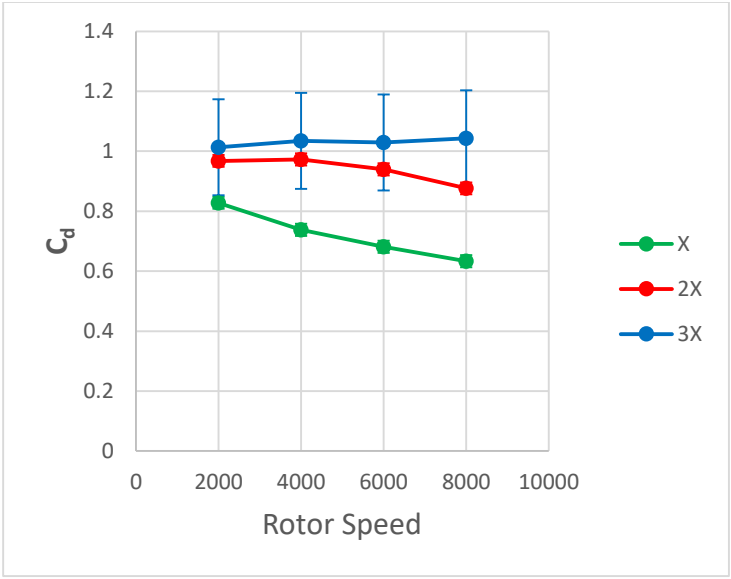

Figure C- 6. C_d versus ω at ε_0 = 0.00 and ΔP = 8.28 bar.

Figure C-7 shows C_d versus ΔP at $\varepsilon_0 = 0.00$ and $\omega = 8$ krpm. C_d generally increases as ΔP increases. As seen in Fig. C-6, C_d also increases as C_r increases.

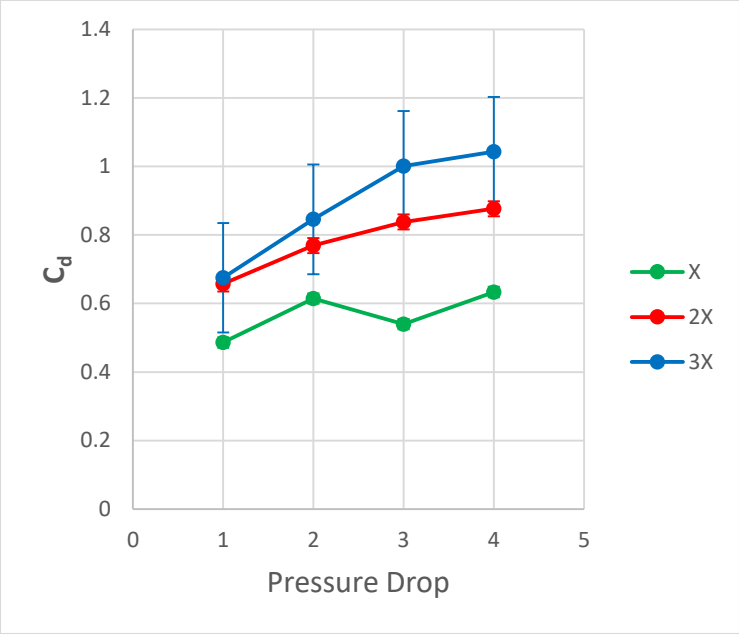

Figure C-7. C_d versus ΔP at ε_0 = 0.00 and ω = 8 krpm.